

BELLCOMM. INC.


TR-67-310-1

Capabilities of the Entry Guidance  
Equations for Earth Orbital Speed Entry

February 14, 1967

I. Bogner  
W. G. Heffron

Work Performed For Manned Space Flight, National Aeronautics  
and Space Administration, Under Contract NASW-417.



# BELLCOMM, INC.

## TABLE OF CONTENTS

Abstract

1.0 Introduction

2.0 AS-204 Entry Description

2.1 SPS Deorbit Entry Description

2.2 RCS Deorbit Entry Description

3.0 Limiting Conditions for Guidance Accuracy

3.1 Effect of Position Variations on SPS Orbit Footprints

3.2 Effect of Position Variations on RCS Orbit Footprints

3.3 Effect of Position and Velocity Indication Errors

3.4 Inertial Measuring Unit Effects

3.5 Effects of L/D Variations

3.6 Effect of Range on Deceleration and Heating

3.7 Other Spacecraft Parameter Variation Effects

3.8 Environment Variation Effects

4.0 Entry Guidance Equations

5.0 Summary and Conclusions

6.0 Acknowledgements

7.0 References

Appendix A - Coordinate Axes and Platform Alignment

Appendix B - Accelerometer Output Quantization Effects

Appendix C - AS-204 Requirements and Directives - Entry Phase

Appendix D - Simulation Computer Programs

ABSTRACT

This report has been prepared as part of Bellcomm, Inc. participation in the activities of the Guidance Software Control Panel of the Manned Spacecraft Center. It examines entry from Earth orbital speeds from the point of view of establishing the variations in initial conditions, indication errors, inertial measuring unit errors, lift to drag ratio (L/D), and environmental factors which can successfully be handled by the entry guidance. A description of entry guidance is included as are discussion of the various coordinate systems used, platform alignment formulas and the effects of the natural quantization of accelerometer outputs on navigation accuracy.

The conclusions resulting from the study include:

1. The flight path angle at entry and the L/D ratio are the most significant factors in entry success. At  $L/D = 0.357$  (old nominal), and nominal flight path angle of  $-1.478^\circ$ , the SPS deorbit margins in flight path angle are  $+0.72^\circ$ , (to the undershoot boundary) and  $-0.43^\circ$ , (to the overshoot boundary). At  $L/D = 0.28$  (new nominal) the margins are  $+0.25^\circ$  and  $-0.40^\circ$ . At  $L/D = 0.24$  (3 $\sigma$  low) they are  $0.07^\circ$  and  $-0.40^\circ$ . With 1 $\sigma$  as  $0.057^\circ$ , the low L/D undershoot margin is too small, and the flight path angle should be adjusted. It seems more desirable, however, to reduce the range to some 1800 NM and steepen the flight path angle to about  $1.48^\circ$ , getting margins of about  $\pm 0.30^\circ$ , which should be safe. If planning is done using  $L/D = 0.24$ , then margins improve if L/D increases.

RCS deorbit margins are  $+0.35^\circ$ ,  $-0.20^\circ$  for  $L/D = 0.357$ ; are  $+0.15^\circ$ ,  $-0.20^\circ$  for  $L/D = 0.28$ ; and are  $+0.05^\circ$ ,  $-0.15^\circ$  for  $L/D = 0.24$ . (1 $\sigma$  for flight path angle is here about  $0.015^\circ$ ). Decreasing the range is not of significant help, so the flight path angle should be made less steep to balance the margins. Again, use of 0.24 L/D in planning is desirable.

2. Inertial Measuring Unit (IMU) errors cause a CEP of 1.30 NM for the SPS deorbit and 1.39 NM for the RCS deorbit, provided the IMU accelerometers are not used for navigation during the free fall after retrofire and before atmospheric entry. If the accelerometers are

used, the CEP's become 2.95 NM (SPS) and 11.7 NM (RCS). The crew may establish the IMU attitude as much as 1 hour before retrofire without significant effect on the CEP's.

3. Guidance accuracy is insensitive to lift orientation errors (in roll) of  $\pm 35^\circ$ , to roll acceleration reductions to  $2^\circ/\text{sec}^2$  (about 40% of the capability of one set of thrusters), to roll rate limits of  $5^\circ/\text{sec}$  ( $15^\circ/\text{sec}$  nominal), to weight variations of  $\pm 20\%$ , to winds of 300 knots from any direction, and to atmospheric density variations of  $\pm 20\%$ . In particular, manual control of roll orientation should be quite feasible.
4. Position and velocity update errors have negligible effect on landing accuracy.

BELLCOMM, INC.

CAPABILITIES OF THE ENTRY GUIDANCE  
EQUATIONS FOR EARTH ORBITAL SPEED ENTRY

1.0 Introduction

This report has been prepared as part of Bellcomm, Inc., participation in the activities of the Guidance Software Control Panel of the NASA Manned Spacecraft Center. Like a similar report for Mission AS-202, it examines the entry guidance equations from two viewpoints. One is the determination of the tolerable range of conditions and hardware errors over which guidance accuracy of 20 NM or less can be maintained. The other, which is brief because the guidance is simple, is to discuss the guidance equations themselves, showing why the entry trajectory is as it is.

Because of the low L/D experienced in AS-202, this report gives special attention to the effects of L/D variations. Because an RCS deorbit is intended as a backup to the nominal SPS deorbit, both trajectories are considered. And because in-flight alignment of the Inertial Measuring Unit is generally required, special attention is paid in Appendix A to relationships between the various coordinate systems used.

This report is not primarily concerned with dispersions or with the CEP at the landing point. That topic is covered in a report issued by MIT/IL [ 2 ] and by an MSC Study [ 21 ]. However, all three studies suggest that the 10 NM CEP requirement for entry accuracy will be met.

The nominal trajectory used in this report is the AS-204 Operational Trajectory [ 3 ], which is also the source of much of the data. It is considered to be a typical earth orbit entry.

The guidance equations were taken from the G&N System Operations Plan (GSOP) [ 1 ] but were corrected to agree with the flight computer program listing [ 8 ]. Computer simulation work was conducted at Bellcomm, Inc. using two different computer programs (See Appendix D).

This report begins with a description of the nominal entry trajectory. The effects of position and velocity variations and uncertainties on guidance accuracy are then examined followed by a discussion of the effects of Inertial Measuring Unit errors.

Then discussions are given on the effects of L/D variations, of variation of other spacecraft parameters, and of variations in environmental factors. These form the first part of the report. The second, and briefer part of the report discusses the guidance equations. They are a small excerpt from the high speed entry guidance equations, sufficient because the entry speed is relatively low (circular speed as opposed to parabolic speed). The conclusions of this report are applicable only for earth orbit entries, and other work is required for the LOR mission equations.

## 2.0 AS-204 Entry Description

This section describes both the SPS and RCS deorbit entries for Mission AS-204. SPS deorbit is the nominal, with RCS deorbit used as backup.

### 2.1 SPS Deorbit Entry Description

The nominal entry for earth orbital missions is initiated by a Service Propulsion System (SPS) deorbit burn, following which the vehicle is positioned in an aerodynamically trim condition with full lift up. For AS-204 at the entry interface altitude of 400,000 feet, the vehicle inertial velocity is 25,158 feet per second at a flight-path angle of  $91.48^\circ$  below the radius vector. Heading is  $79.47^\circ$  E relative to true north. The entry point is at  $31.18^\circ$  N geodetic latitude and  $97.84^\circ$  W longitude. Target coordinates for parachute opening (at 23,500 feet altitude) are  $60^\circ$  W longitude and  $31.01^\circ$  N latitude, 2064 NM from the entry point.

Guidance accuracy is achieved by rolling the CM to put the lift vector in the proper direction. Both downrange and lateral range are controlled simultaneously in this way.

The general structure of the guidance scheme may be described by referring to Figure 1. Based upon updated initial conditions and the outputs of on-board integrating accelerometer, vehicle position and velocity (R,V) are determined in the navigation block. Targeting encompasses the computations of range-to-go and the predicted lateral miss. The downrange logic involves flying a ballistic trajectory until, as determined by first occurrence of a specific aerodynamic deceleration, the vehicle penetrates the atmosphere. The vehicle then flies along a stored reference trajectory to the target. During the atmospheric portion of the flight, the commanded lift needed to meet the range is monitored

by acceleration control logic. This logic compares vehicle altitude rate with a computed altitude rate which would result in excessive deceleration. If the rate of descent exceeds the computed bound, the range logic lift is superceded by a full lift up command.

The lift command is also filtered through the lateral logic. Here the function is to reflect the commanded roll angle about the vertical when necessary, in a manner which keeps the predicted lateral miss within acceptable bounds. The computer generates a quantity called Y, which is a conservative estimate ( $Y < 40$  NM) of the remaining lateral range capability of the CM. If full lift up or down is required for range control, then lateral control is permitted only to the extent of  $\pm 15^\circ$  rotation of the lift from full up or down. Rotation is reversed when the predicted lateral miss exceeds  $Y/2$ . If full lift, up or down, is not required, then the roll command changes sign when the predicted lateral miss exceeds Y.

Figure 2 shows the SPS deorbit entry trajectory relative to the earth beginning at the entry point (400,000 ft. altitude). Figure 3 shows altitude and inertial velocity vs. time. Altitude always decreases, and at a fairly uniform rate. This differs from what will occur at higher speeds, for then an increase in altitude (a ballistic skip, out of the sensible atmosphere) is an integral part of the guided trajectory. Here the velocity is approximately circular and there is no skip.

Figure 4 shows the roll angle history and includes the lateral miss and the criteria Y which determines roll right or left. Lift is up during the initial phase of entry and for some 72 seconds into the final phase. Then the range prediction is satisfactory and lateral control comes into action. The CM rolls left then right four times while adjusting the lateral miss and keeping the range under control. Low angular rates can be used: The roll should be smooth for the crew. The miss is less than 0.5 NM.

Figure 5 shows the heating history for the entry. As is discussed later, heating is slight compared with the heat shield capabilities.

Figure 6 shows the deceleration history. At 3.16 g maximum, the deceleration is well within the 10 g maximum requirement. Peak g's occur when the CM is 238 NM from the target, at 163,145 ft.

Figures 7 and 8 show altitude vs. inertial velocity and range-to-go vs. inertial velocity respectively and are traditional

graphs in discussing entry guidance. Note that most of the range is covered at high velocity and altitude. At the lower velocities earth orbital missions use, the final descent is not dramatic, but the general trend of entry trajectories is suggested by this graph.

## 2.2 RCS Deorbit Entry Description

Should the SPS engine fail to ignite for its deboost burn, the spacecraft makes one more orbit and then retrofires the RCS engines. In addition to the postponement of approximately 92 minutes in reaching entry altitude, there are a number of other changes in the entry trajectory. The vehicle is oriented for a  $180^\circ$  roll (lift down) prior to reaching the 400,000 foot altitude, entry starts further west at a longitude of  $-106.16^\circ$  and at  $32.65^\circ$  N latitude, the entry velocity is 25830.5, 72.5 fps greater than for SPS deboost, and the flight path angle is more shallow:  $-0.934^\circ$  vs.  $-1.478^\circ$  for the SPS entry. The initial heading is  $87.53^\circ$  with respect to North. Target coordinates are also changed to  $-57.65^\circ$  longitude and  $23.75^\circ$  latitude. This corresponds to a change in initial range-to-go from 2064 NM (for SPS deboost) to 2767 NM.

Figure 9 shows the trajectory relative to the earth. Lift is down when the spacecraft passes the 400,000 foot interface ( $t = 0$  sec) and remains so until the aerodynamic acceleration builds up to  $6.5 \text{ fps}^2$  at 378 seconds. The guidance first commands a roll of  $0^\circ$  (full lift up), and then modulates the roll commands, so as to fly along a stored reference trajectory, in order to reach the landing site. Nominal drogue parachute deployment occurs 880 seconds after the start of entry at an altitude of 23,500 feet with the vehicle less than 0.6 NM from the target.

## 3.0 Limiting Conditions For Guidance Accuracy

### 3.1 Effect of Position Variations on SPS Deorbit Footprints

This section considers the effects of position variations from nominal at the entry altitude upon the accuracy of landing at the target. Perfect navigation data at the start of entry and nominal L/D are assumed.

Figure 10 shows the two curves which are used to illustrate the above effects. The outer curve is the conventional unguided footprint. It is the locus of spacecraft terminal points when the roll is held fixed at the values marked. The inner curve shows that part of the footprint in which the target can be located



and reached by the CM with a miss of 20 NM or less. Except at the shortest ranges, the two curves are essentially identical. These curves are thus an indirect approach to finding the effect of position variations at entry. By showing where the CM could go, given nominal entry conditions, they imply where it could come from to reach the target.

The CEP specified in the general Apollo Program Specification [6] is 10 NM, i.e., 50 % of the flights should miss by less than 10 NM. Using 20 NM is an arbitrary choice of the authors of this report as a conservative criterion for accurate guidance.

The unguided footprint extends from 1362 NM to 2601 NM from the entry point. The accurate guidance region extends from 1511 NM to the full extent of the unguided range (2601 NM), and is  $\pm 109$  NM wide at its broadest point. The general Apollo Program Specification [6] requires 1500 NM to 2500 NM, which is essentially met under the nominal AS-204 entry conditions, although the requirement was deleted for AS-204. It is stressed that these curves apply only for the initial position and velocity conditions at the start of entry. While it is unlikely that the target will be changed just prior to entry, the guided footprint shows the boundary within which this can be done.

The above discussion was based upon the entry point inertial velocity remaining unchanged. Consider now velocity variations from this nominal value. Indication errors are assumed zero, i.e., the ground has perfectly updated the position and velocity estimates in the G&N systems. The position at entry is taken as nominal as is the L/D ratio (0.357).

Figures 11, 12, and 13 are of interest. Figure 11 shows flight path angle and velocity magnitude effects, considering azimuth as nominal. The upper curve is the overshoot boundary, the lower the undershoot boundary.

At the nominal SPS deorbit entry velocity of 25,758 fps, the minimum tolerable angle is  $-1.05^\circ$  where the nominal is  $-1.478^\circ$ . This represents a variation 193 fps up. Reference 21 gives a  $1\sigma$  value on the order of 2.6 fps, so 193 fps is  $74.3\sigma$ . The numbers suggest that overshoot is not a problem.

The lower curve in Figure 11 shows the boundary beneath which the CM will fall short of its target. The critical flight path angle is  $-2.2^\circ$ , an unlikely variation of -325 fps ( $125\sigma$ ). This lower boundary is not a  $10\text{ g}$  boundary, which is much further

below and is not shown. Deceleration considerations are discussed in Section 3.6.

Figure 12 shows azimuth and velocity magnitude effects considering flight path angle as nominal. At nominal velocity, a large range of azimuths can be tolerated, between  $76.5^\circ$  and  $82.8^\circ$  with  $79.469^\circ$  as nominal. Since one degree of azimuth represents approximately 450 fps laterally, these limits are some 1350 fps left and 2800 fps to the right. Reference [21] gives approximately  $4.7$  fps as  $1\sigma$ .

Figure 13 completes the discussion showing the flight path angle and azimuth effects for nominal velocity magnitude.

Assuming that the uncertainties are even roughly correct and that the L/D is nominal (0.357), these curves indicate that the spacecraft should experience no difficulty, from these considerations, in hitting the target site. Section 3.5 discusses the effect of L/D variation from nominal.

### 3.2 Effects of Position Variations on RCS Deorbit Footprints

This section considers the effects of position variations from nominal at the entry altitude upon the ability of the spacecraft to land at the designated target assuming an RCS deboost. Figure 14 shows the guided and unguided footprints which are used to depict this capability.

The guided footprint extends from 2,030 NM to 3,165 NM and is approximately  $\pm 111$  NM wide. Several points may be made based upon the figure and upon data obtained while generating the curves.

With the RCS deorbit, which is a backup mode, the entry guidance still achieves better than 1000 NM range span in meeting landing point accuracy requirements (10 NM). A shallow entry flight path angle ( $-0.934^\circ$ ) precludes meeting the general accuracy specification in the 1500 to 2030 NM range.

The heel of the guided entry locus is also the 10G acceleration boundary. Targets located nearby produce trajectories with peak accelerations of 9 to 11 g.

It was somewhat unexpected to find the guided locus outside the unguided locus. An explanation is difficult to give

without detailed comparison of guided and unguided trajectories to points in this short range region, but basically the additional lateral capability is due to better control of altitude and time of flight when guidance is used. When the trajectory is guided, the initial roll is about  $180^\circ$  and the CM enters the sensible atmosphere somewhat sooner. But then, instead of permitting an unchecked descent, the guidance uses less lift down, the better to sustain the altitude, and lifts to the side to make the necessary turn. Thus guidance makes more time available with useful levels of lift, and thereby gains additional lateral capability.

### 3.3 Effect of Position and Velocity Indication Errors

The duration of Earth orbital missions is generally so long that the ground must supply position and velocity data to the G&N system prior to deorbit. This data is derived from the MSFN tracking network, with  $1\sigma$  accuracies of about 1000 ft. and 0.8 fps in each axis [4]. In this section, the effects of these errors are discussed. The actual trajectory at deorbit is assumed to be nominal and the estimate supplied to the G&N system to be in error.

Table 1 shows the results for the SPS deorbit at  $3\sigma$  levels. The downrange and crossrange data are the changes in the actual misses caused by the indication errors noted. They are small. The error in indicated altitude is also given: it is large enough to justify the use of barometric devices to measure altitude and control parachute deployment during the descent, as is actually done.

Additional analysis shows that errors greater than  $20\sigma$  values are required before the miss begins to exceed 20 NM.

Table 2 gives the results for RCS deorbit. The errors are larger, because the descent takes longer, but are still tolerable. Errors greater than  $10\sigma$  are required to cause misses over 20 NM.

All of these miss data are inherently uncertain to about 1 NM. This is because the entry guidance has an inherent dead zone of about that size about the target, i.e., it does not attempt to get any closer than about 1 NM to the target, particularly in the crossrange direction. Even small perturbations in conditions can cause the miss to change from, say +0.4 NM to -0.4 NM: both

TABLE 1

Effect of Position and Velocity Indication Errors - SPS Deorbit

<u>Indication Error (<math>3\sigma</math>)</u>	<u>Downrange Miss NM</u>	<u>Crossrange Miss NM</u>	<u>Altitude Indication Error - Feet</u>
Downrange Position 3000 Ft.	-1.0	-0.28	3644
Crossrange Position 3000 Ft.	-0.35	-0.38	-447
Altitude 3000 Ft.	-1.77	-0.60	9074
Downrange Velocity 2.4 fps	-0.13	-0.33	5461
Crossrange Velocity 2.4 fps	0.12	0.07	-457
Altitude Rate 2.4 fps	-1.18	-0.36	2850
RSS Effect ( $3\sigma$ )	2.38	0.90	11575

TABLE 2

Effects of Position and Velocity Indication Errors - RCS Deorbit

<u>Indication Error (<math>3\sigma</math>)</u>	<u>Downrange Miss NM</u>	<u>Crossrange Miss NM</u>	<u>Altitude Indication Error - Feet</u>
Downrange Position 3000 Ft.	-1.20	-0.65	2,470
Crossrange Position 3000 Ft.	0.08	-0.37	-558
Altitude 3000 Ft.	-3.71	-1.87	14,859
Downrange Velocity 2.4 fps	-2.61	-1.09	11,690
Crossrange Velocity 2.4 fps	-0.20	0.11	-602
Altitude Rate 2.4 fps	-1.10	-0.61	2,079
RSS Effect ( $3\sigma$ )	4.82	2.37	19,198

results are satisfactory, and which would be the case in an actual entry is impossible to predict.

### 3.4 Inertial Measuring Unit Effects

The Inertial Measuring Unit (IMU) in the CM is aligned before SPS retrofire so that the Flight Director Attitude Indicator (FDAI) reads  $0^\circ$ ,  $0^\circ$  at retrofire, which aids manual monitoring or control of the burn. Appendix A discusses alignment (and other related factors) in great detail. Briefly, the IMU Y axis is normal to the orbit plane, and the X and Z axes are in the orbit plane, except for compensations for the engine thrust misalignment. At SPS retrofire, the X axis is about  $40^\circ$  from the radius vector, pointed up and forward. At the entry point, it is  $17.8^\circ$  from the radius vector and to the rear, and at the end of entry it is about  $52.6^\circ$  to the rear of the radius vector.

Alignment procedures are completed well before retrofire. MIT/IL assumes the procedure completed and the IMU in inertial mode some 15 minutes before retrofire. Because this puts some pressure on the crew, a period of 60 minutes was also considered in the present study: there were negligible differences in the results.

The error sources used were those given in the GSOP [2] and tests were conducted at the  $3\sigma$  level. The results depend strongly upon whether or not the IMU accelerometers are used for navigation during the 15 minute (SPS) or 30 minute (RCS) free fall between retrofire and 400,000 ft. altitude. This is controllable by the crew. If they are used, the  $1\sigma$  levels for the actual miss are 2.51 NM downrange and 2.20 NM crossrange for a CEP of about 2.95 NM for the SPS deorbit, and for the RCS deorbit, the  $1\sigma$  levels are 10 NM downrange, 5.5 NM crossrange and a CEP of about 11.7 NM. If they are not used, the  $1\sigma$  levels are 1.09 NM downrange and 0.96 NM crossrange with a CEP of about 1.30 NM for the SPS and 0.81 NM downrange, 1.18 NM crossrange and 1.39 NM CEP for the RCS.

MIT/IL gives 0.69 NM CEP for the SPS deorbit, and 3.32 NM CEP for the RCS deorbit, and thus apparently does not use the accelerometers during the coast. TRW [21] gives the miss as less than 3 NM due to all error sources for the SPS deorbit, and does not give an estimate for the RCS deorbit.

Not included in the above errors is the effect of the accelerometer pulse method of sensing deceleration due to lift and drag. The analysis of this problem is complex and is contained in Appendix B, but the effect is completely negligible.

The "Average-G" Navigation algorithm is found to be very good.

### 3.5 Effects of L/D Variations

The operational trajectory for AS-204 was calculated for a hypersonic trim L/D of 0.357, which was the value assigned for the CM prior to AS-202. In AS-202, it will be remembered, the CM fell about 200 NM short; this miss was due to a reduction of L/D to about 0.285 plus a slightly steep entry angle. Although the CM for AS-204 was not rebalasted (to change the L/D), the MSC ASPO changed the nominal L/D to about 0.28 with  $3\sigma$  tolerance of  $\pm 0.04$ . This section discusses the effects of varying L/D, flight path angle, and range on the accuracy of guidance.

Figures 15-26 show curves for misses of 20 NM, 100 NM, and 300 NM for three velocities (nominal, nominal +200 fps, and nominal -200 fps), and for four ranges (1660 NM, a reasonable minimum range; 2060 NM, the SPS deorbit nominal range; 2460 NM, a possible maximum range for SPS deorbit, and 2767 NM, the RCS deorbit range).

Consider first the nominal SPS deorbit, Figure 15, with velocity variations effects given in Figures 16 and 17. At the nominal SPS flight path angle and  $L/D = 0.357$ , there are margins of  $+0.72^\circ$  and  $-0.4^\circ$  in flight path angle. (A positive margin applies for undershoots, a negative margin for overshoots.) Variations to be expected are given by MIT/IL as about  $0.00091^\circ$  ( $1\sigma$ ) due to platform drift [2], and about  $0.0026^\circ$  ( $1\sigma$ ) from update errors of 1000 ft. and 0.8 fps in each axis [2]. TRW [21] gives a larger value of  $0.057^\circ$  and considers other error sources as well. In any instance it would appear that with  $L/D$  of 0.357 there will be no problem. If the  $L/D$  is reduced to 0.28, the margin shrinks considerably, to  $+0.25^\circ$  and  $-0.40^\circ$ , but is still adequate. At  $L/D = 0.24$ , they become  $+0.07^\circ$ ,  $-0.40^\circ$  which is too low an undershoot margin.

From Figure 16, if the velocity is reduced 200 fps, the margin for  $L/D = 0.28$  is then  $+0.1^\circ$  and  $-0.6^\circ$ , while if the velocity is increased by 200 fps (Figure 17), the margins are  $+0.5^\circ$  and  $-0.2^\circ$ . Since the SPS deorbit  $\Delta V$  total is about 553 fps, the variations of  $\pm 200$  fps are extreme; but the variations show that control of the  $\Delta V$  for deorbit is important and that the  $L/D$  and the flight path angle must be considered carefully. It would appear from the curves in Figure 15 that with  $L/D = 0.28$ , the entry flight path angle should be  $-1.41^\circ$  (for margins of  $\pm 0.32^\circ$ ) rather than  $-1.48^\circ$  as the operational trajectory has it. There is apparently no advantage in changing the speed, the range in acceptable flight path angle being the same for the three speeds. But

if the L/D should fall as low as 0.24 then a flight path angle of  $-1.3^\circ$  is more desirable, giving margins of  $\pm 0.23^\circ$ . To protect against such a contingency, this  $-1.3^\circ$  value appears better operationally; the margin against overshoot is then satisfactory for any L/D greater than 0.24, and the margin against undershoot is adequate even if the L/D is 0.24.

Another way of improving margins for the SPS deorbit is to delay retrofire, reducing the range for entry. Figures 18-20 show what happens if the range is reduced to 1660 NM. It is immediately obvious that the deorbit burn needs adjusting, for the flight path angle is too shallow. Using  $-1.6^\circ$  and 25558 fps velocity as a nominal, (Figure 19) the margins for L/D = 0.24 are  $\pm 0.35^\circ$ , better than the  $\pm 0.25^\circ$  possible for nominal range, and are independent of velocity over the  $\pm 200$  fps range. Changing the flight path angle to  $-1.6^\circ$  from  $-1.48^\circ$  requires about 80 fps additional  $\Delta V$  at SPS deorbit, so there is a trade-off between increasing the SPS deorbit burn and reducing the range. This should be evaluated during the flight when the actual SPS fuel remaining is known. Nominal entry velocity is reduced at the same time the entry is made steeper, because the nominal deorbit burn attitude is maintained.

Figures 21-23 show that the range for SPS deorbit should not be increased, particularly if an L/D of 0.24 is considered. The curves also show a strong dependency of desirable flight path angle with velocity; if the long range deorbit becomes necessary, it will be necessary to adjust the CM attitude at retrofire, possibly losing the pilot's line of sight to the horizon. Fortunately, there is no reason for forcing the long range entry, so the problem should not come up.

For the SPS deorbit, therefore, it seems better to reduce the entry range. At 1800 NM, a flight path angle of  $-1.48^\circ$  should have margins of about  $\pm 0.30^\circ$ . Naturally, it is necessary to plan the deorbit burn to adjust to the real-time situation, and use of a pessimistic L/D of 0.24 is desirable since results for higher L/D's are always better.

These last figures (21-23) are also of interest as a short range RCS deorbit and entry. RCS deorbit entry velocity is 25830 fps, 72 fps faster than the SPS deorbit entry velocity so Figures 21 and 23 are of greater interest than Figure 22. For the pessimistic L/D of 0.24, the margin is about  $+0.15^\circ$ ,  $-0.1^\circ$  at 25758 fps. Actually Figures 15-23 all show that RCS deorbit should not be planned for 2400 NM or less.



Figures 24-26 show the conditions for the nominal RCS entry range of 2767 NM, for RCS nominal entry velocity and for RCS entry velocity  $\pm 200$  fps. The RCS deorbit  $\Delta V$  is 137 fps, so  $\pm 200$  fps are, again, extreme variations. For the nominal velocity, (Figure 24) the margins at  $L/D = 0.357$  are  $+0.35^\circ$ ,  $-0.20^\circ$ ; at  $L/D$  of 0.28 are  $+0.15^\circ$ ,  $-0.2^\circ$ , and at  $L/D = 0.24$  are  $+0.05^\circ$ ,  $-0.15^\circ$ . Note that the miss goes up rapidly if the margins are exceeded, especially if the entry is too shallow.

MIT/IL suggest  $0.012^\circ$  as  $1\sigma$  for RCS deorbit entry flight path angle dispersion. This seems reasonable to the writers. Compared with the SPS deorbit, the  $\Delta V$  is much smaller, so engine performance errors (which MIT/IL did not include in either case) are less and MIT/IL's result should be only slightly low. To be a bit conservative, a  $1\sigma$  value of  $0.015^\circ$  seems appropriate.

Using the  $0.015^\circ$ , then, the RCS deorbit will have a relatively small margin against undershoot if the  $L/D$  is 0.24, but otherwise it will be satisfactory. It seems desirable to make the flight path angle slightly less steep.

For a faster velocity (Figure 25) the margins are reduced and the entry flight path angle must be adjusted. For a slower velocity the margins are more desirable (Figure 26); at an  $L/D$  of 0.24, with a flight path angle of  $-0.63^\circ$ , the margins would be  $\pm 0.17^\circ$  and would increase as  $L/D$  increases. But such a lower velocity (200 fps slow) is an undesirable (or impossible) requirement for the RCS deorbit with the standard attitude during the burn.

The above point up a definite need for real time planning of the RCS deorbit if it is needed. The crew must fine align the IMU and the ground must both update the position and velocity data and carefully calculate the optimum RCS burn. It seems prudent to do this using the low  $L/D$  of 0.24, since the situation always improves as  $L/D$  increases.

### 3.6 Effect of Range on Deceleration and Heating

Figure 27 shows how maximum g's, peak heat rate and total heat vary with range to the landing point. SPS deorbit entry conditions were used.

The maximum deceleration curve shows a typical reduction in g's with range, but has two unusual variations. The peak at about 1600 NM range is due to nearly simultaneous requirements from the lateral miss control and from the g limiter. What happens at the 1600 NM range, for example, is the following. During

the final phase, the downrange control is operating with little predicted range miss and a bank angle of about  $+90^\circ$ . The lateral miss control comes into action and commands a roll angle of about  $-90^\circ$ , because the lateral miss has just drifted over the acceptable limit. Because of the particular situation, the spacecraft goes from  $+90^\circ$  to  $-90^\circ$  through  $180^\circ$ , i.e., it momentarily causes full lift down. This causes deceleration to build up to 10.6 g's even though the g-limiter takes over and calls for full lift up. A particular set of lateral miss and range conditions are required for these events to occur in just this way; having slightly different initial lateral miss, for example, would have caused the lateral correction to occur at a different time, and the high peak would not have occurred.

The Reentry Studies Section of the Mission Planning and Analysis Division, MSC, it is known, has recognized this problem and instructed MIT/IL not to permit rolling through  $180^\circ$  if the deceleration is greater than  $175 \text{ fps}^2$  [22]. Within the capabilities of the authors of this report to understand the listing of the AS-204 flight program, no such special logic is included and was therefore not included in the Bellcomm simulations.

The second unusual variation is that the g's are not uniformly low at high ranges. This is due to the commands given in the final phase of the entry guidance. It is interesting to note that the initial phase lasts for about 1000 NM regardless of total range, so that the final phase range goes up fairly equally with total range. Final phase initial conditions uniformly have a velocity of about 25700 fps, an altitude of about 255,000 ft. and a flight path angle of  $-1.22^\circ$ . The final phase for short ranges begins lift down almost immediately, leading to the high g's shown on the graph. As the range increases, lift is maintained up for more and more time. The guidance trades off velocity and rate of descent to achieve the proper range - at ranges of about 2000 NM the deceleration is fairly uniform during the descent yielding a low maximum g of only 3 g. At long ranges (2600 NM), the deceleration is low while the CM stays at high altitude, but when the final descent is begun the velocity is low enough that the maximum deceleration is again about 3 g. But at intermediate ranges (2450 NM), the trade off is not so good - the CM stays at high altitude for too long and does not lose enough velocity, and the deceleration during the final descent builds up to about 4.5 g. This is not high enough to make desirable any changes in the guidance equations, although it might be considered while planning the mission. It is interesting to note that these peak g's occur when the CM is 100 to 300 NM from the landing point, being closest when the total range is greatest.

The total heat curve is as expected, increasing steadily with range. Most of the heating occurs at high altitudes (and velocities). When the range is short, so that flight time is reduced, the total heat is reduced. This increases the peak heat rate, which occurs at high altitude and velocity. As range increases, peak heat rate reduces.

Earth orbital speed entries are not heat shield tests. Figure 28 shows pertinent data on the heat shield design requirements, on LOR-mission expectations, and on particular flights. There should not be any heat shield problem.

### 3.7 Other Spacecraft Parameter Variation Effects

In addition to the L/D variation effects discussed in the previous section, the effects of other spacecraft parameters were investigated.

Roll Orientation of Lift, that is the angle by which the lift is not in the spacecraft X-Z plane, was investigated. A  $\pm 35^\circ$  error was inserted; the miss remained under 1.0 NM for both SCSS and RCS entries. This is because the actual lift force is sensed by the accelerometers. The roll angle time history is affected by this variation, but the guidance equations successfully cope with it. This error would also correspond to readout errors (or misalignment) of the roll gimbal resolver.

Roll Acceleration and Rate Limits were also checked. The simulations used in this study did not include a perfect simulation of the autopilot, although the simulations are thought to be reasonable. Nominal roll acceleration was  $5^\circ/\text{sec}^2$  and nominal roll rate limit was  $15^\circ/\text{sec}$  (about the CM X axis). Reducing the acceleration to  $2^\circ/\text{sec}^2$  did not affect the guidance accuracy. Reducing the roll rate as low as  $5^\circ/\text{sec}$  with  $2^\circ/\text{sec}^2$  acceleration also does not affect the guidance accuracy. In both cases, the guidance equations adjust the roll angle time history to compensate for the variations. This is of interest especially for manual control of entry or for use of only one of the two roll thruster sets. Autopilots for attitude control during orbital entry should be as simple as possible - high accuracy is simply not required.

Weight of the spacecraft, for  $\pm 20\%$  variations, has no important effect on the guidance accuracy. This is because the deceleration is sensed. If the weight is reduced, the drag force causes greater deceleration. There is some self stabilizing effect in that the resulting slower velocity would reduce the drag force, but, in any case, the entry guidance equations adjust the roll angle time history to compensate for the change.

### 3.8 Environment Variation Effects

Variation of atmospheric density by  $\pm 20\%$  does not affect guidance accuracy, for both SPS and RCS nominal deorbits. This is because the deceleration effect of the atmosphere is sensed by the G&N system, and the guidance makes appropriate changes in the roll angle commands.

Winds of 300 knots above 65,000 ft. from any direction do not affect guidance accuracy. Again, this is because the effect is sensed by the G&N system and the trajectory corrected.

The G&N system stops guiding the trajectory at about 60,000 ft., when the relative velocity falls below 1,000 fps. From there to touchdown, winds could deflect the CM, but it would take the jet stream at 300 knots to cause it to move two miles. Thus, winds are not a problem.

### 4.0 Entry Guidance Equations

Figures 29-35 are flow charts for the entry guidance. Taken from the GSOP [1] and supplemental information [8, 14, 15], they are annotated to show how they operate for Mission AS-204. The nominal mission sequence of events, insofar as entry is concerned, begins with platform alignment on the order of one hour prior to retrofire. The operational trajectory [3] lists retrofire as approximately 13D, 18H, 20M after lift-off. By the time the CM reaches the entry interface altitude 881S later, it is at the required entry attitude. The pitch and yaw angles are set for aerodynamic trim of the CM and the roll angle is  $0^\circ$ , for full lift up. Entry heading is such that the target is slightly to the right and 2,064 NM downrange. (For the remainder of this section  $t = 0$  when the CM passes through the 400,000 ft. altitude.)

The CM is in a ballistic phase in which little aerodynamic force is exerted. While the CM guidance has the ability to attempt to correct for predicted lateral misses, the conditions do not warrant any roll maneuvers. Full lift up (with an accompanying slow buildup of lateral miss) is maintained until the senses aerodynamic deceleration reaches  $6.5 \text{ fps}^2$ , when a new guidance phase is initiated. This occurs about 228 seconds into entry, at an altitude of 257,102 feet with a range to go of about 1102 NM. In this, the final phase, the range which will result from the present trajectory is computed, using present velocity magnitude, vertical velocity, and deceleration as the independent variables. The guidance technique employs a reference trajectory

(range, vertical velocity and deceleration vs. velocity magnitude) and influence coefficients about that trajectory to predict the range which will be covered. This is compared with the range to the target and the error is converted into an L/D command using another influence function. Note that range control is attempted only during the final phase. It is assumed that the retrofire and ballistic phase result in the CM velocity and position being within the range capability of the final guidance phase.

Lateral Control (Figure 35) is attempted throughout the flight. But vertical L/D requirements for longitudinal control take precedence, and lateral control is reduced to a question of rolling right or left. That is, suppose the vertical L/D wanted can be achieved by a roll angle of  $+60^\circ$  or  $-60^\circ$  ( $L/D_{\text{vertical}} = L/D_{\text{max}} \cos(\text{roll angle})$ ); then the lateral control determines whether the  $+60^\circ$  or  $-60^\circ$  is to be used. To reduce the amount of rolling, the lateral logic permits the lateral error to drift back and forth between limits given as the quantity Y. That is, suppose the roll angle actually is  $+50^\circ$ , and the commanded roll is  $+60^\circ$ . Lateral logic will use  $+60^\circ$  unless the lateral miss now exceeds Y, in which case the  $-60^\circ$  will be used.

If full lift up or down is required for longitudinal control, not much is available for lateral control. The logic in Figure 35 permits roll angles of  $\pm 15^\circ$  from  $0^\circ$  or  $180^\circ$  in such a case. This gives some lateral control, but not as much as might be desired. So  $Y/2$  is then used as the switching criteria, i.e., a more strenuous effort is made to keep the target dead ahead. Y is always conservative and so is  $Y/2$ .

Lateral motion should be acceptable from the viewpoint of crew comfort. Trajectory data indicates four roll reversals during the entry.

## 5.0 Summary and Conclusions

This study has investigated the conditions under which accurate guidance in the entry phase is maintained. Accurate guidance is arbitrarily defined as a miss less than 20 NM at the 23,500 ft. altitude where the parachute opens. For this study, trajectory initial conditions and similar data were taken from the AS-204 Operational Trajectory [3]. The results of the study include the following:

1. The G&N system following an SPS deorbit can accurately guide the command module to any point in an area extending from 1511 NM to 2601 NM downrange from the entry point and up to  $\pm 109$  NM to the side. The nominal target is 2064 NM downrange in the center of this area. In the backup mode, where the RCS is used for deorbit, accurate guidance is achieved from 2030 NM to 3165 NM downrange and  $\pm 111$  NM to the side. The nominal target in this case is 2767 NM downrange.
2. Expectable variations in entry position (position at 400,000 ft. altitude), and in velocity magnitude and heading angle have negligible effects on guidance accuracy, provided they are known to the G&N System.
3. Expectable errors in position and velocity update data from the MSFN do not importantly affect guidance accuracy.
4. Inertial Measuring Unit (IMU) errors cause a CEP of 1.30 NM for the SPS deorbit and 1.39 NM for the RCS deorbit, provided the IMU accelerometers are not used for navigation during the free fall after retrofire and before atmospheric entry. If the accelerometers are used, the CEP's become 2.95 NM (SPS) and 11.7 NM (RCS). The Crew may establish the IMU attitude as much as 1 hour before retrofire without significant effect on the CEP's.
5. The flight path angle at entry and the L/D ratio are the most significant factors in entry success. At  $L/D = 0.357$  (old nominal), and nominal flight path angle of  $-1.478^\circ$ , the SPS deorbit margins in flight path angle are  $+0.72^\circ$  (to the undershoot boundary) and  $-0.43^\circ$  (to the overshoot boundary). At  $L/D = 0.28$  (new nominal) the margins are  $+0.25^\circ$  and  $-0.40^\circ$ . At  $L/D = 0.24$  ( $3\sigma$  low) they are  $0.07^\circ$  and  $-0.40^\circ$ . With  $1\sigma$  as  $0.057^\circ$ , the low L/D undershoot margin is too small, and the flight path angle should be adjusted. It seems more desirable, however, to reduce the range to some 1800 NM and steepen the flight path angle to about  $-1.48^\circ$ , getting margins of about  $\pm 0.30^\circ$ , which should be safe. If planning is done using  $L/D = 0.24$ , then margins improve if L/D increases.

RCS deorbit margins are  $+0.35^\circ$ ,  $-0.20^\circ$  for  $L/D = 0.357$ ; are  $+0.15^\circ$ ,  $-0.20^\circ$  for  $L/D = 0.28$ ; and are  $+0.05^\circ$ ,  $-0.15^\circ$  for  $L/D = 0.24$  (1 $\sigma$  for flight path angle is here about  $0.015^\circ$ ). Decreasing the range is not of significant help, so the flight path angle should be made less steep to balance the margins. Again, use of 0.24  $L/D$  in planning is desirable.

6. Deceleration, peak heat rates and total heat load for Earth orbital speed entry are all quite tolerable.
7. Guidance accuracy is insensitive to lift orientation errors (in roll) of  $\pm 35^\circ$ , to roll acceleration reductions to  $2^\circ/\text{sec}^2$  (about 40% of the capability of one set of thrusters), to roll rate limits of  $5^\circ/\text{sec}$  ( $15^\circ/\text{sec}$  nominal), to weight variations of  $\pm 20\%$ , to winds of 300 knots from any direction, and, to atmospheric density variations of  $\pm 20\%$ . In particular, manual control of roll orientation should be quite feasible.

#### 6.0 Acknowledgements

Mrs. S. B. Watson programmed necessary modifications to the computer simulations and expertly operated the computer to obtain the data in this report.

The Reentry Studies Section, MPAD, MSC, headed by C. B. Graves gave full cooperation to the authors during this study. Their assistance is greatly appreciated.

2012-<sup>IB</sup>  
WGH-mrr

  
I. Bogner

  
W. G. Heffron

## BELLCOMM, INC.

### REFERENCES

1. "Guidance and Navigation System Operations Plan, Apollo Mission 204A/205 (U)", J. M. Dahlen et al, Massachusetts Institute of Technology Instrumentation Laboratory, Vol. 1, October 1966 (R-507 Rev. 1).
2. "Guidance and Navigation System Operations Plan, Apollo Mission 204A/205 (U)", J. M. Dahlen et al, Massachusetts Institute of Technology Instrumentation Laboratory, Vol. 2, October 1966, (Error Analysis, Confidential).
3. "Spacecraft Operational Trajectory for AS-204 (U)", D. J. Griffith et al, MSC Internal Note 66-FM-101, October 17, 1966.
4. "Preliminary MSFN Error Analysis, AS-204 (U)", P. T. Pixley, MSC Internal Note 65-FM-106, August 5, 1965.
5. "Apollo Flight Mission Assignments (U)", M-D MA500-11 SE 010-00-1, Sept. 10, 1965 (Confidential).
6. "Apollo Program Specification (U)", SE 005-001-1, Rev. A (last Rev. Oct. 11, 1966).
7. "AS-204 Appendix to the Apollo Program Specification (U)", SE 005-001-1, Revision A.
8. Program Assembly Listing "YUL System for AGC - New Program SNSPT247 by NASA 1021107-031", MIT/IL, Sept 15, 1966. (Unclassified)
9. "Natural Environment and Physical Standards for the Apollo Program", M-DE 8020.008B, SE 015-001-1, OMSF, NASA, April 1965 (Unclassified).
10. "Project Apollo Coordinate System Standards", SE 008-001-1, OMSF, NASA, June 1965 (unclassified).
11. "The American Ephemeris and Nautical Almanac - 1966", US Government Printing Office.
12. "The American Ephemeris and Nautical Almanac - 1967", US Government Printing Office.
13. "Explanatory Supplement to the Astronomical Ephemeris and the American Ephemeris and Nautical Almanac:, Her Majesty's Stationery Office (U.K.).



14. "Re-entry Guidance for Apollo", Raymond Morth, MIT/IL Report R-532, V1 (Unclassified), V2 (Confidential), January 1966.
15. "Description of Apollo Entry Guidance", I. Bogner, Bellcomm, Inc. TM 66-2012-2, August 4, 1966.
16. "Capabilities of the Entry Guidance Equations for Mission AS-202", I. Bogner, W. G. Heffron, Bellcomm, Inc. TR-66-310-5, August 9, 1966.
17. "Updated Alignment Equations for AS-204 and AS-205 (U)", G. R. Kimball, MSC Memorandum 66-FM 25-463, Sept. 20, 1966.
18. "Notes for Ephemeris Programs for the AGC", L. Brock, MIT/IL, SGA Memorandum 20-65, Sept. 29, 1965.
19. "Noise Analysis of the Apollo Powered Flight Navigation Equations", H. Heffes, Bell Telephone Laboratories, Whippany, N. J., MM66-4264-13, August 31, 1966.
20. "Two Body Linear Guidance Matrices", R. E. Stearns and L. P. Abramson, MIT Experimental Astronomy Laboratory Report RE-14, March 1965 (revised June 1965).
21. "Apollo Mission AS-204 Spacecraft Dispersion Analysis", MSC Internal Note 66-FM-139, November 17, 1966.
22. "Reentry Guidance Logic", C. A. Graves, Memorandum 66-FM53-183, MSC, NASA, June 21, 1966.

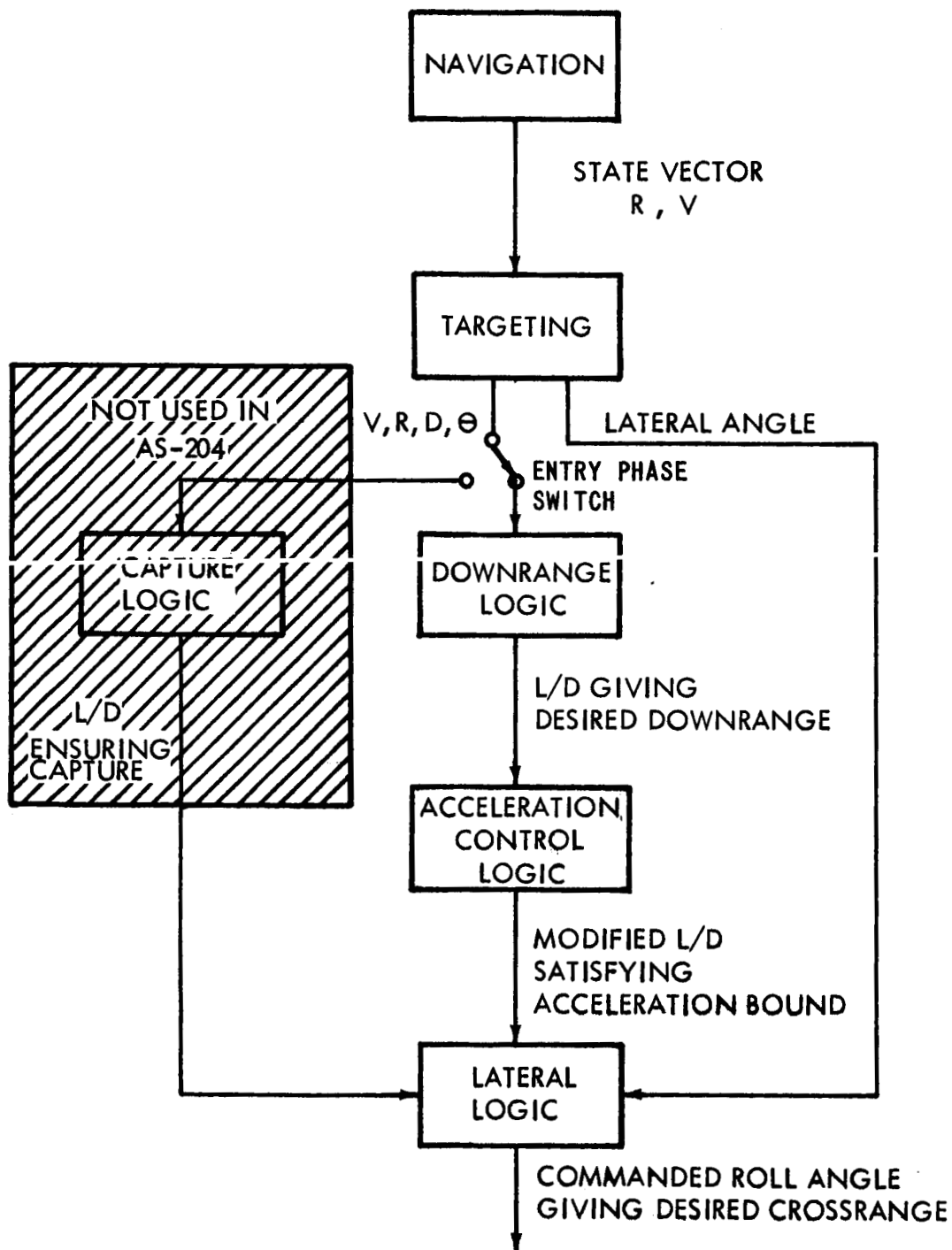
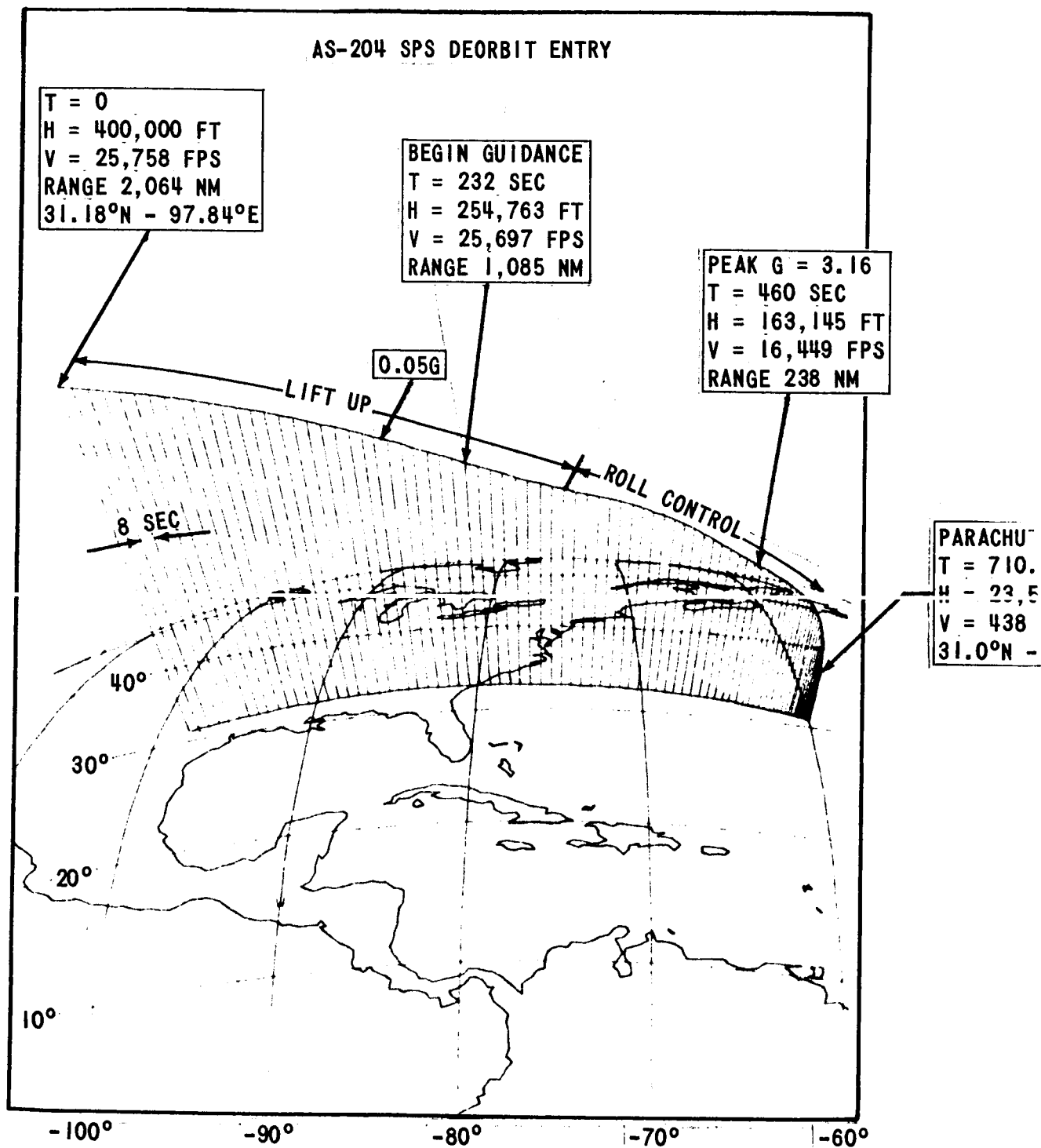


FIGURE 1 - GENERAL STRUCTURE OF THE GUIDANCE SYSTEM



**FIGURE 2 - AS-204 SPS DEORBIT ENTRY TRAJECTORY  
(ALTITUDE EXAGGERATED 20X)**

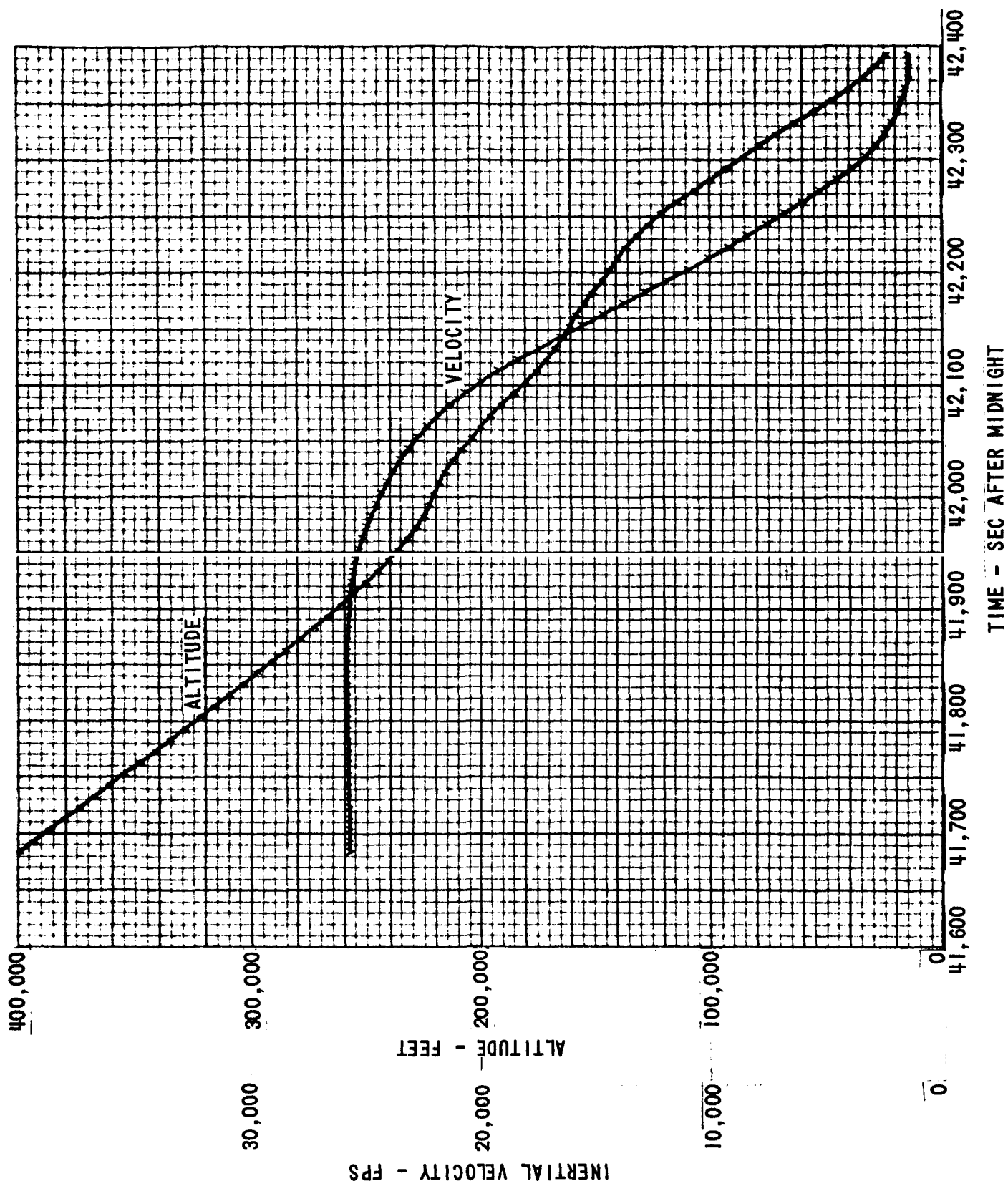


FIGURE 3 - SPS REORBIT ALTITUDE AND VELOCITY

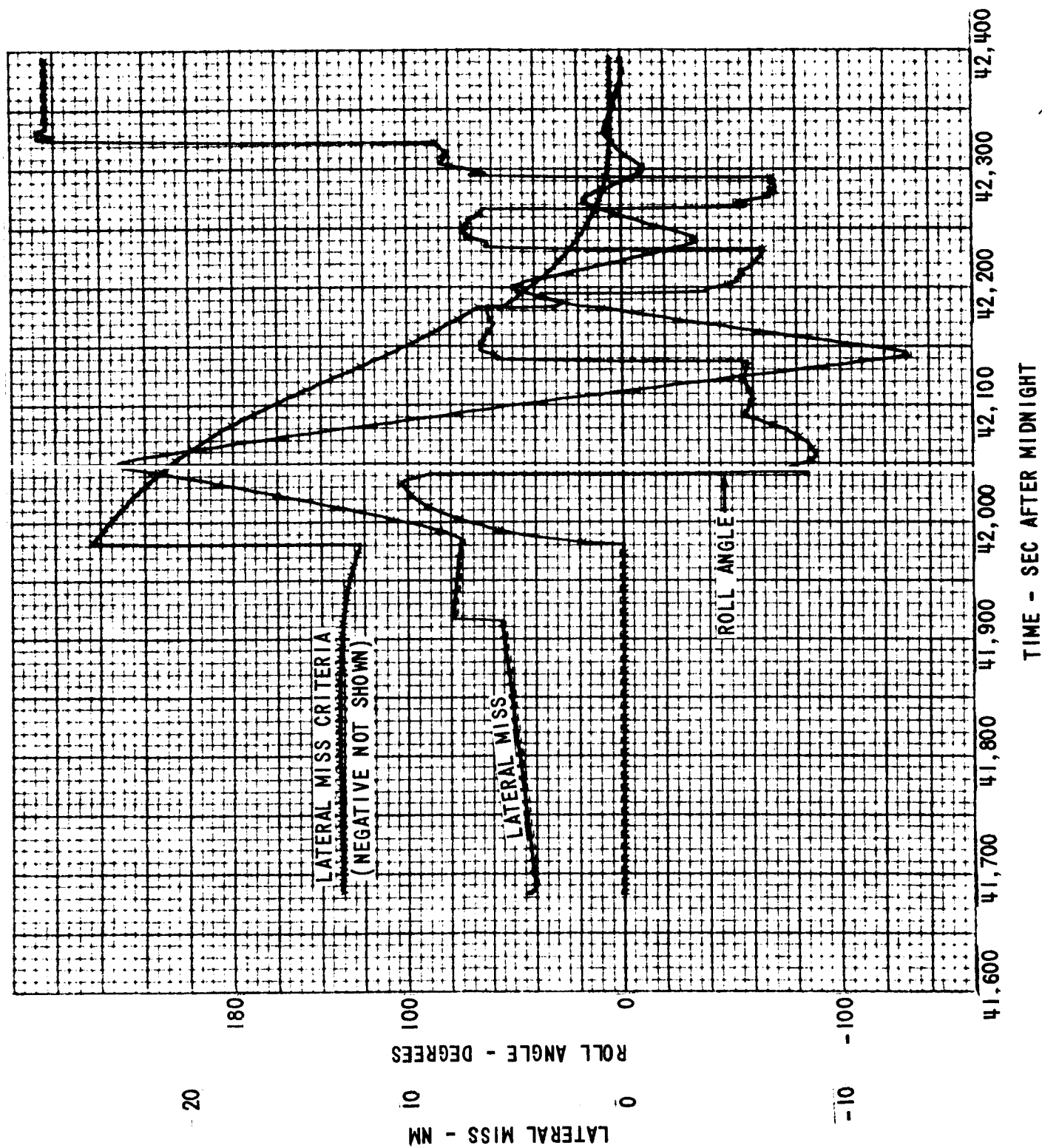


FIGURE 4 - SPS ORBIT - ROLL ANGLE AND LATERAL MISS

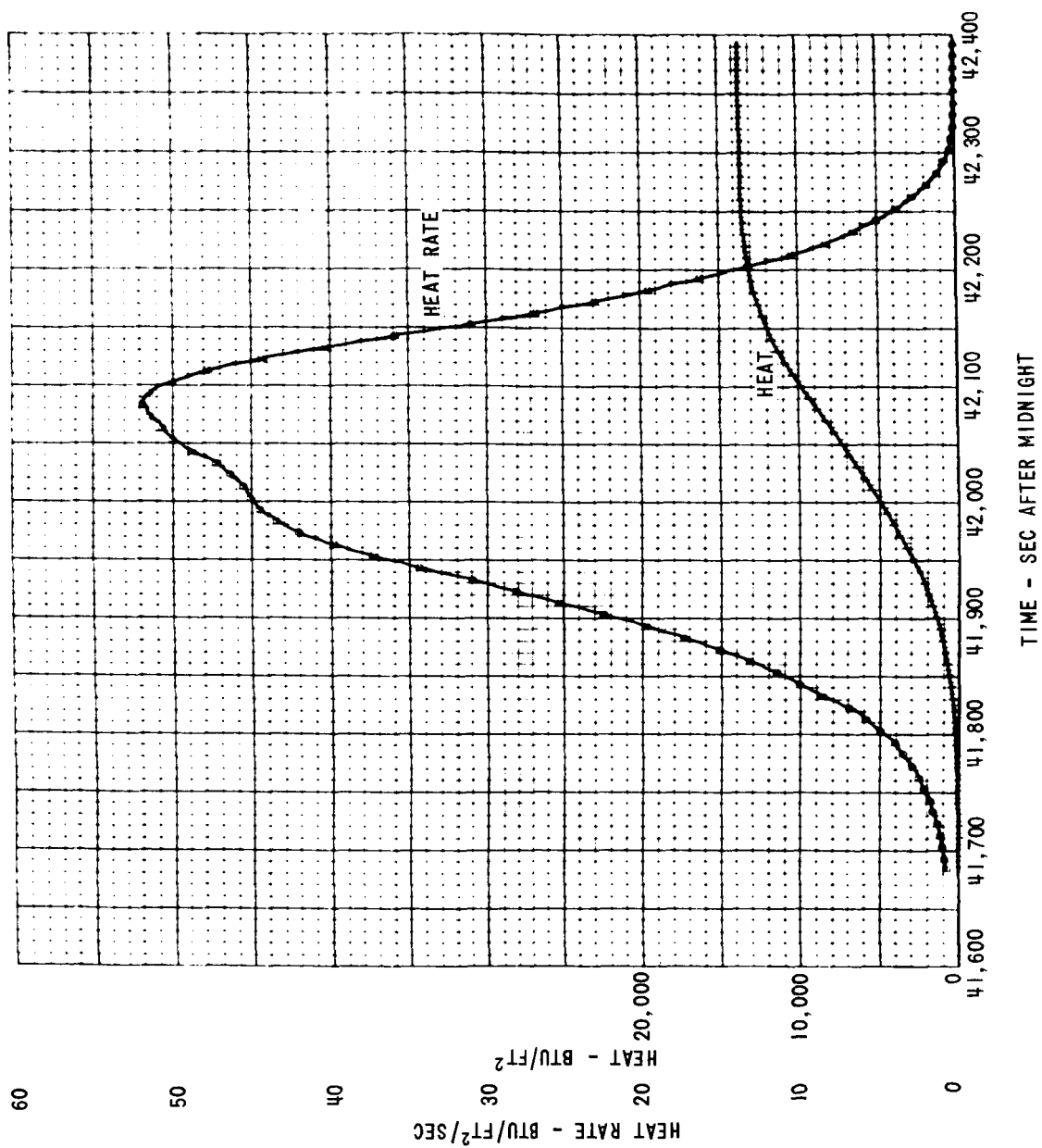


FIGURE 5 - SPS DEORBIT HEATING

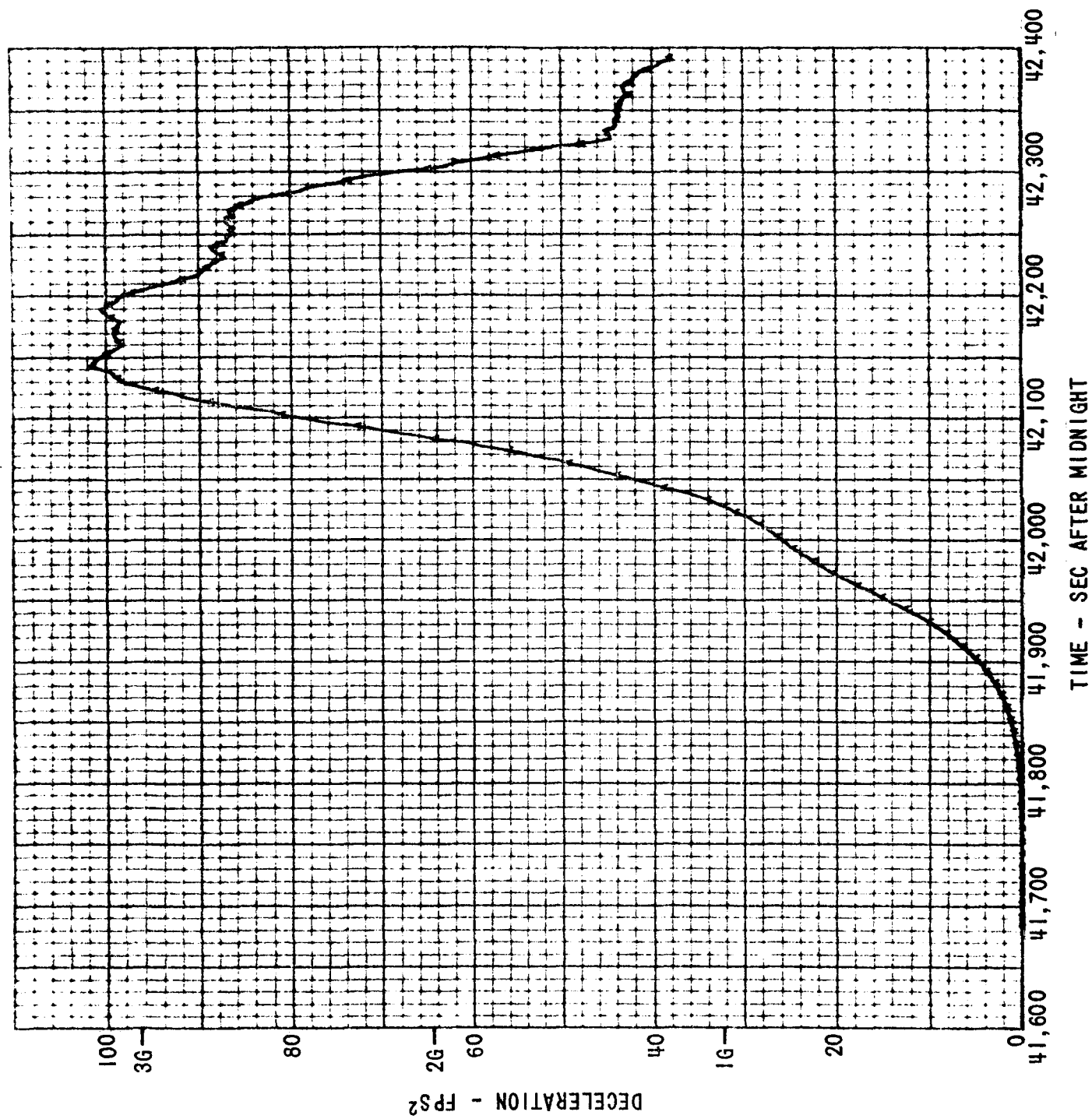


FIGURE 6 - SPS DEORBIT DECELERATION

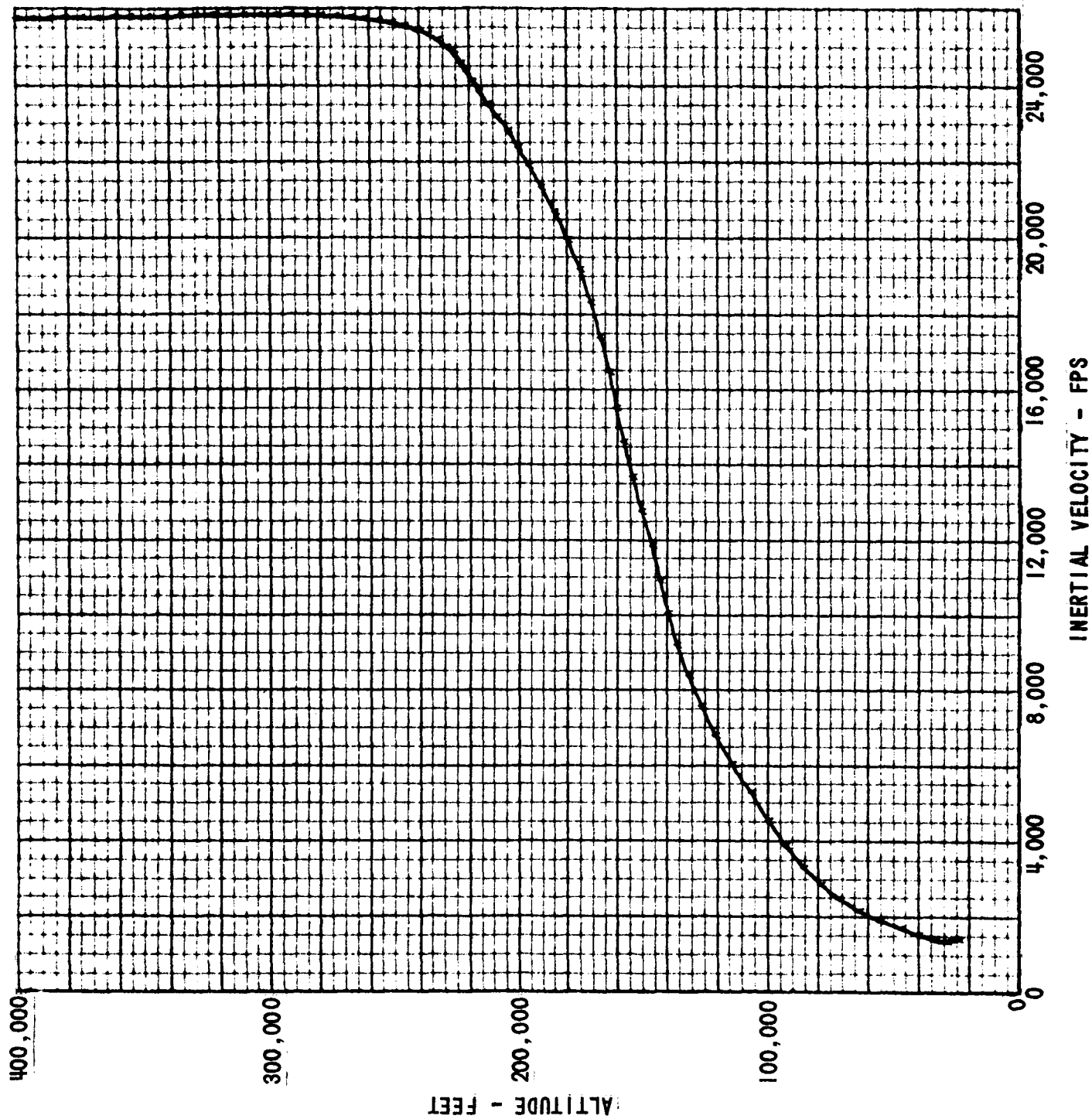


FIGURE 7 - SPS DEORBIT - ALTITUDE VS. VELOCITY



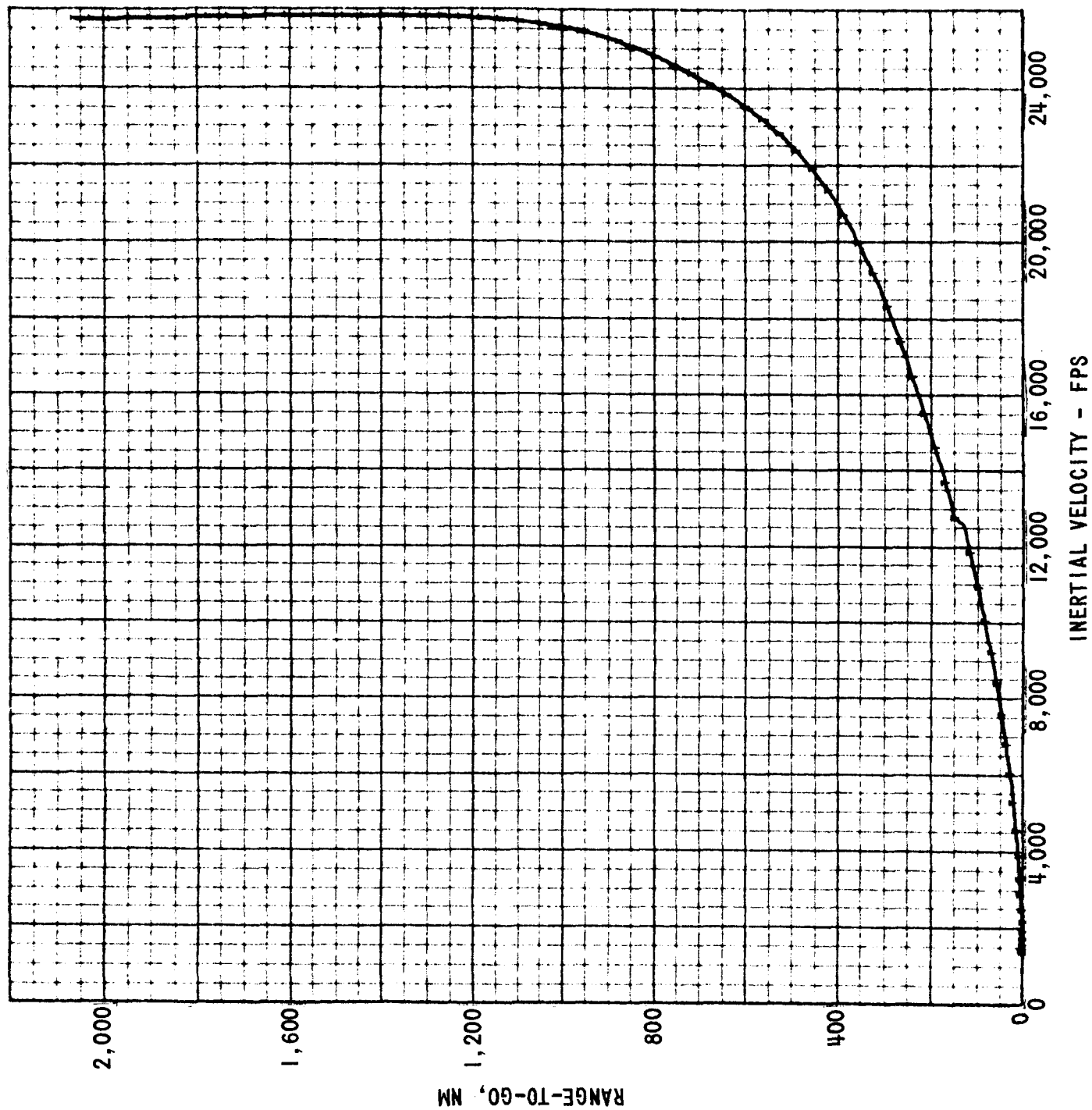
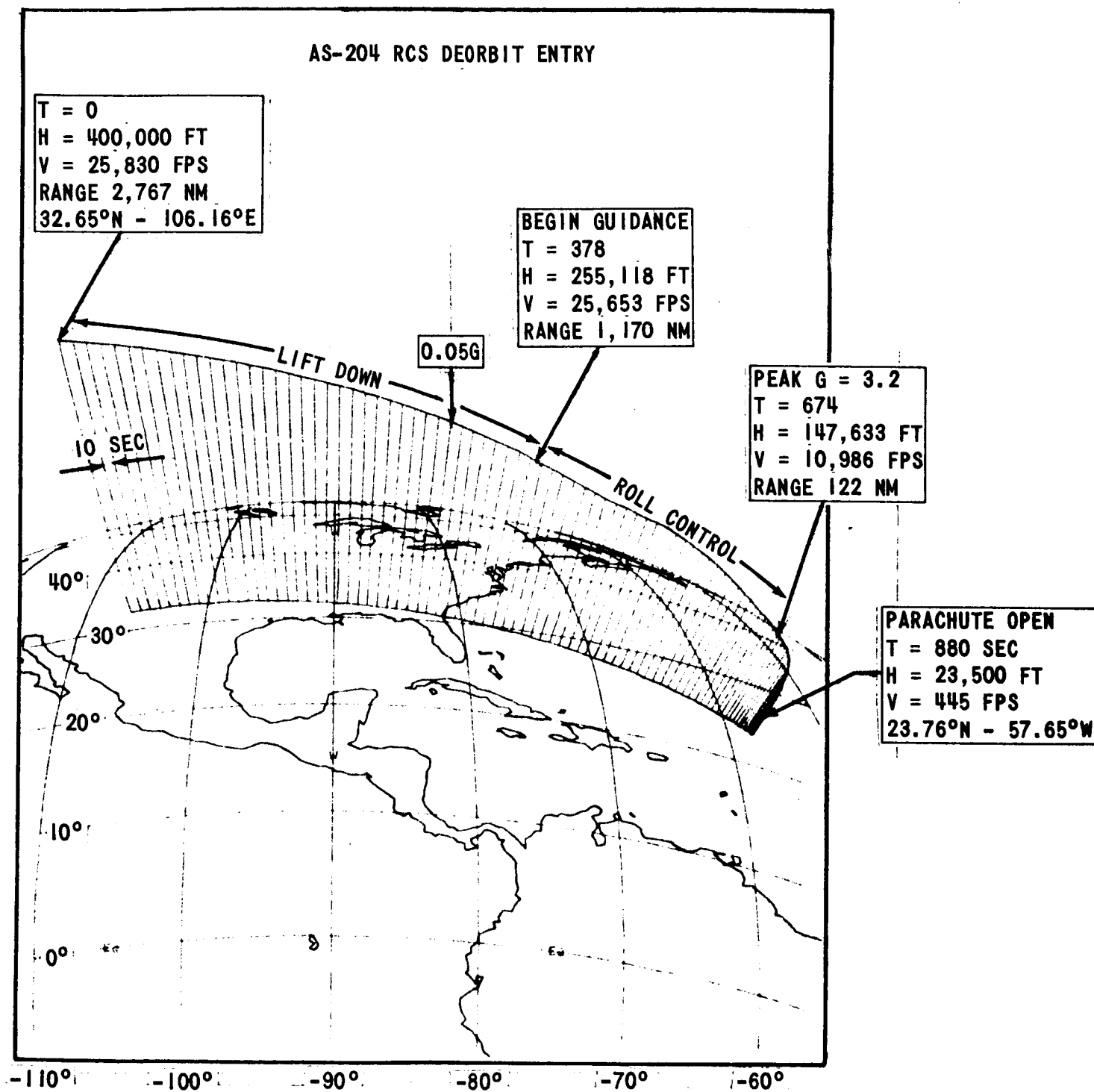


FIGURE 8 - SPS DEORBIT - RANGE-TO-GO VS. VELOCITY



**FIGURE 9 - AS-204 RCS DEORBIT ENTRY TRAJECTORY  
(ALTITUDE EXAGGERATED 20X)**

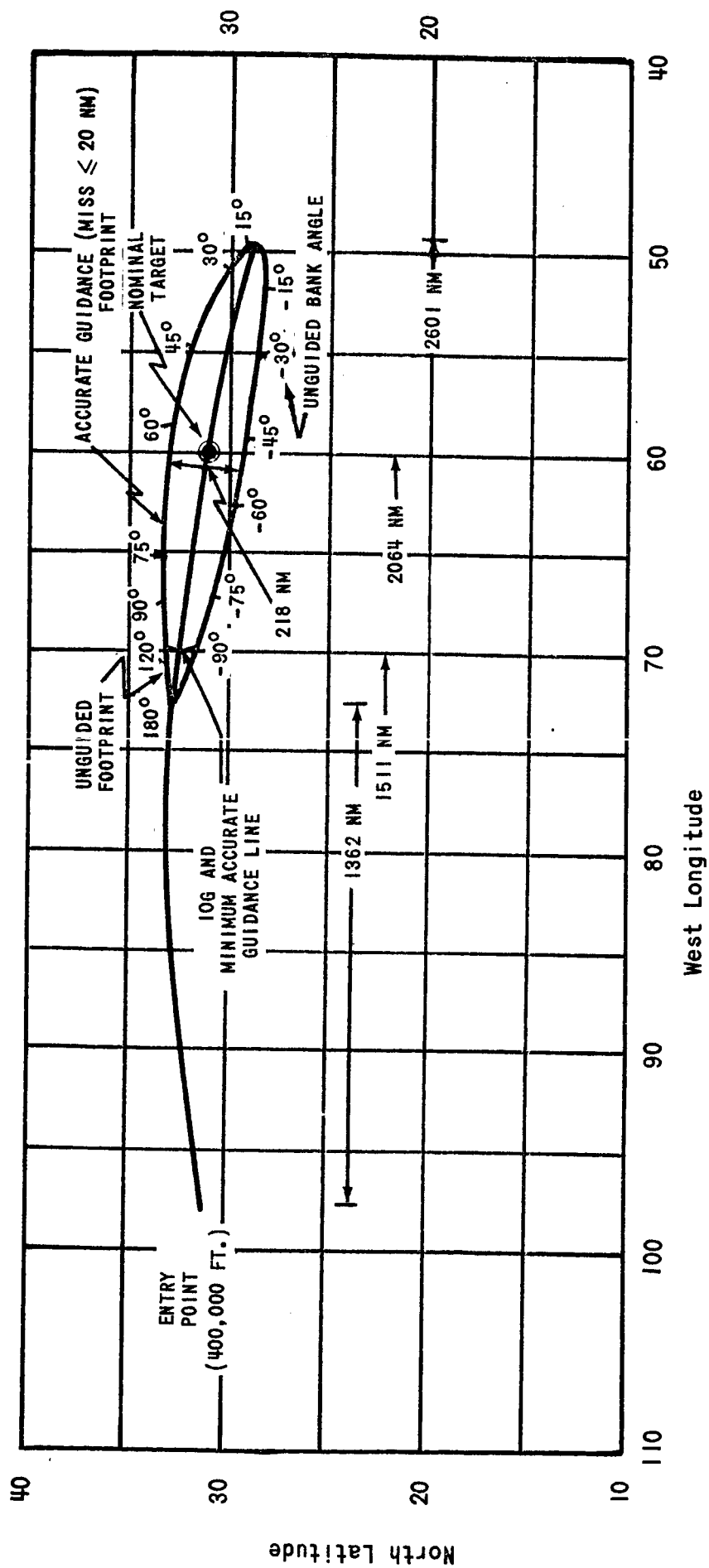


FIGURE 10 - AS-204 GUIDED AND UNGUIDED FOOTPRINTS - SPS DEBOOST  $L/D = 0.357$

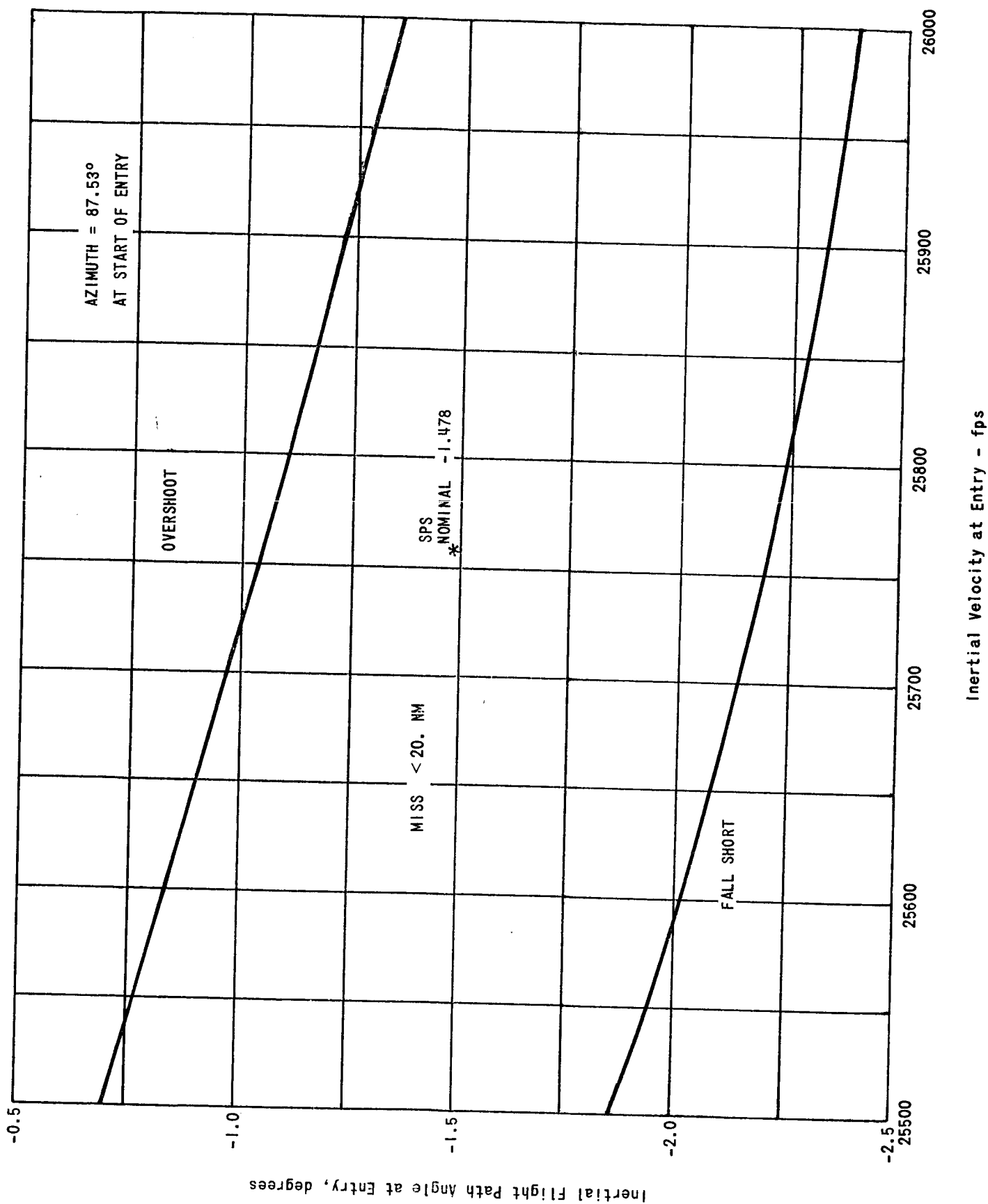


FIGURE 11 - EFFECT OF ENTRY VELOCITY AND FLIGHT PATH ANGLE ON GUIDANCE ACCURACY

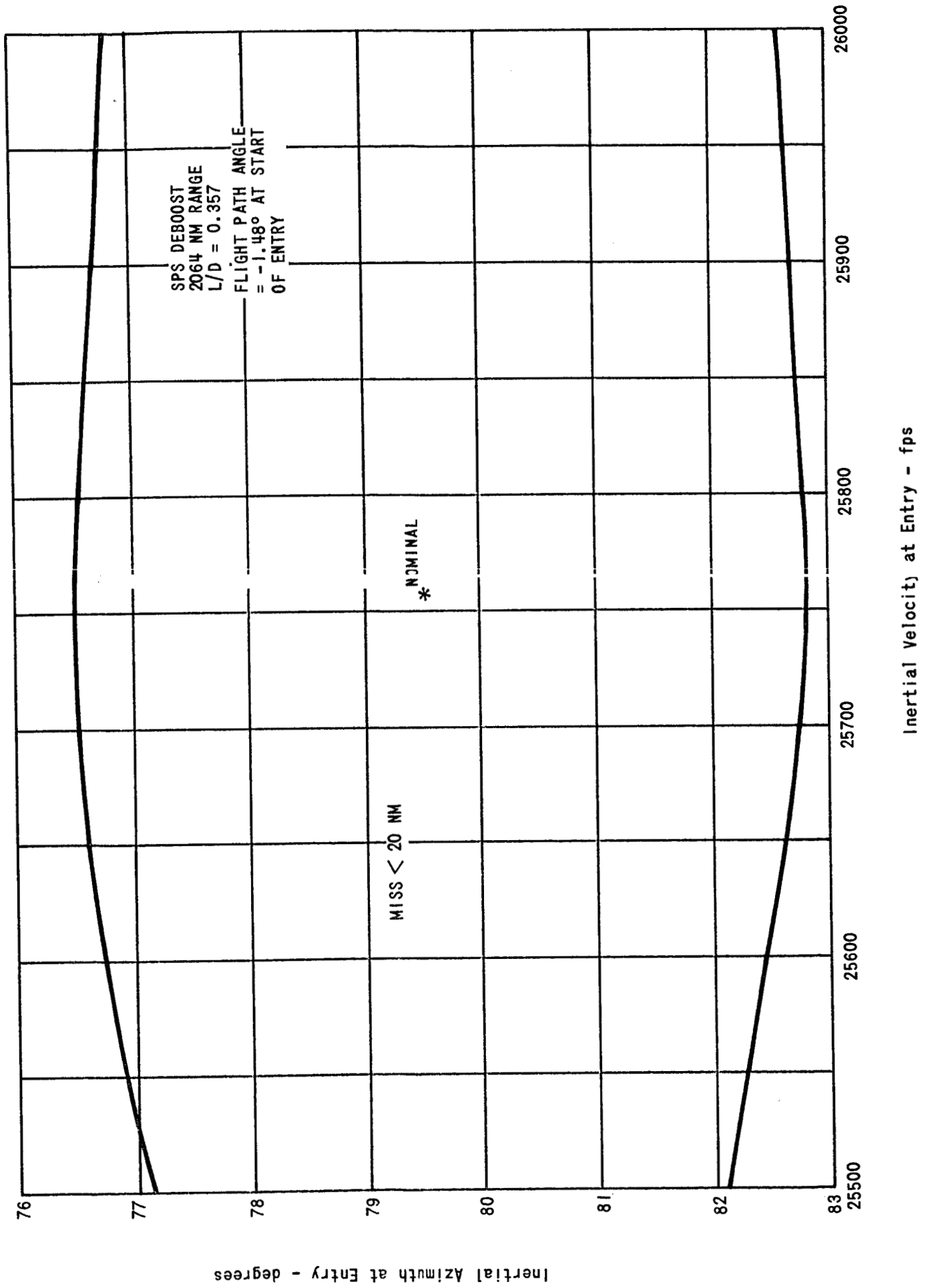


FIGURE 12 - ACCURATE GUIDANCE LIMITS IN FLIGHT PATH ANGLE AND AZIMUTH

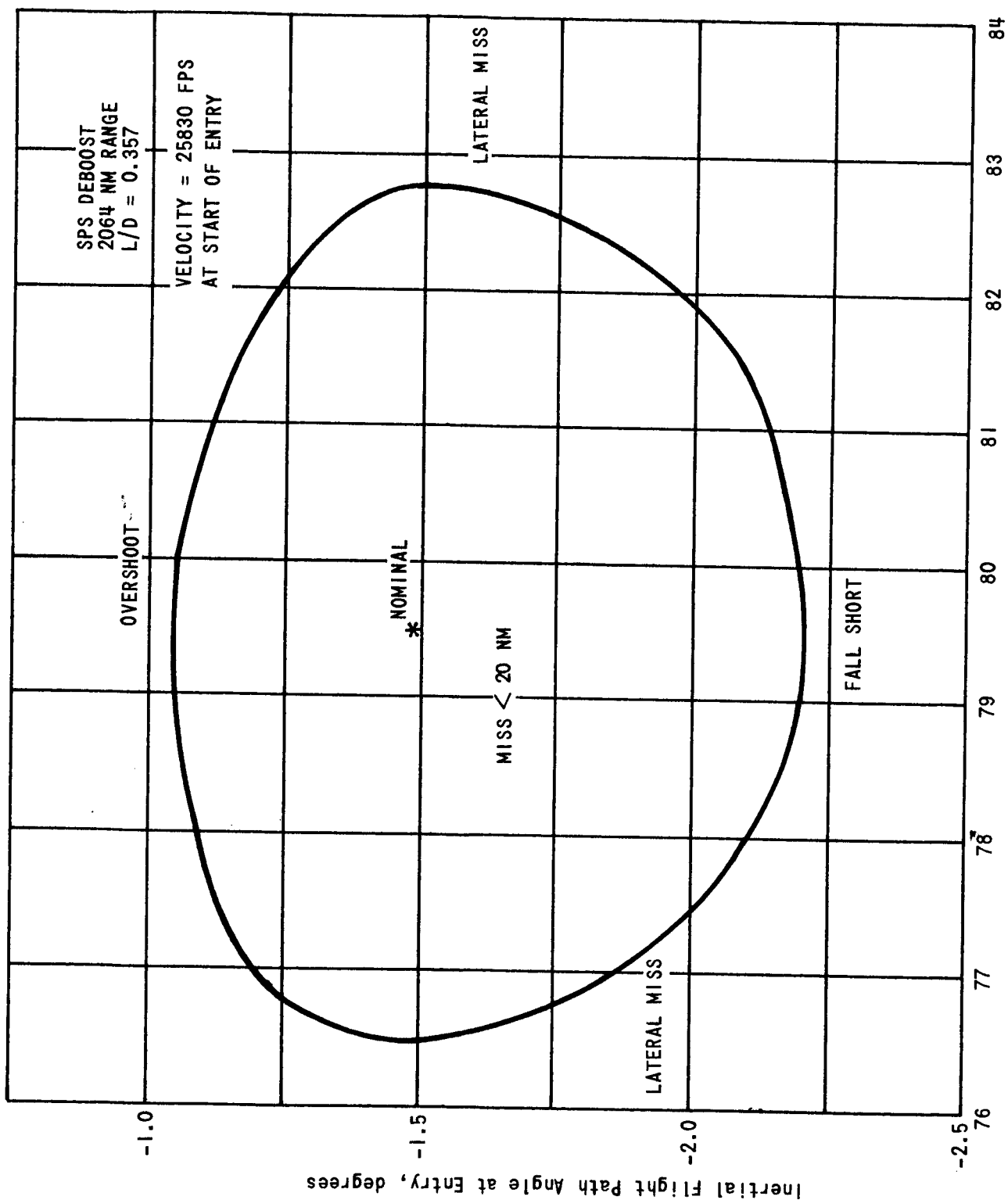


FIGURE 13 - ACCURATE GUIDANCE LIMITS IN AZIMUTH AND VELOCITY

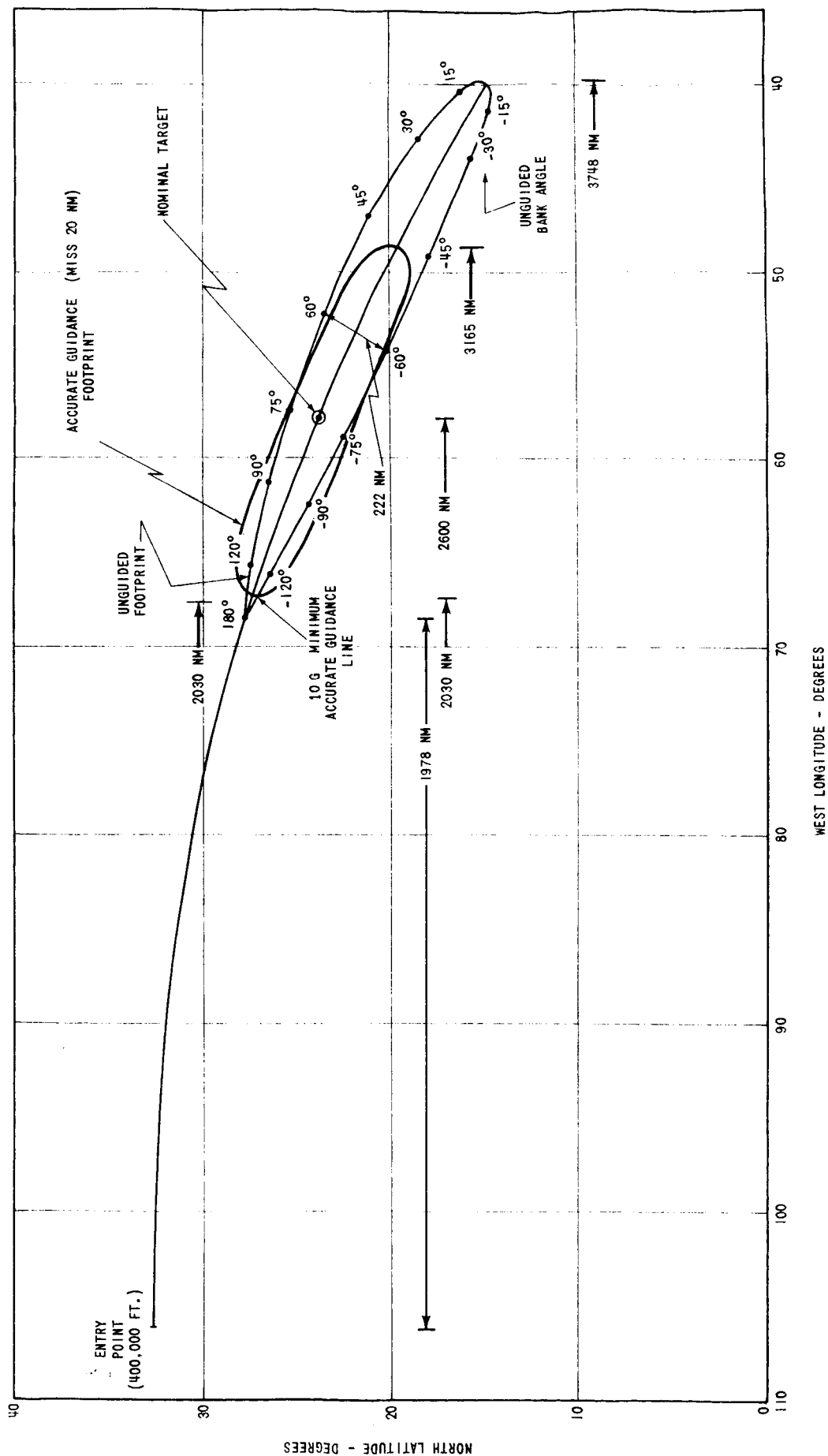


FIGURE 14 - AS-204 GUIDED AND UNGUIDED FOOTPRINTS - RCS DEBOOST L/D = 0.357

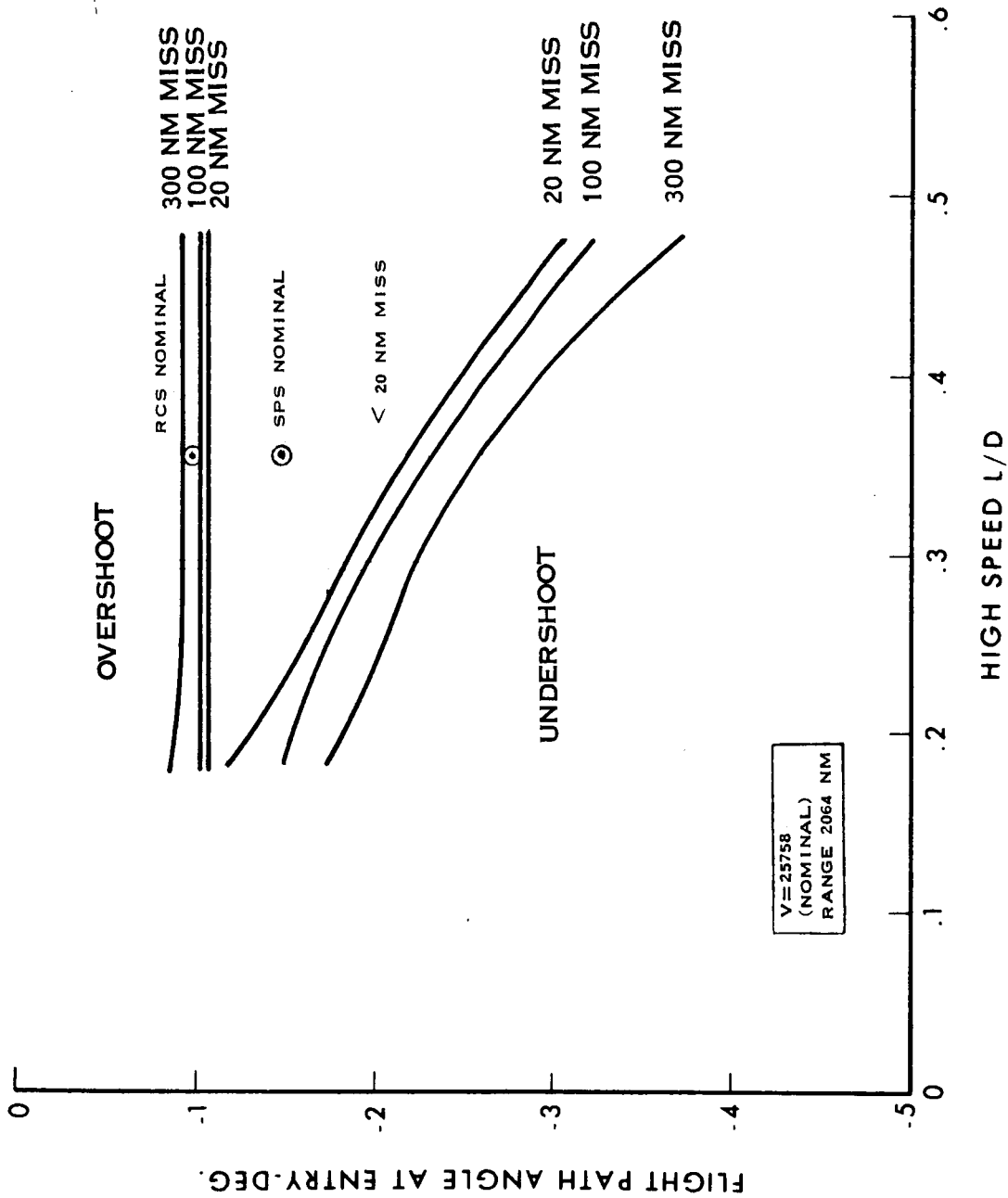


FIGURE I5 - L/D VS. FLIGHT PATH ANGLE



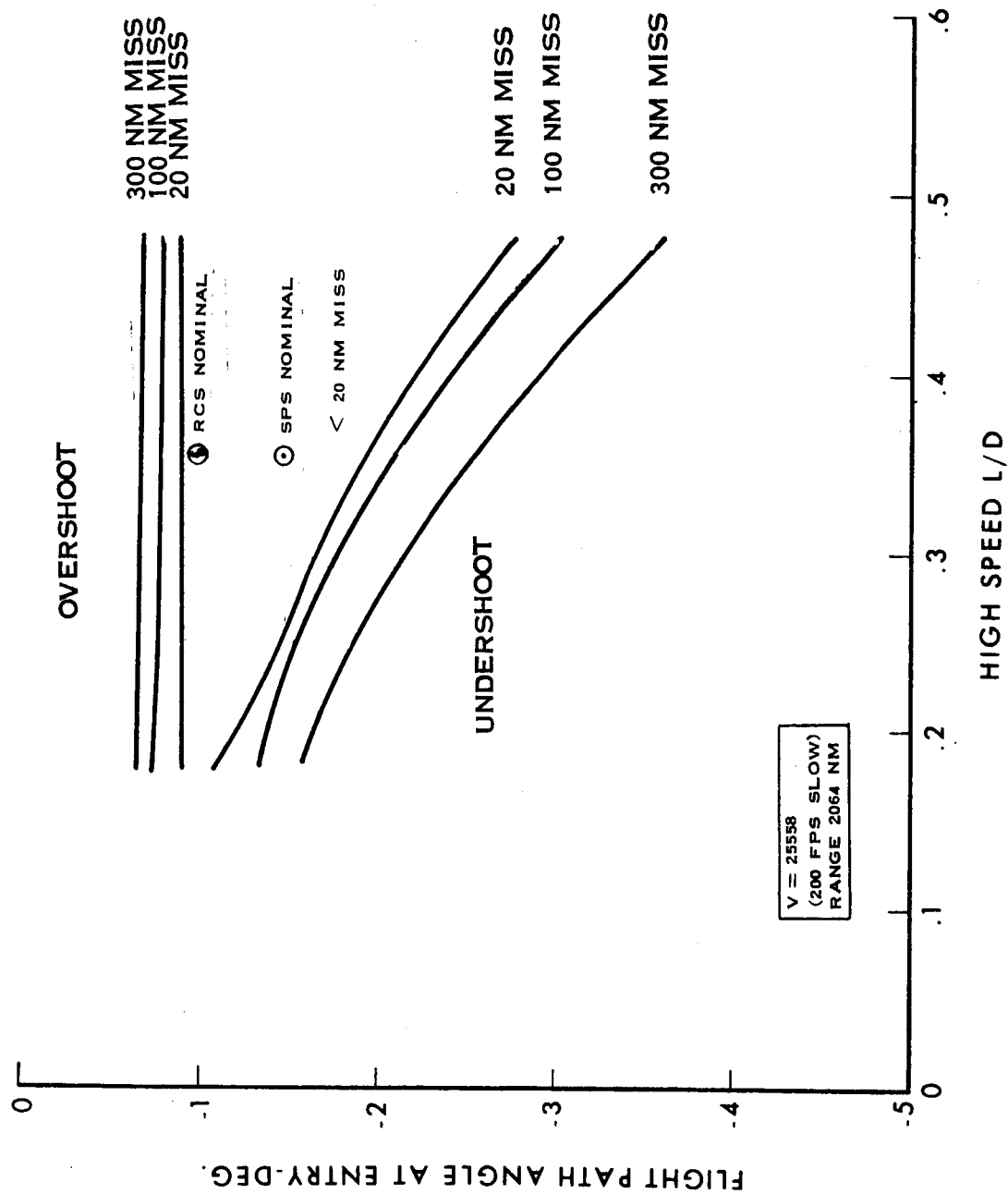


FIGURE 16 - L/D VS. FLIGHT PATH ANGLE

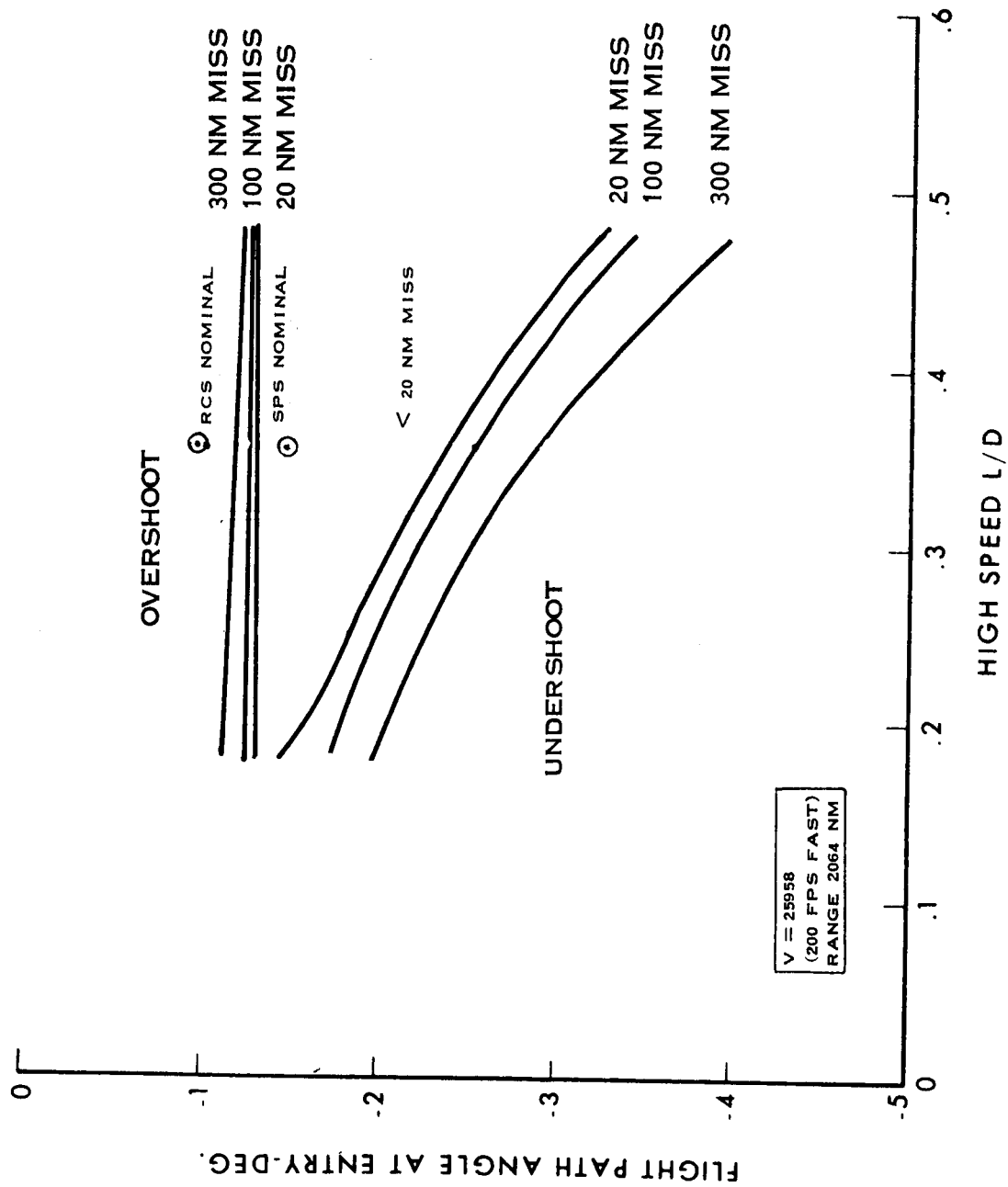


FIGURE 17 - L/D VS. FLIGHT PATH ANGLE

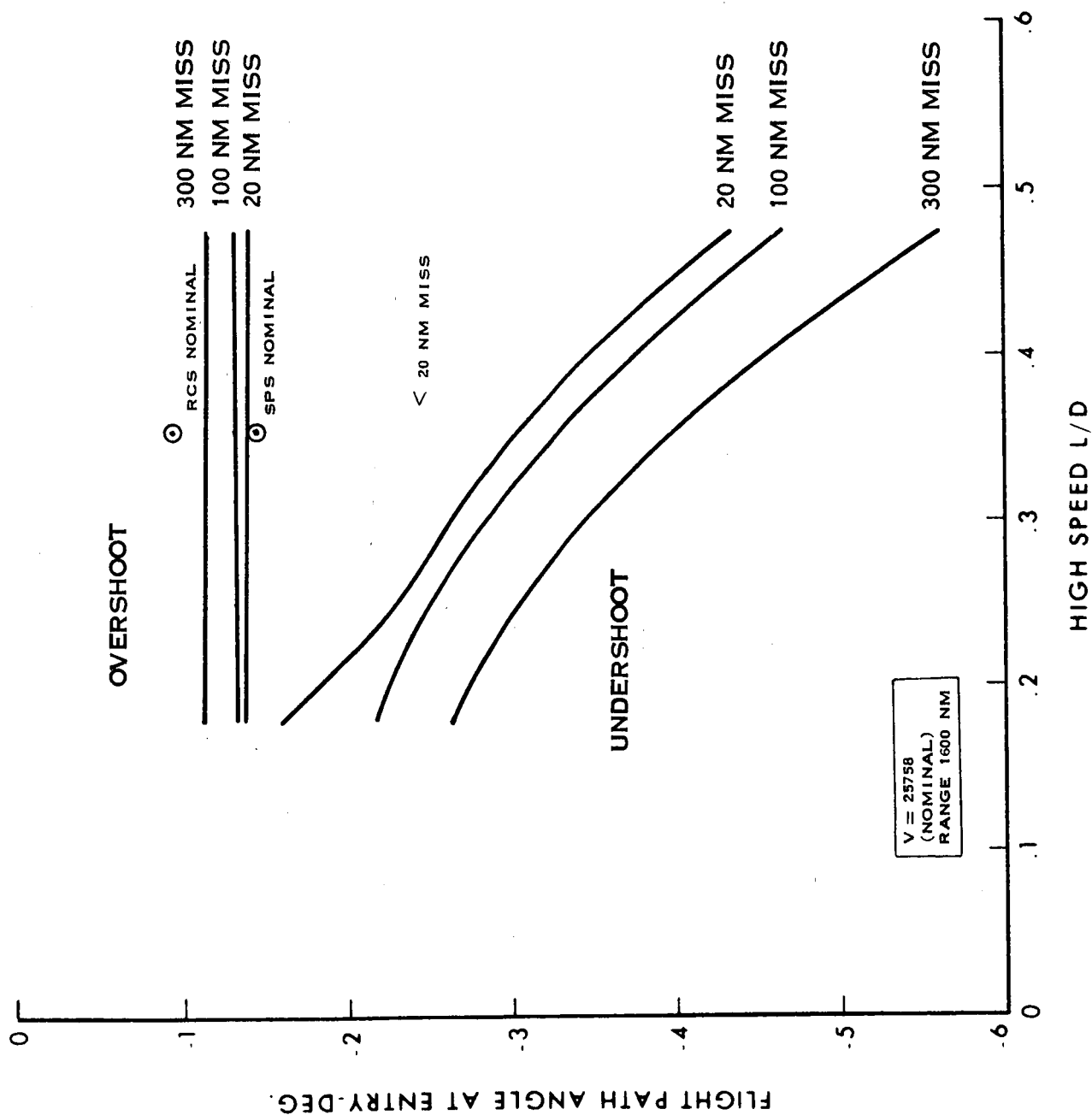


FIGURE 18 - L/D VS. FLIGHT PATH ANGLE

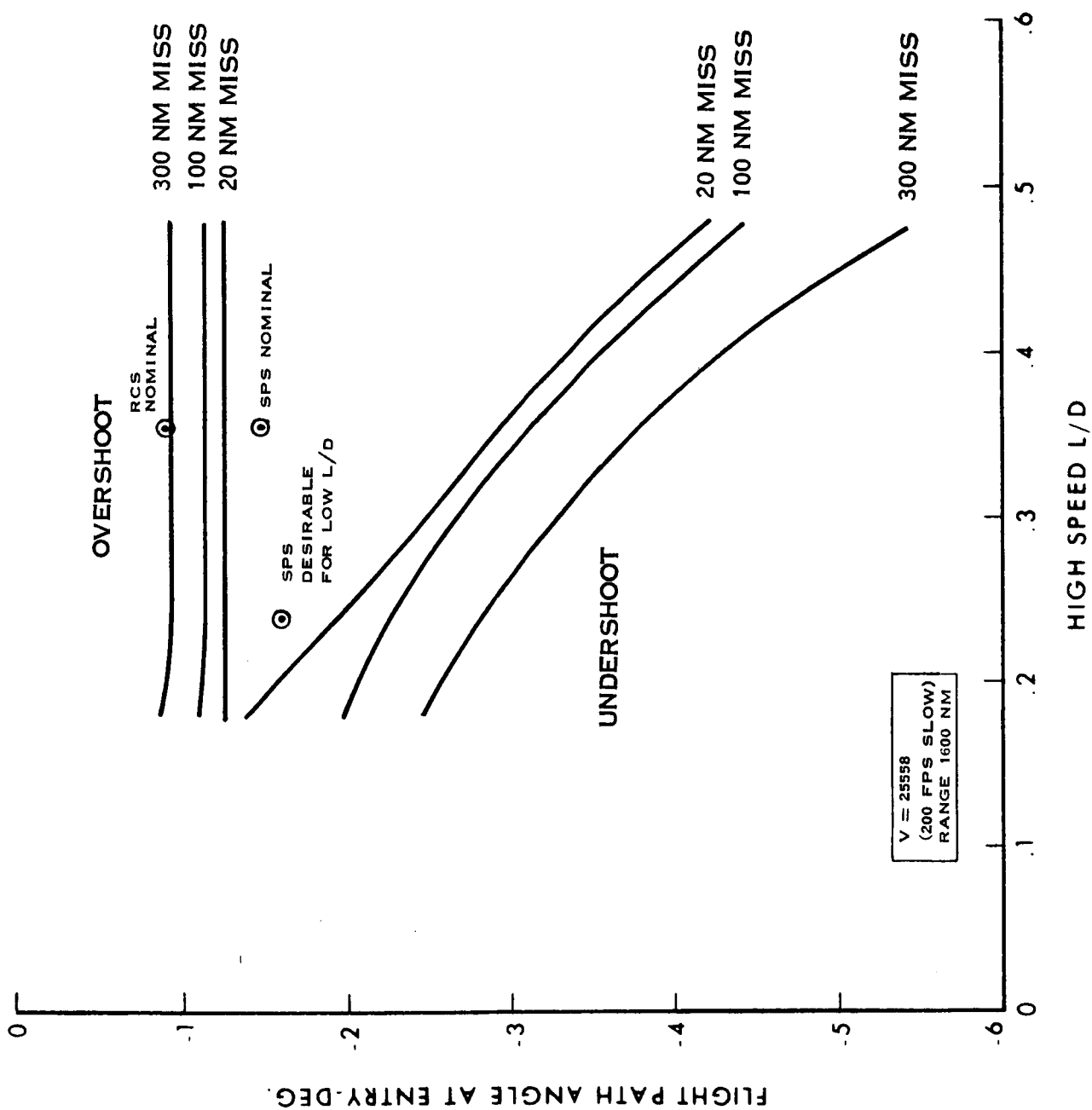


FIGURE I9 - L/D VS. FLIGHT PATH ANGLE

OVERSHOOT

⊙

RCS  
NOMINAL

300 NM MISS  
100 NM MISS  
20 NM MISS

SPS NOMINAL

UNDERSHOOT

20 NM MISS

100 NM MISS

300 NM MISS

V = 25958  
(200 FPS FAST)  
RANGE 1600 NM

FLIGHT PATH ANGLE AT ENTRY-DEG.

HIGH SPEED L/D

FIGURE 20 - L/D VS. FLIGHT PATH ANGLE

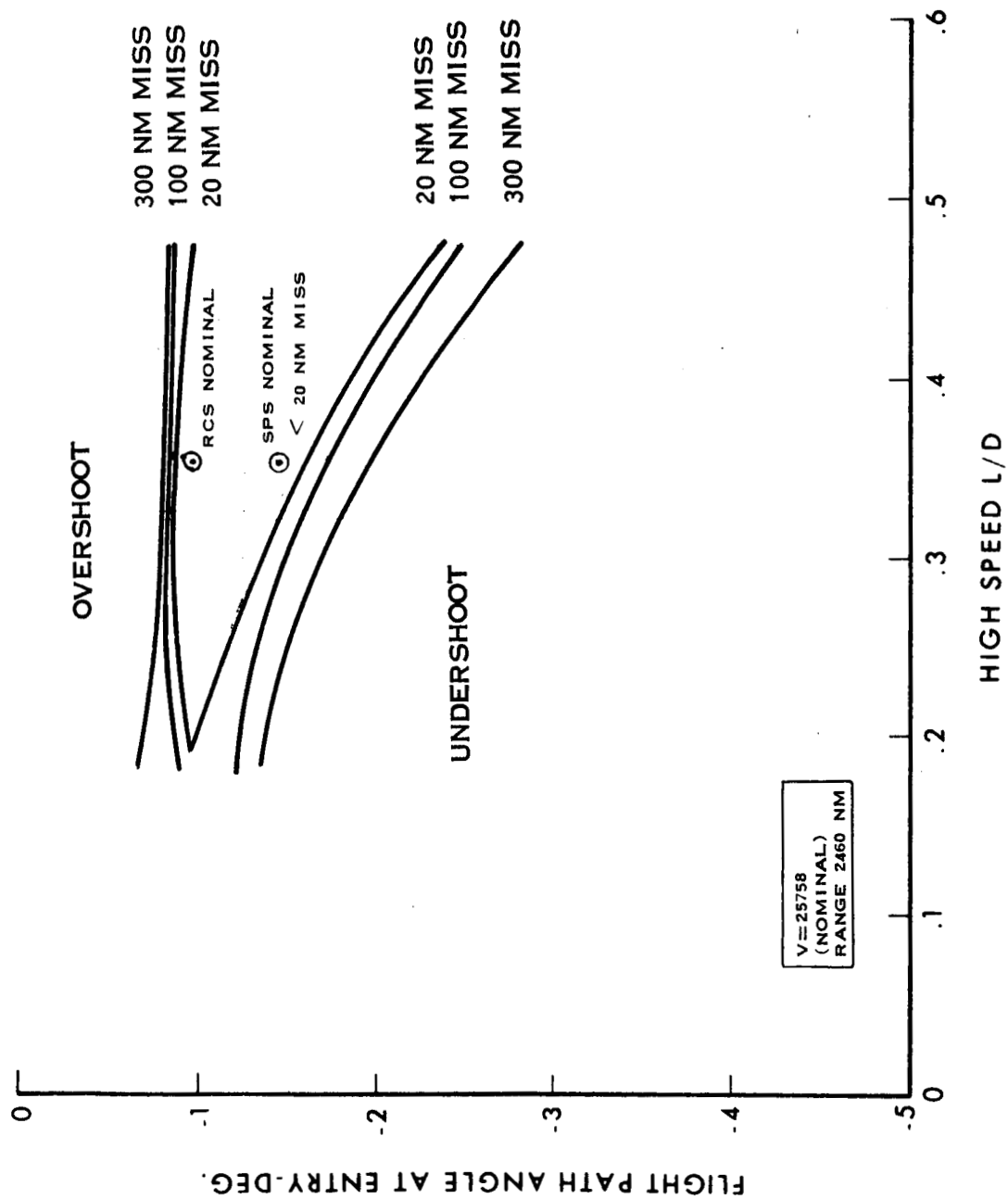


FIGURE 21 - L/D VS. FLIGHT PATH ANGLE

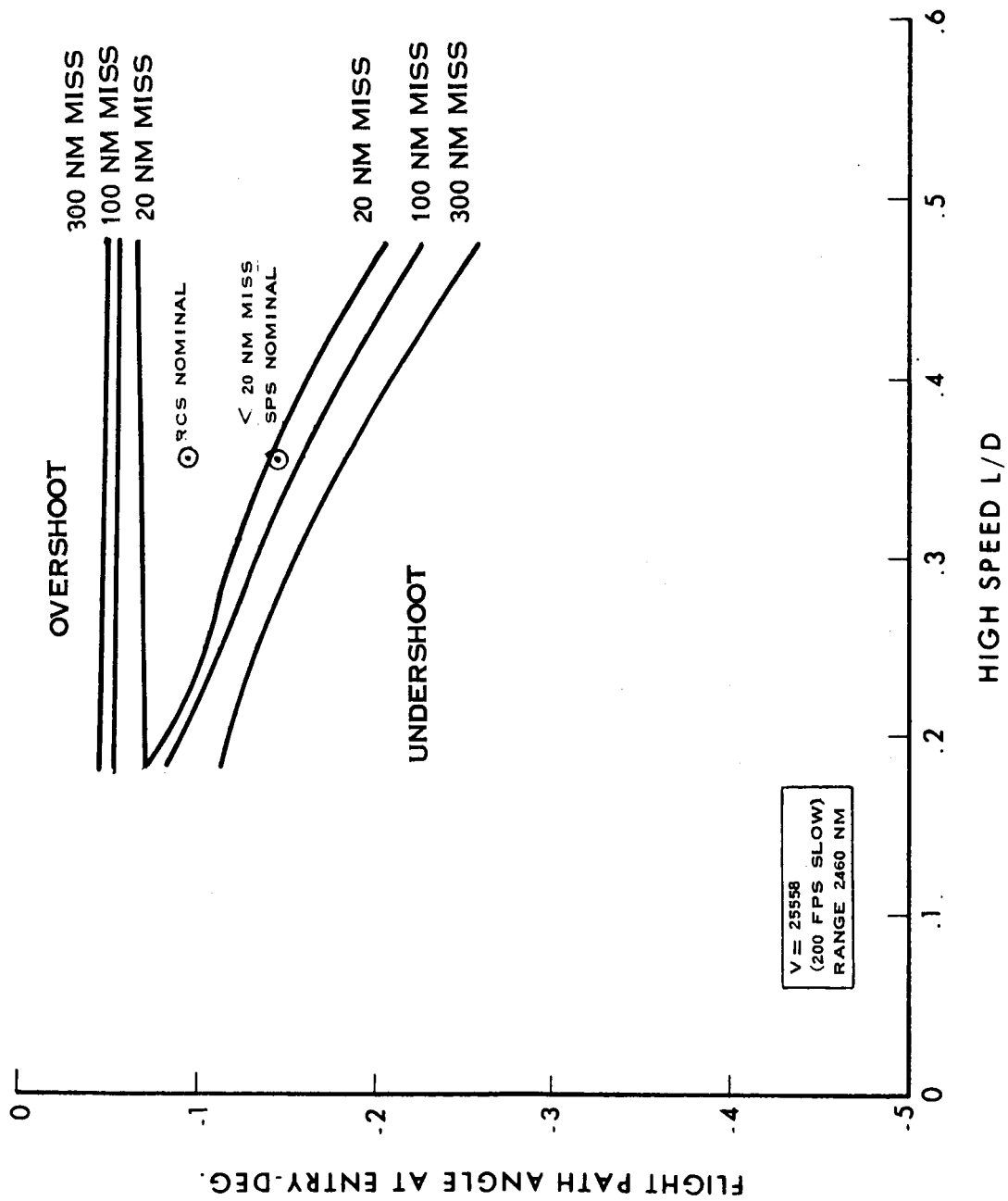


FIGURE 22 - L/D VS. FLIGHT PATH ANGLE

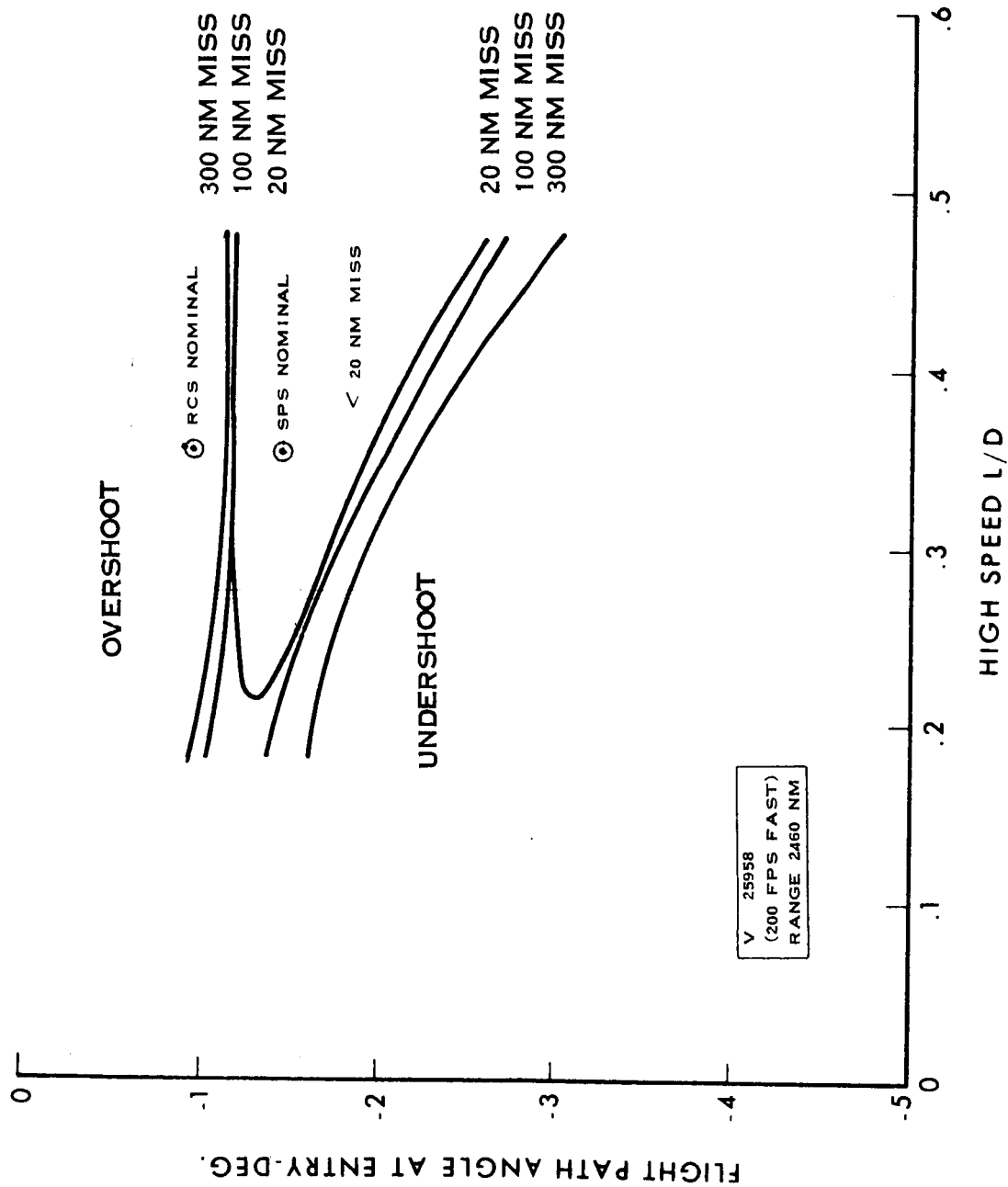


FIGURE 23 - L/D VS. FLIGHT PATH ANGLE



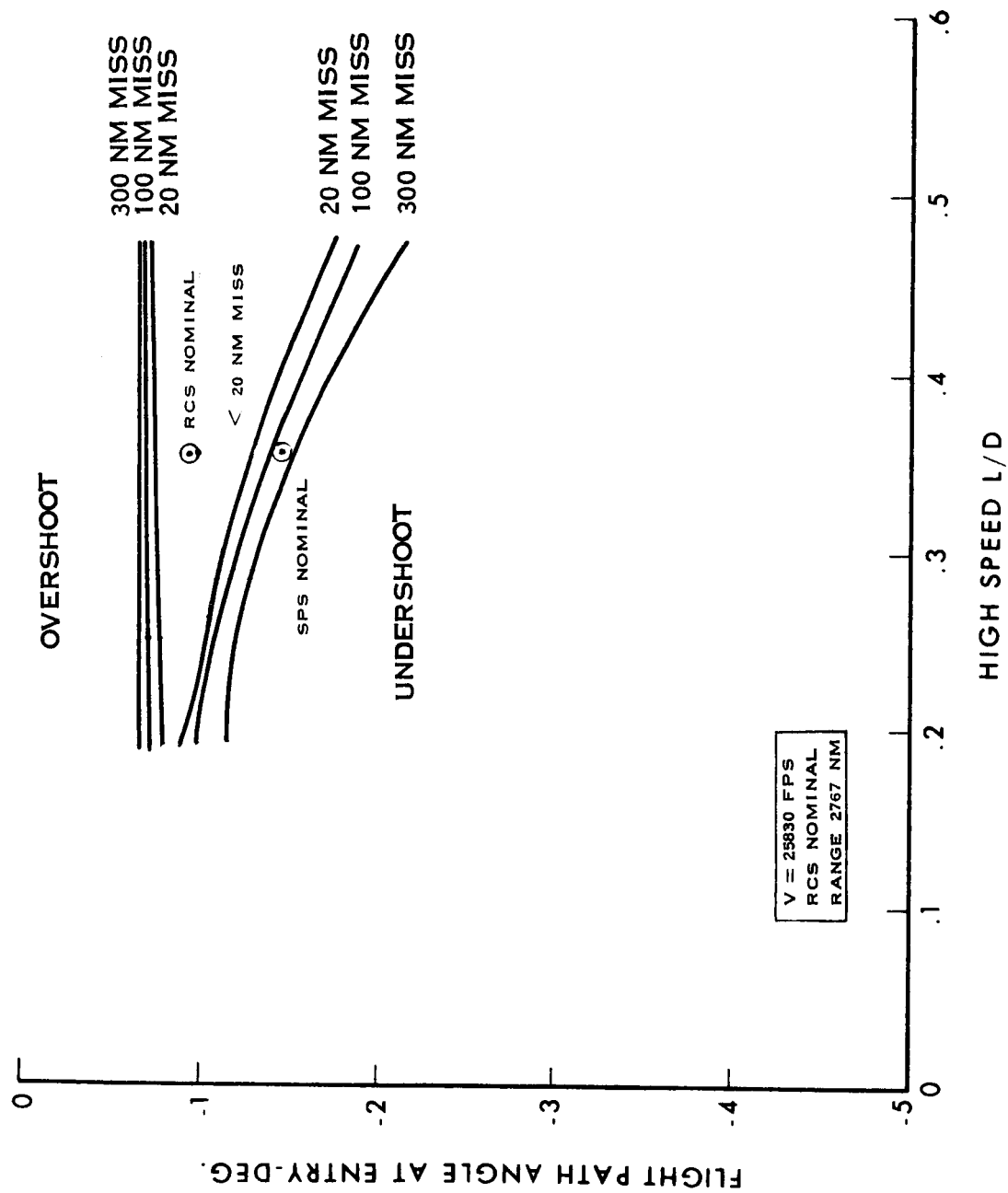


FIGURE 24 - L/D VS. FLIGHT PATH ANGLE

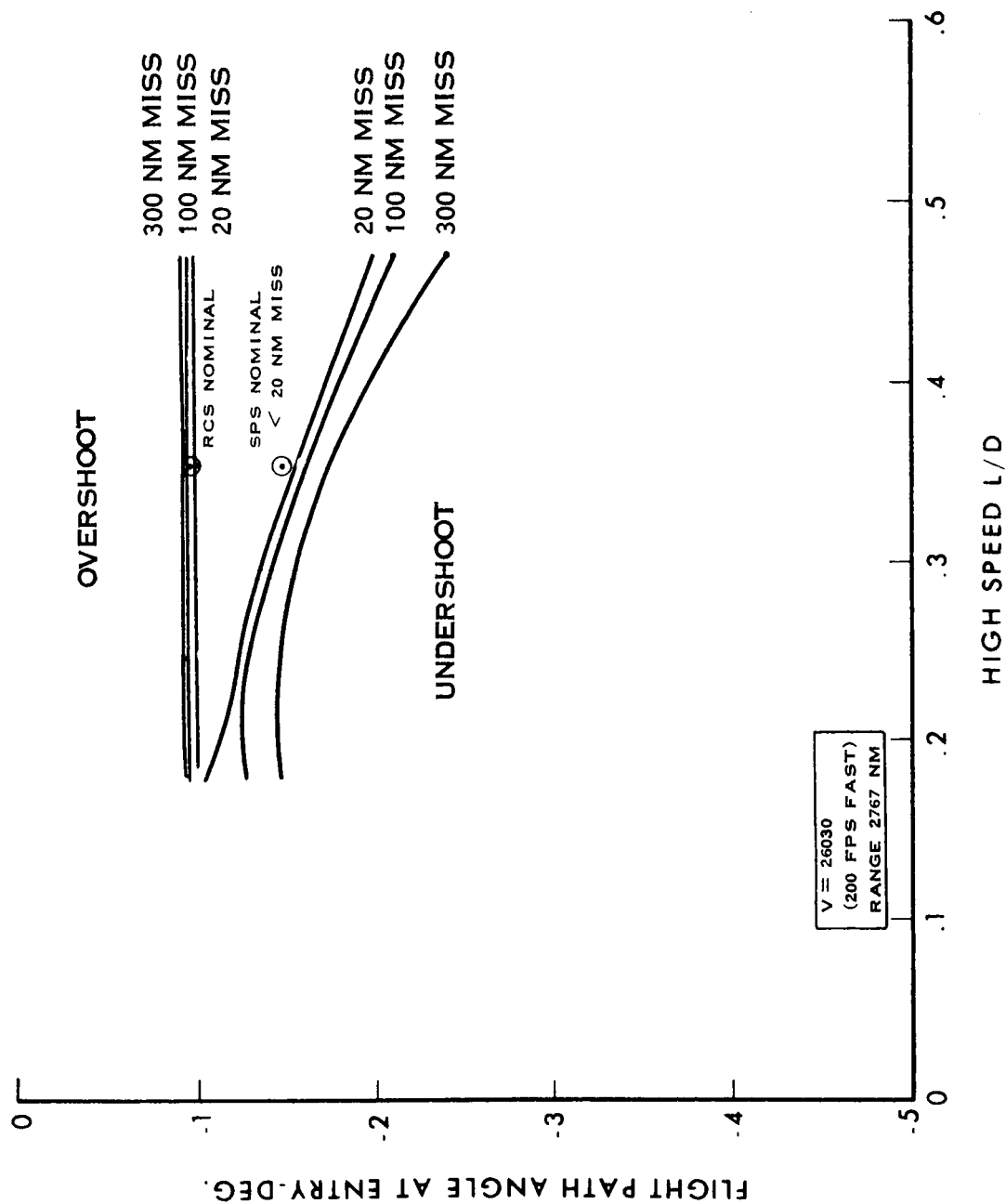


FIGURE 25 - L/D VS. FLIGHT PATH ANGLE

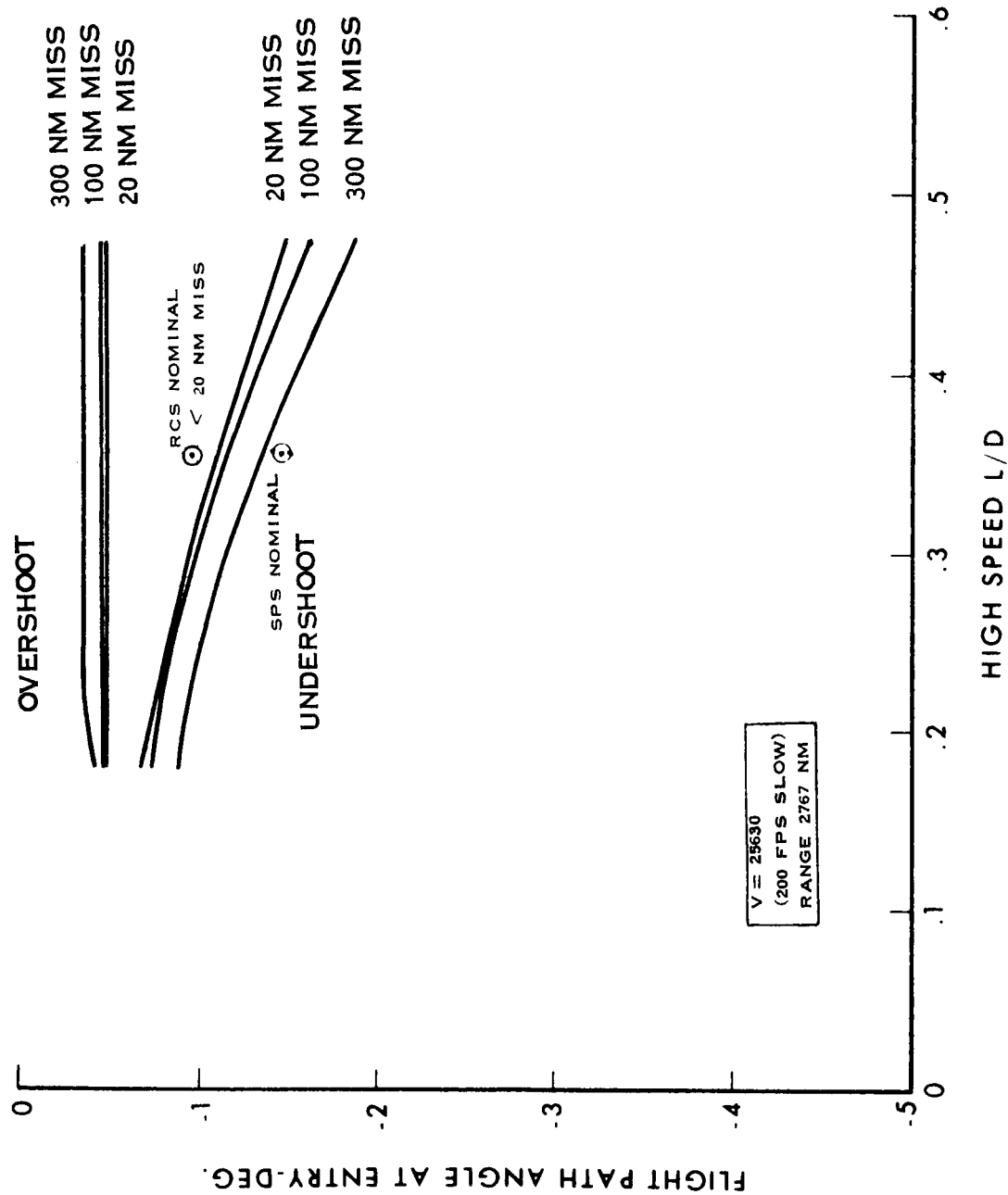


FIGURE 26 - L/D VS. FLIGHT PATH ANGLE

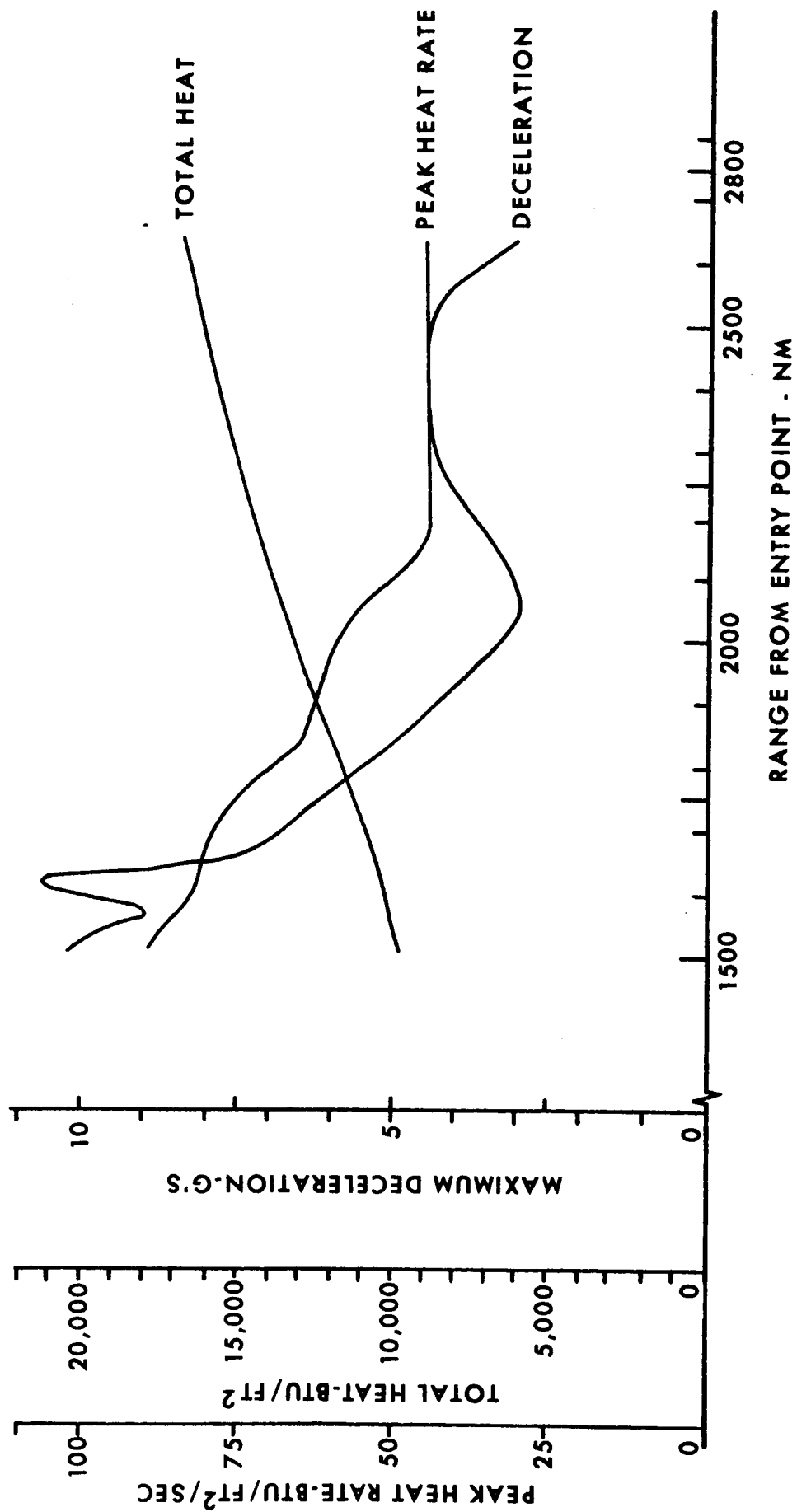


FIG. 27 EFFECT OF RANGE ON G'S AND HEATING

PANEL REVIEW BOARD  
 NASA-S-66-2364 MAR 14, 1966

# APOLLO FLIGHT REGIME ( TESTS )

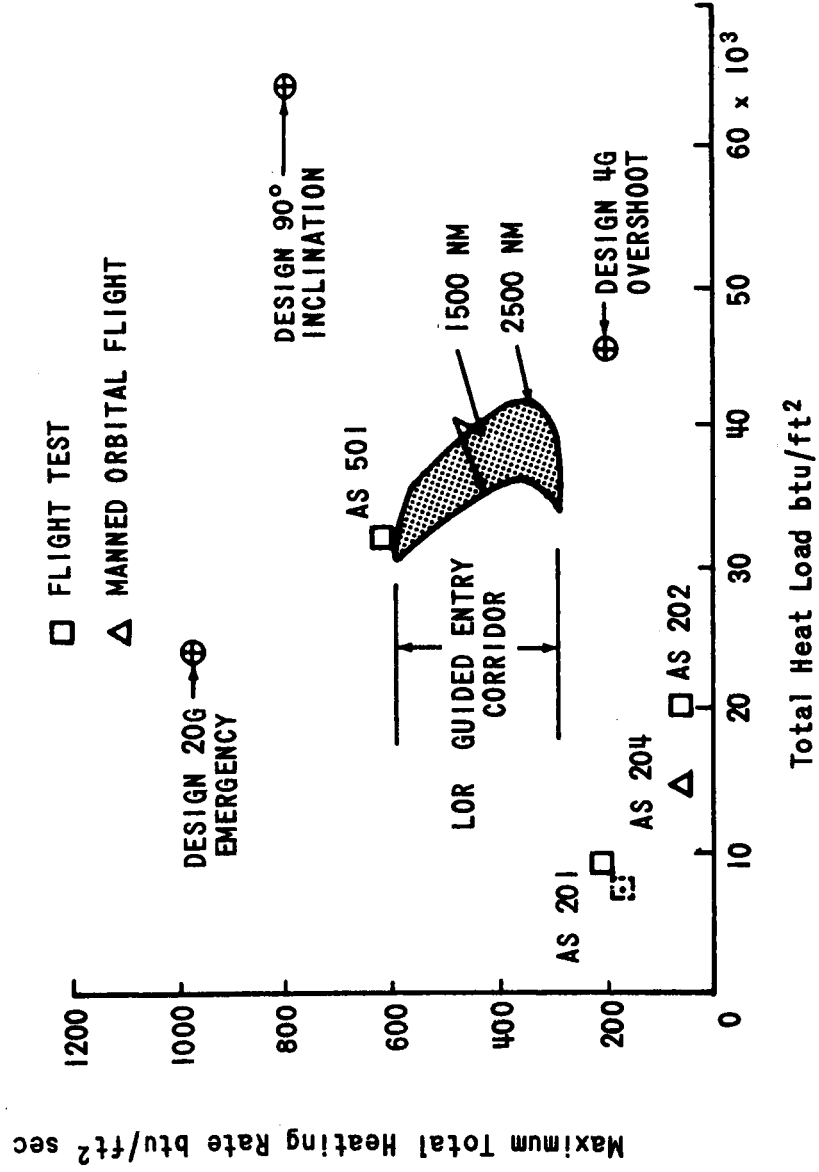
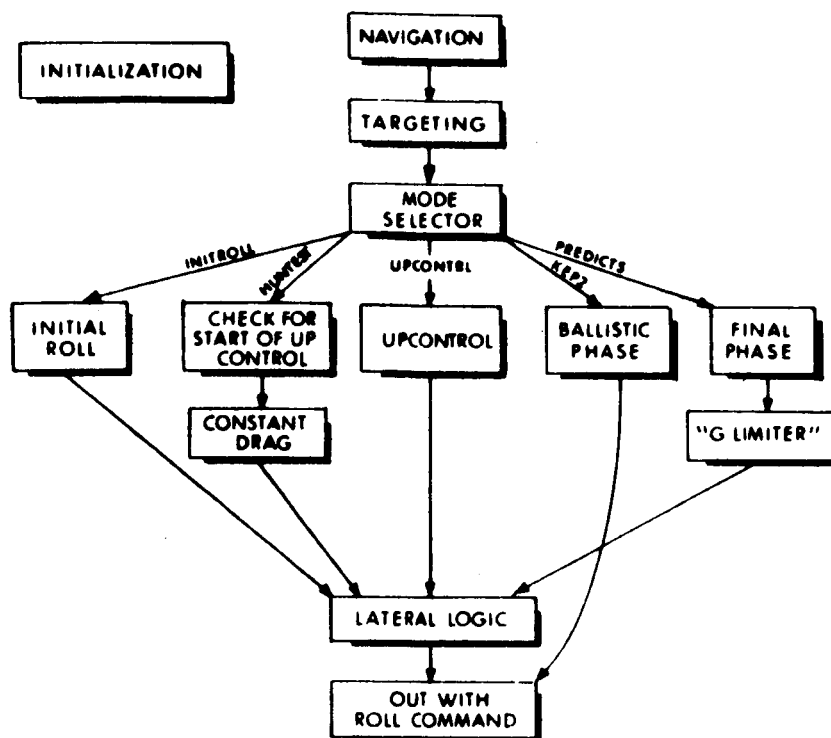


FIGURE 28 - HEAT RATE AND TOTAL HEAT FOR APOLLO HEAT SHIELDS



TRAJECTORY CONDITIONS USING SPS DEORBIT

PHASE	"ENTRY" ALTITUDE		BALLISTIC (.05 g)	FINAL PHASE	23500 FT ALTITUDE
Time (relative), sec.	0.	INITIAL ROLL,	176.	228.	710.8
Range to go nm	2064.		1322.	1102.	0.
Lateral miss nm	4.	CONSTANT DRAG,	5.	5.	.03
Altitude feet	400,000.		287,538.	257,102.	23,500.
Inertial velocity, fps	25,758.	UPCONTROL,	25,845.	25,704.	1419
Flight path angle, deg	-1.48		-1.37	-1.22	-17.8
Roll angle, deg	0.	NOT USED	0.	0.	264.1

TRAJECTORY CONDITIONS USING RCS DEORBIT

PHASE	"ENTRY" ALTITUDE		BALLISTIC	FINAL PHASE	25000 FT ALTITUDE
Time (relative), sec.	0.	INITIAL ROLL,	296.	378	881.2
Range to go nm	2767		1517	1170	0.
Lateral miss nm	-9	CONSTANT DRAG,	-5	-2	0.5
Altitude feet	400,000		287,198.	255,118.	23,500.
Inertial velocity, fps	25,830.	UPCONTROL,	25,883.	25,653.	1458.
Flight path angle, deg	-0.934		-0.77	-0.97	-17.4
Roll Angle, deg	164.8	NOT USED	164.8	15.20	-123.

FIGURE 29 - MIT ENTRY GUIDANCE - TRAJECTORY PHASES FLOW CHART

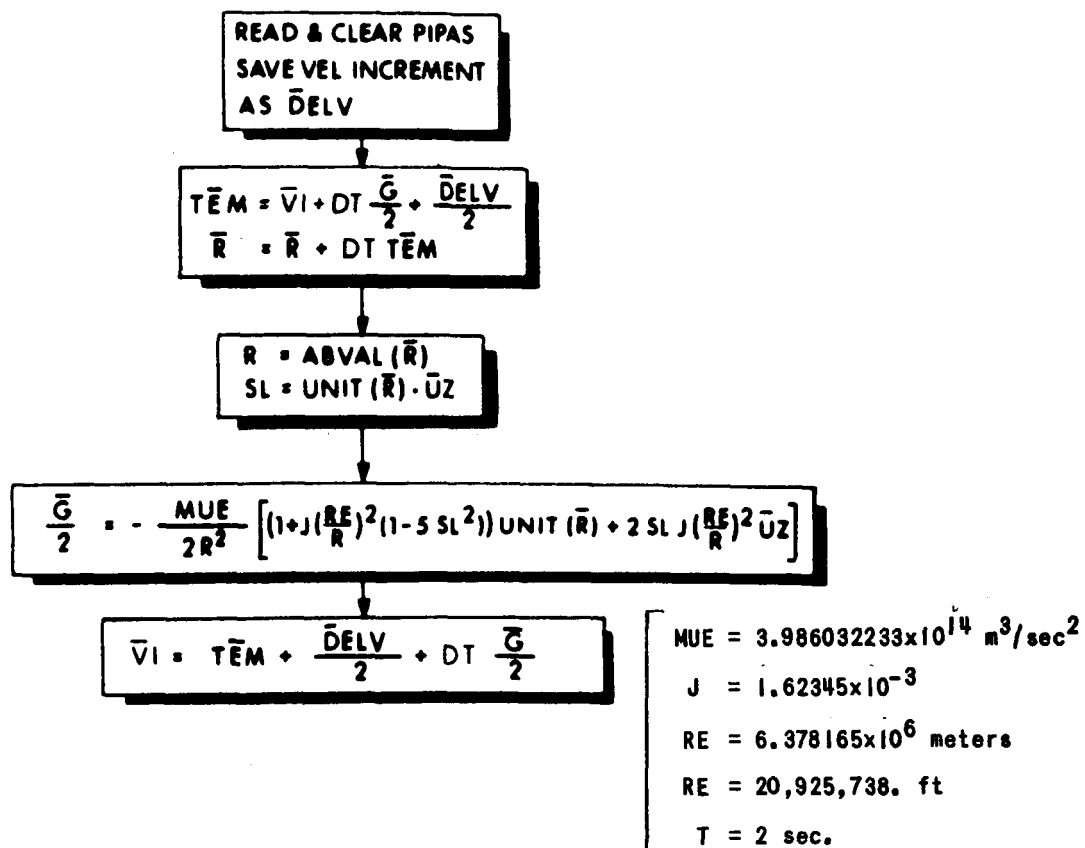


FIGURE 30 MIT AVERAGE G NAVIGATION FLOW CHART

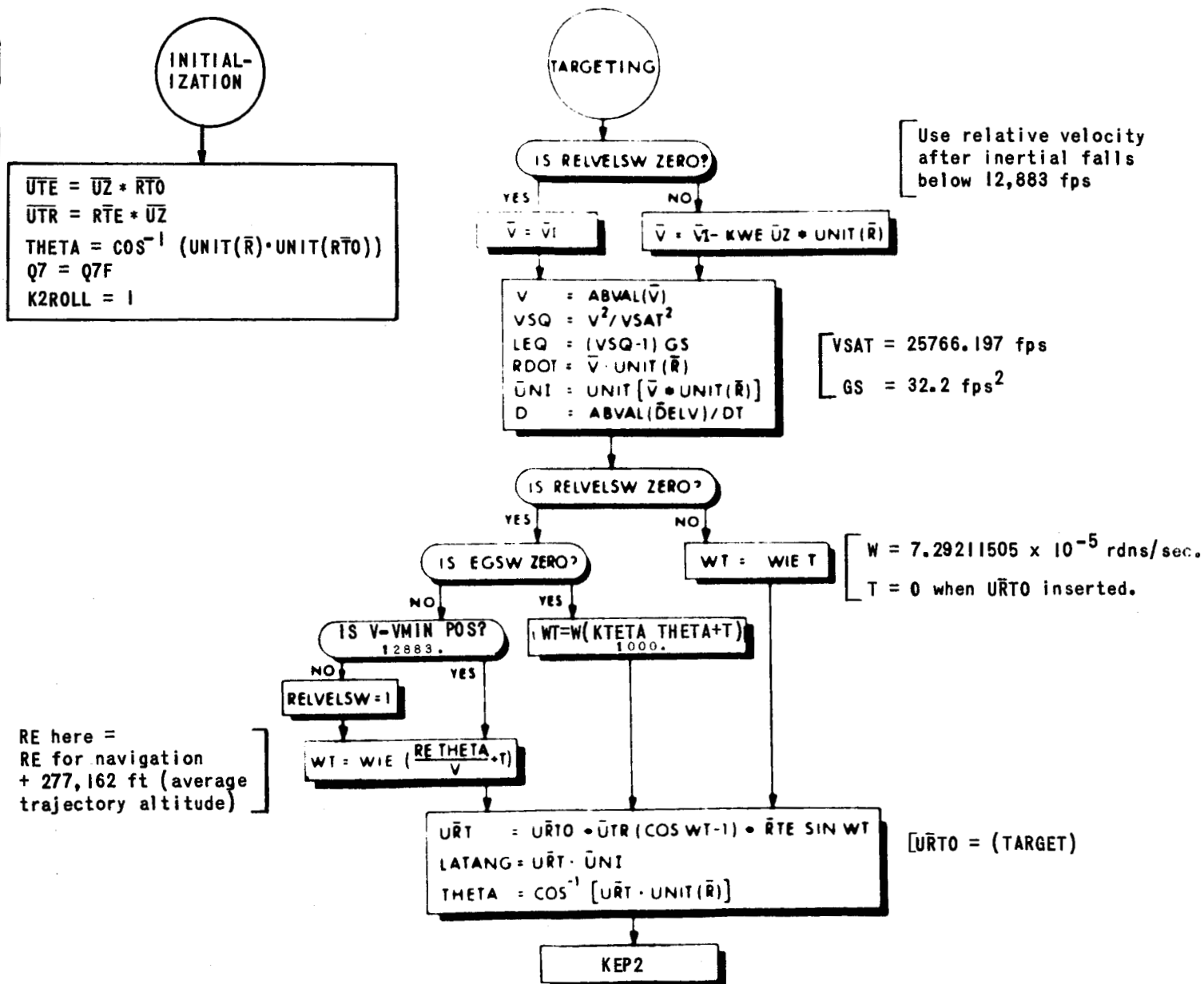


FIGURE 31 FLOW CHART - INITIALIZATION AND TARGETING COMPUTATIONS



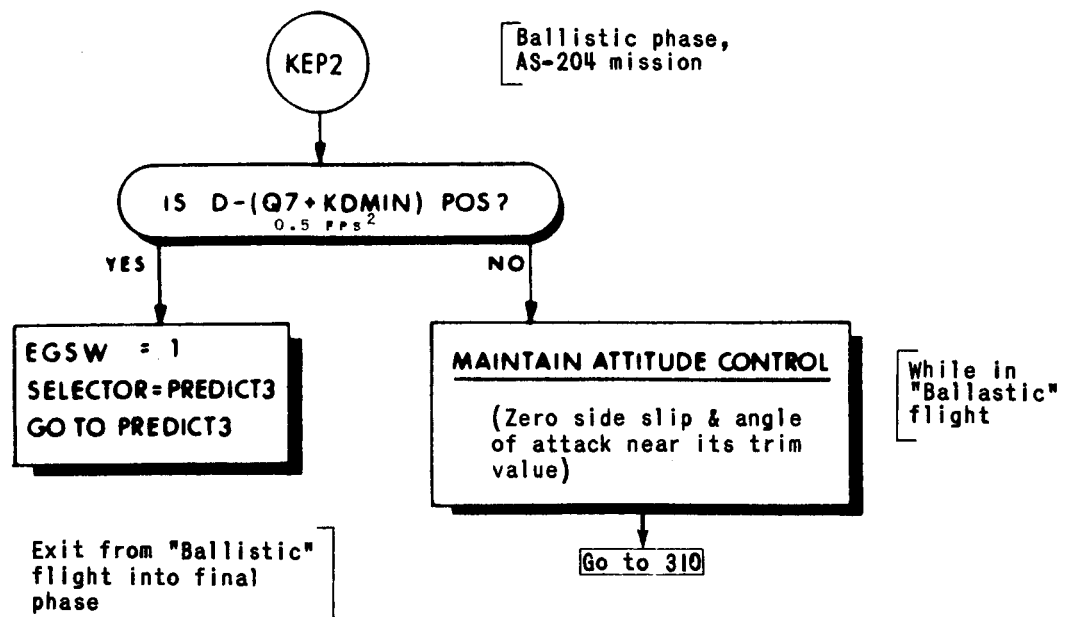


FIGURE 32 MIT FLOW CHART - BALLISTIC FLIGHT PHASE

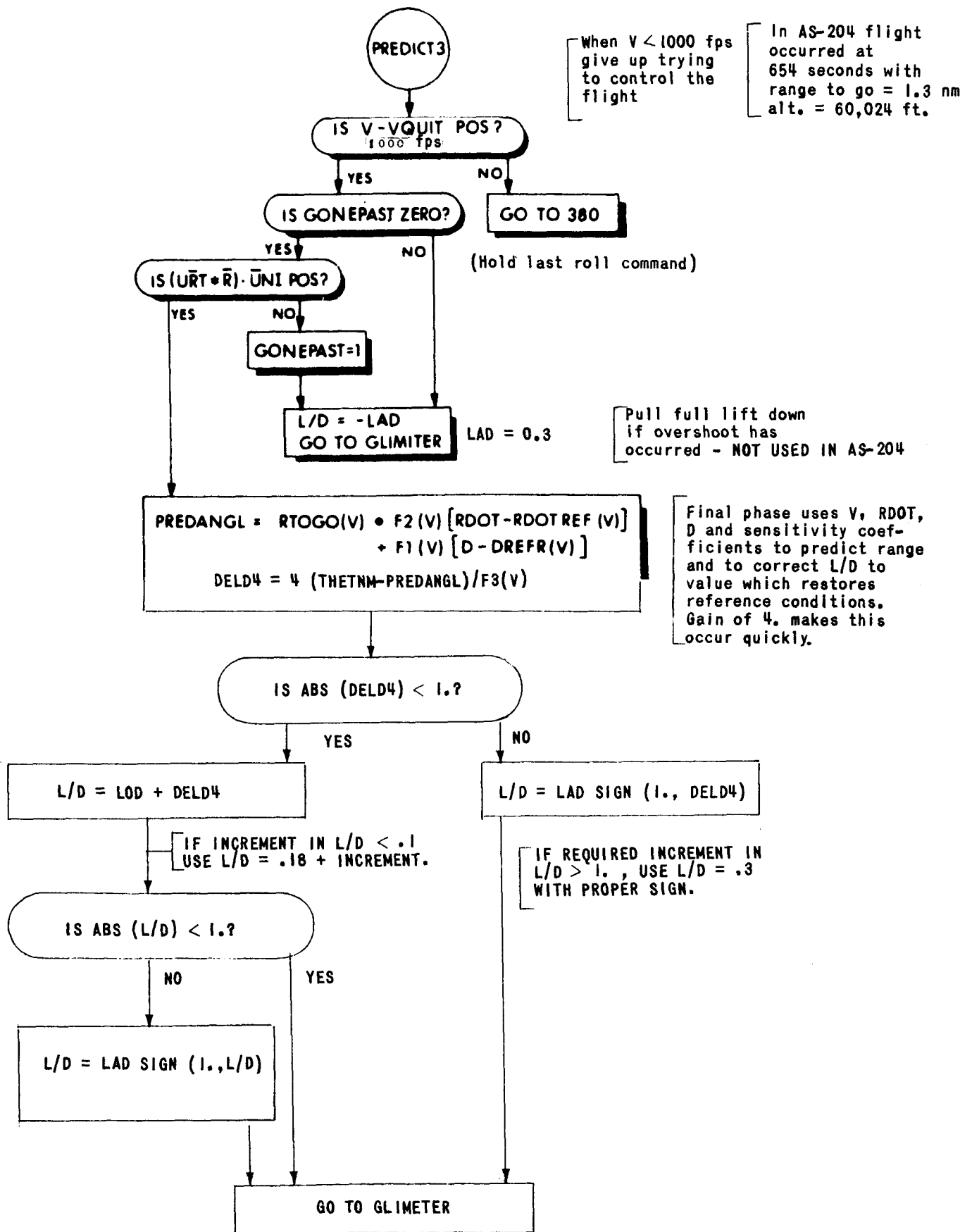


FIGURE 33 MIT FLOW CHART - FINAL PHASE

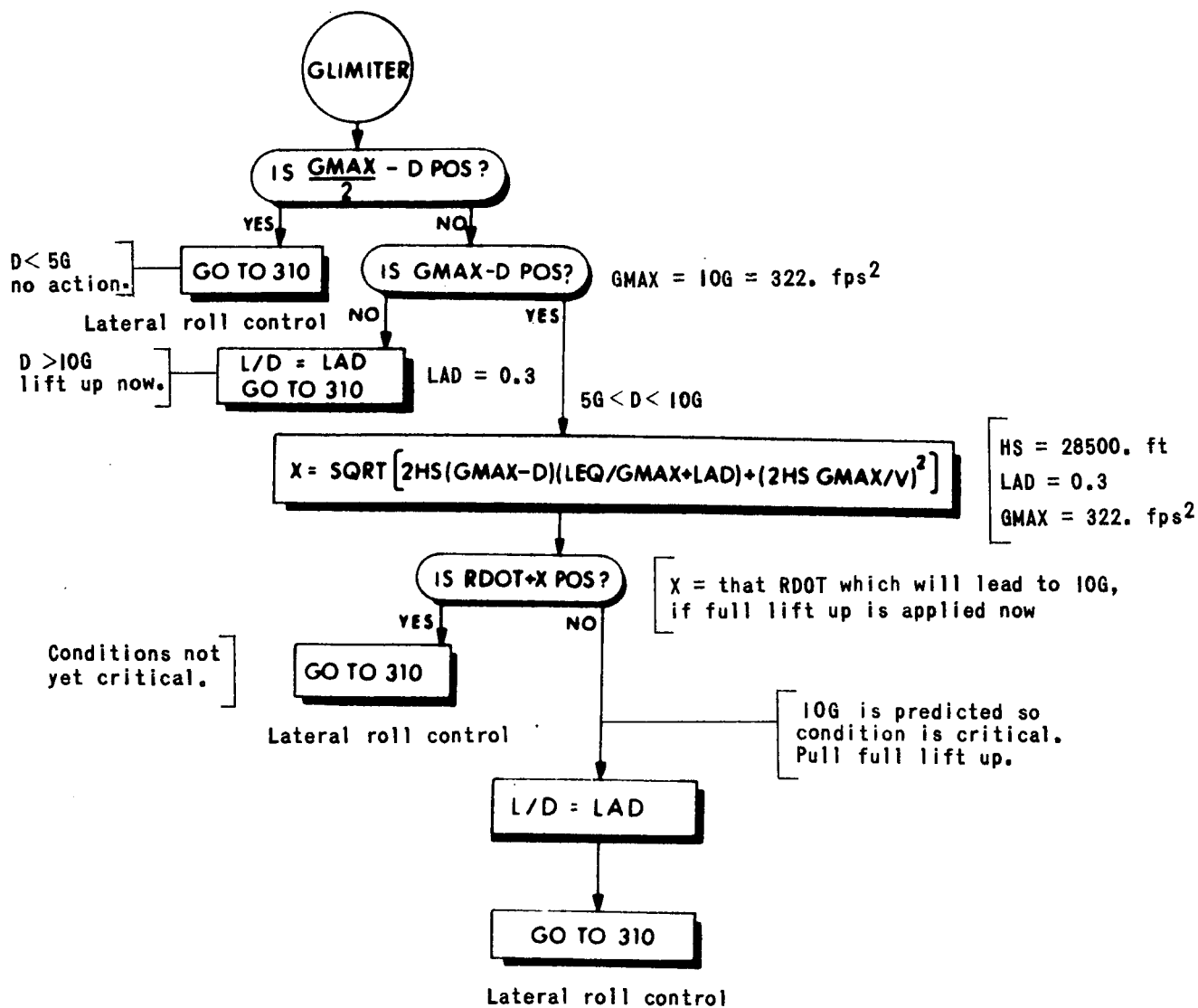


FIGURE 34 MIT FLOW CHART - G LIMITER CONTROL

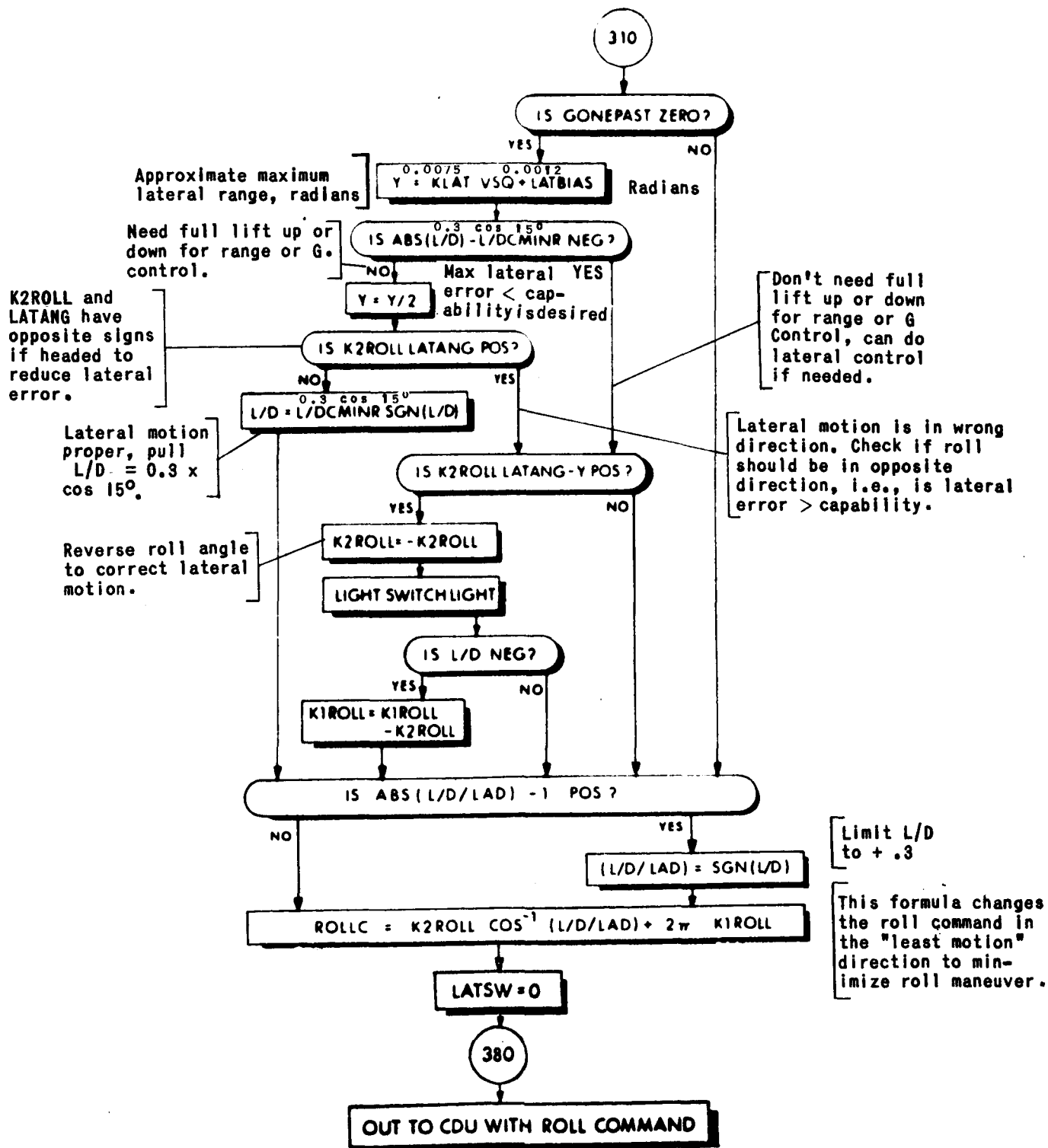


FIGURE 35 MIT FLOW CHART - LATERAL LOGIC

VREF	RDOTREF	DREFR	DR/DRDOT	DR/DA	RTOGO	DR/DL/D
FPS	FPS	FPSS	F2 NM/FPS	F1 NM/FPSS	NM	F3 NM
0*	-331	34.1	0	-.02695	0	1
337*	-331	34.1	0	-.02695	0	1
1080	-693	42.6	.002591	-.03629	2.7	6.44 x 2
2103	-719	60.	.003582	-.05551	8.9	10.91 x 2
3922	-694	81.5	.007039	-.09034	22.1	21.64 x 2
6295	-609	93.9	.01446	-.1410	46.3	48.35 x 2
8531	-493	98.5	.02479	-.1978	75.4	93.72 x 2
10101	-416	102.3	.03391	-.2372	99.9	141.1 x 2
14014	-352	118.7	.06139	-.3305	170.9	329.4
15951	-416	125.2	.07683	-.3605	210.3	465.5
18357	-566	120.4	.09982	-.4956	266.8	682.7
20829	-781	95.4	.1335	-.6483	344.3	980.5
23090	-927	28.1	.2175	-2.021	504.8	1385
23500	-820	6.4	.3046	-3.354	643.0	1508
35000	-820	6.4	.3046	-3.354	643.0	1508

\* INCLUDED IN FLIGHT PROGRAM BUT NOT NEEDED SINCE GUIDANCE STOPS FOR VELOCITY LESS THAN 1000 FPS

FIGURE 36 TABULAR DATA FOR FINAL PHASE COMPUTATIONS

# BELLCOMM. INC.

## APPENDIX A

### Coordinate Axes and Platform Alignment

#### Introduction

The navigation system uses two coordinate systems. One is a mean equinox and equator system with epoch as the nearest Besselian New Year, and the other the stable member coordinate system, aligned for ease of use of the Flight Director Attitude Indicator (FDAI) instrument and with consideration given to such matters as gimbal lock of the platform and accuracies of the individual gyroscopes and accelerometers mounted on the stable member. The calculation of the direction cosines between these two coordinate systems (MIT/IL calls the matrix of direction cosines REFSMAT) is of fundamental interest, and is considered in this appendix.

The first section shows how to calculate position and velocity vectors in a true equinox and equator system, given geodetic latitude, longitude, altitude, azimuth and the epoch for which they apply. The second section discusses nutation effects, showing how to convert position and velocity from true equinox and equator axes to mean equinox and equator axes (at the same epoch). The third section discusses precession, showing how to convert from mean equinox and equator axes at the given epoch to the reference inertial axes (which are the mean equinox and equator axes at the nearest Besselian New Year epoch, as noted above). The fourth section discusses universal and ephemeris time and the fifth section shows how platform alignment is computed, and gives sample calculations.

Since the Besselian New Year axes are to be used for missions which occur within a half year of the Besselian New Year, the sixth section shows how much this may affect navigation accuracy. These results are compared with the techniques to be used by MIT/IL [18] to determine true equator and equinox coordinates.

The distinction between true equator and equinox of present instant and mean equinox and equator at the Besselian New Year is important in two areas: (a) gravity, as affected by oblateness, requires knowledge of the direction of the true North Pole of the earth, (b) computations of longitude and latitude require true coordinates (plus Greenwich Hour Angle) for accurate computations.

## Appendix A

Position and Velocity in True Equator and Equinox Axes

Consider how  $\bar{R}$  and  $\bar{V}$  are determined given earth fixed position. Suppose the ignition position and velocity are given as geodetic latitude  $\phi$ , longitude  $\lambda$ , altitude  $H$ , velocity magnitude  $V$ , flight path angle  $\gamma$ , and azimuth East from true North  $\psi$ , where standard definitions [10] are used. Let the retrofire (and alignment epoch) Julian date of midnight be  $d$ , plus  $t$  seconds after midnight.

In a mean equinox system of date  $d$ , the Greenwich mean hour angle (the angle between the mean equinox of date  $d$  and the Greenwich meridian at  $0^h$  U.T.) is given by Newcomb's formula [13, p 75]: in terms of degrees with Jan 0.0, 1950 (J.D. 2433281.5) as the reference epoch, this formula is

$$\text{GMHA} = 99^\circ.08989513 + 0^\circ.9856473460d + 2^\circ.90151 \times 10^{-13} d^2$$

where  $d$  is the integral member of days since the reference epoch (and refers to  $0^h$  U.T. at the specified epoch).

To this must be added the rotational effect of the earth. Its sidereal (inertial) rate is given by

$$\omega = \frac{360}{86164.09972 + 0.0449 \times 10^{-6} d} \text{ deg/sec}$$

where  $d$  is as above. This formula can be given also in the form

$$\omega = (360.985608784 - 1.8811 \times 10^{-10} d) / 86400 \text{ deg/sec}$$

The sum of GMHA and  $\omega t$  is then the longitude between the mean equinox at  $0^h$  and Greenwich at  $t$ . Since latitude and longitude are referred to the true equator and pole, it is necessary to account for the difference between the mean equinox

## Appendix A

at  $O^h$  and the true equinox at  $t$ . This is caused by nutation (discussed later in this appendix) and by the motion of the mean equinox.

The motion of the mean equinox is closely approximated for short intervals by the angle  $m$  (discussed later). While the later discussion gives  $m$  on an annual basis (365.25 days) the daily rate is

$$m = 0^{\circ}.00003506 + 5^{\circ}.8089 \times 10^{-9} D \text{ deg/day}$$

where  $D = d/10^4$  and  $d$  is measured from 1950.0 (J.D. 2433281.5). Since the motion of the mean equinox is retrograde, the value for  $m$  for the fractional part of the day should be added to the GMHA computed from the above formula.

The difference in right ascension between the mean and true equinox is the "equation of the equinoxes", also discussed later. It can be computed, but is best found by interpolation (for the fractional part of the day required) between values found in the American Ephemeris (Universal and Sidereal Time Table). The value found also should be added to GMHA.

The result of these two corrections may be called GTHA, Greenwich True Hour Angle.

The GTHA being known, the formulas to be used to compute the position and velocity in true equinox coordinates with epoch  $d$  and  $t$  are as follows:

Coordinates of the sub-vehicle point in the local meridian plane

$$u = a[1 + (b \tan \phi/a)^2]^{-1/2}$$

$$v = u(b/a)^2 \tan \phi$$

where  $a$  and  $b$  are the major and minor axes of the reference earth ellipsoid. [9]



## Appendix A

Coordinates of the vehicle in the local meridian plane

$$w = u + H \cos \phi \qquad z = v + h \sin \phi$$

Coordinates of the vehicle in the equatorial plane

$$x = w \cos (\lambda + \omega t + GTHA)$$

$$y = w \sin (\lambda + \omega t + GTHA)$$

The vector position  $\bar{R}_{d,t}$  is the triad (x,y,z).

Direction cosines between up, East, North axes at the vehicle position and true equinox axes of d,t

	UP	EAST	NORTH
X			
M = Y	Unit( $\bar{R}_{d,t}$ )	Unit( $\overline{\text{North Pole}} \times \bar{R}_{d,t}$ )	$\bar{U}_p \times \bar{E}_{ast}$
Z			

where  $\overline{\text{North Pole}} = (0,0,1)$

Then the velocity vector  $\bar{V}_{d,t}$  is given by

$$\bar{V}_{d,t} = M \begin{bmatrix} V \sin \gamma \\ V \cos \gamma \sin \psi \\ V \cos \gamma \cos \psi \end{bmatrix}$$

## Appendix A

Note that the position calculation places the altitude along the zenith ray, which is perpendicular to the reference ellipsoid at the sub-vehicle point: horizontal then means tangent to the reference ellipsoid, not perpendicular to the radius vector. Conversely, horizontal for velocity does mean perpendicular to the radius vector, and does not involve the ellipsoid. This inconsistency is part of the standards.

Nutation

Nutation is the somewhat irregular circular motion of the true pole about the mean pole, and has a period of about 18.6 years and an amplitude of about 9".21. It depends a great deal upon the longitude of the node of the Moon's orbit, which has the period and amplitude noted.

Nutation effects are described by three angles,  $\Delta\psi$  the nutation in longitude,  $\Delta\epsilon$  the nutation in obliquity and  $\epsilon$  the obliquity angle (see Figure A-1). The Astronomical Ephemeris [11] (or other ephemerides, such as the JPL tapes used as Apollo Program Standards) lists  $\Delta\psi$  in the Sun tables, gives  $\Delta\psi \cos \epsilon$  (the "equation of the equinoxes", or nutation in right ascension) in the Universal and Sidereal Time tables. The computation of  $\Delta\psi$  and  $\Delta\epsilon$  involves five angles ( $\ell, \ell', F, D, \Omega$ ) and is of the form

$$\Delta\psi = \sum_i (a_i + b_i T) \sin (c_i \ell + d_i \ell' + e_i F + f_i D + g_i \Omega)$$

$$\Delta\epsilon = \sum_i (a'_i + b'_i T) \cos (c_i \ell + d_i \ell' + e_i F + f_i D + g_i \Omega)$$

where T is the number of Julian centuries since 1900, and a, a', b, b', c, d, e, f, g are coefficients given in table 2.5 of reference 13. Formulas for  $\ell, \ell', F, D, \Omega$  are given there. The obliquity angle formula is as given above.

These nutation terms involve both long period terms and short period terms, with the shortest period being some 5.5 days. Perusal of the tables cited show the day to day variation in  $\Delta\psi$  to be less than 0".2, and of  $\Delta\epsilon$  to be less than 0".05.

## Appendix A

The matrix of direction cosines to be used is

	$X_m$	$Y_m$	$Z_m$
$X_T$	1	$-\Delta\psi \cos \epsilon$	$-\Delta\psi \sin \epsilon$
$N = Y_T$	$+\Delta\psi \cos \epsilon$	1	$-\Delta\epsilon$
$Z_T$	$+\Delta\psi \sin \epsilon$	$+\Delta\epsilon$	1

and this can be used to convert between a true equinox and equator coordinate system ( $X_T Y_T Z_T$ ) and a mean equinox and equator coordinate system ( $X_m Y_m Z_m$ ) for the time specified. This matrix is not a perfectly orthonormal matrix, as direction cosine matrices should be, but the error is trivial. The matrix has the sense defined by the equation

$$\bar{R}_{\text{true equinox of date}} = N \bar{R}_{\text{mean equinox of date}}$$

### Precession Effects

It remains to convert to the Besselian New Year mean equinox system. The variations are those due to precession.

"General" precession is the motion of the mean poles of the equator and ecliptic. It is caused by luni-solar precession (a smooth retrograde motion of period some 26,000 years, due to the gravitational action of the Sun and Moon on the equatorial bulge of the Earth) and by planetary precession (the effects of the planets on the orbit plane of the Earth). The effect is given by three Eulerian angles ( $\zeta_0, \theta, z$ ) relating

## Appendix A

mean equinox axes of some date  $t_0$  ( $X_0 Y_0 Z_0$ ) to mean equinox axes of some later date  $t$  ( $XYZ$ ) (see Figure A-2). The direction cosines between these axes are

	$X_0$	$Y_0$	$Z_0$
X	$C_{\zeta_0} C_\theta C_z - S_{\zeta_0} S_z$	$-S_{\zeta_0} C_\theta C_z - C_{\zeta_0} S_z$	$-S_\theta S_z$
P = Y	$C_{\zeta_0} C_\theta S_z + S_{\zeta_0} C_z$	$-S_{\zeta_0} C_\theta S_z + C_{\zeta_0} C_z$	$-S_\theta S_z$
Z	$C_{\zeta_0} S_\theta$	$-S_{\zeta_0} S_\theta$	$C_\theta$

Here  $t_0$  represents the Besselian New Year, and  $t$  the date of interest, and  $\bar{R}_t = P \bar{R}_{\text{BNY}}(t_0)$ .

The angles are given by Newcomb's formulas, here converted to degrees and days since Jan. 0.0, 1950 (J.D. 2433281.5).  $d$  and  $d_0$  should include fractional parts of days in these formulas.

J.D. Initial Epoch  $t_0$ : 2433281.5 +  $d_0$  · J.D. Final Epoch,  $t$ :

2433281.5 +  $d_0$  +  $d$

$$D = d/10^4$$

$$\begin{aligned} \zeta_0^\circ = & (0^\circ.175\ 298\ 3 + 29.0694 \times 10^{-6} D_0) D + 6.289 \times 10^{-6} D^2 \\ & + 0.1025 \times 10^{-6} D^3 \end{aligned}$$

## Appendix A

$$z^{\circ} = \zeta_0 + 16.4694 \times 10^{-6} D^2$$

$$\theta^{\circ} = (0.152\ 4946 - 17.761 \times 10^{-6} D_0) D \\ - 8.869 \times 10^{-6} D^2 - 0.2394 \times 10^{-6} D^3$$

Because the angles are small, approximations are quite accurate for the direction cosines. For the initial and final epochs as computed above, the approximations are

$$(X_0, X) - 1 = -10^{-8} \{ (2226.056 + 0.534 D_0) D^2 + 0.2668 D^3 \}$$

$$(Y_0, X) = -(X_0, Y) = -10^{-8} \{ (611906.556 + 101.573 D_0) D \\ + 13.874 D^2 - 4.5357 D^3 \}$$

$$(Z_0, X) = -(X_0, Z) = -10^{-8} \{ (266039.907 - 31.034 D_0) D \\ - 15.517 D^2 - 1.9703 D^3 \}$$

$$(Y_0, Y) - 1 = -10^{-8} \{ (1872.163 + 0.616 D_0) D^2 + 0.3078 D^3 \}$$

$$(Y_0, Z) = + (Z_0, Y) = -10^{-8} \{ (813.932 + 0.041 D_0) D^2 \}$$

$$(Z_0, Z) - 1 = -10^{-8} \{ (353.893 - 0.082 D_0) D^2 \}$$

The above is satisfactory for long term use.

## Appendix A

Approximate formulas for precession angles serve well for intervals of the order of a year or less. The situation is represented in Figure A-3, which shows clearly that luni-solar precession is along the ecliptic while planetary precession is along the equator. The following formulas give the annual (365.25 days) changes in the angles (in degrees) using the epoch 1950.0 (J.D. 2433281.5) as the reference epoch, and  $D = d \times 10^{-4}$ ,  $d$  = the number of days since that epoch

$$\psi' = 0^{\circ}.013\ 9929 + 0^{\circ}.38029 \times 10^{-6} D$$

$$\lambda' = 32^{\circ}.029 \times 10^{-6} - 1^{\circ}.43059 \times 10^{-6} D$$

$$p = 0^{\circ}.013\ 9635 + 1^{\circ}.6883 \times 10^{-6} D$$

$$m = 0^{\circ}.012\ 8056 + 2^{\circ}.1217 \times 10^{-6} D$$

$$n = 0^{\circ}.005\ 5675 + 0^{\circ}.6525 \times 10^{-6} D$$

and the obliquity is

$$\begin{aligned} \epsilon = & 23^{\circ}.445\ 788 - 0^{\circ}.003\ 563 D - 0^{\circ}.06632 \times 10^{-6} D^2 \\ & + 0^{\circ}.01032 \times 10^{-6} D^3 \end{aligned}$$

### Time

Common time is actually "UT2", which is a mathematical, nearly uniformly flowing prediction of Universal time, and which is also known as Greenwich Mean Time and Greenwich Civil Time

## Appendix A

( $O^h$  being at midnight). It must be distinguished from Greenwich Mean Astronomical Time (GMAT) which begins at noon, and proceeds at the same rate as universal time. Ephemeris Time is also used, being necessary for the JPL Ephemerides for example, and is related to UT by the formula

$$E.T. = U.T. + \Delta T$$

E.T. is the time used in celestial mechanics computations and flows absolutely smoothly, while UT varies as the earth wobbles. The correction  $\Delta T$  is determined empirically post facto annually. Predictions are available in the American Ephemeris to the nearest second of time ( $36^s$  for 1966.5).

The distinction is unimportant for the present application, none of the quantities varying rapidly enough to make any difference. It becomes important only in locating the moon, which moves about 24 miles in 36 seconds.

Platform Alignment

Consider now the alignment of the stable member. Fundamental quantities are the vector position  $\bar{R}$ , velocity  $\bar{V}$  and time  $t$  of ignition of deboost retrofire, which are predicted well ahead of the event. The platform is to be aligned so  $X_{SM}$  (stable member X axis) is approximately opposite to the thrust vector at this instant and so the horizon appears level in the window of the spacecraft with a "look angle" for the pilot of  $31.7^\circ$ . Alignment is to include thrust misalignment angles CGY and CGZ which are angles (positive in the right hand sense) by which the engine nozzle must be rotated relative to the spacecraft to put the thrust through the spacecraft, c.g., (see Figure A-4). Figure A-5 shows the vectors associated with alignment. At the left in this figure is the vector to the earth's horizon.  $31.7^\circ$  below this must lie a scribed horizontal line on the CM window, so the pilot will see the horizon merging with the line. This would be all of the information needed except for the pitch and yaw trim gimbal angles. The thrust vector must be in the orbit plane and is thus above the scribed line by the angle CGY. To accommodate the yaw angle CGZ, while keeping the thrust in the orbit plane, the spacecraft X axis is put out of plane by the yaw angle CGZ. This

## Appendix A

theoretically puts the highest point of the horizon off the center of the scribed line, but the actual effect is relatively nil, the horizon being relatively flat.

To keep the FDAI on dead center ( $0^\circ$  in pitch, yaw, and roll) which permits easy manual attitude monitoring or control, the platform is aligned with the spacecraft, except that the X and Y axes are oppositely directed between the spacecraft and platform.

The computational formulas are [17]

Forward horizontal vector  $\bar{I}_H$

$$\bar{I}_H = \text{unit } [(\bar{R} \times \bar{V}) \times \bar{R}] \quad (\text{at ignition})$$

thrust angle  $\phi$

$$\phi = \sin^{-1} \left( \frac{R_E}{R} \right) - 31.7^\circ + \text{CGY}$$

$$R_E = 20909869.1 \text{ ft.}$$

thrust vector  $\bar{TS}$

$$\bar{TS} = - \text{unit } [R] \cos \phi - \bar{I}_H \sin \phi .$$

Approximate Axes  $\bar{L}$ ,  $\bar{M}$ ,  $\bar{N}$

$$\bar{L} = \bar{TS}$$

$$\bar{M} = \text{unit } (\bar{L} \times \bar{R}) \quad \begin{array}{l} \text{plus for heads up (SPS),} \\ \text{minus for heads down (RCS)} \end{array}$$

$$\bar{N} = \bar{L} \times \bar{M}$$



## Appendix A

## Spacecraft and Stable Member Axes

$$\bar{X}_{SCD} = -\bar{X}_{Sm} = \text{unit} [\bar{L} + \bar{N} \sin CGY - \bar{M} \sin CGZ]$$

$$\bar{Y}_{SCD} = -\bar{Y}_{Sm} = \text{unit} [\bar{M} - (\bar{X}_{SCD} \cdot \bar{M}) \bar{X}_{SCD}]$$

$$\bar{Z}_{SCD} = \bar{Z}_{Sm} = \bar{X}_{SCD} \times \bar{Y}_{SCD}$$

## Alignment matrix REFSMAT

$$\text{REFSMAT} = \begin{bmatrix} -\bar{X}_{Sm}^T & - \\ -\bar{Y}_{Sm}^T & - \\ -\bar{Z}_{Sm}^T & - \end{bmatrix}$$

such that  $\bar{R}_B$  and  $\bar{R}_{SM}$  (position in Besselian and Stable member axes) are related by

$$\bar{R}_{SM} = [\text{REFSMAT}] \bar{R}_B$$

Sample Numerical Data

Tables I-1, 2, 3 show sample nutation matrices N, precession matrices P, and the product matrix NP, and the platform alignment matrix REFSMAT for three dates of interest. Table I-1 is for the retrofire time (and location) as given in the AS-204 Operational Trajectory (December 15th).

## Appendix A

Table I-2 is for July, 1966, about 6 months before the Besselian New Year, and Table I-3 is for June 13, 1967, about 6 months after the Besselian New Year.

In these matrices, the small numbers off the diagonal can be considered as angles of rotation (in radians) between the axes noted, with the general format given by the well known matrix for small rotations

1	$\Delta\theta_Z$	$-\Delta\theta_Y$
$-\Delta\theta_Z$	1	$\Delta\theta_X$
$\Delta\theta_Y$	$\Delta\theta_X$	1

The largest of these angles in the combined nutation-precession matrix is 0.00015676 radians (0.00898°) and is about the Pole axis. If it were neglected, longitude would be in error by this amount, which is equivalent to an East-West position error of some 0.538 NM or 3220 feet, a value which is greater than the errors expected of the MSFN system. Similarly, the greatest latitude error is 0.0000681 radians (0.0039°) equivalent to about 0.234 NM or 1450 feet. Therefore, it is reasonable to include precession and nutation when converting from longitude and latitude to position components XYZ. For the inverse conversion from XYZ components to longitude and latitude for information purposes to the flight crew, the error is barely capable of being displayed on the DSKY, and may well be neglected.

The guidance computer performs its navigation functions using the Mean Pole at the Besselian New Year as the true polar axis at the present instant. That is, the true polar axis is represented as the vector (0,0,1). On December 15, 1966, the more accurate representation is (-2.739E-5, 2.912E-5, 1.0), which indicates a total angle between the two axes of 0.0000478 radians (0.00273°). This affects the oblateness term in gravity, which is never more than 0.00162 times the principal part, for a total error of some 0.000000045 times the principal part of gravity in the X and Y directions. This is trifling: the assumption is certainly justifiable.

## Appendix A

Comparison with Computer Software Methods

The methods used in the program for the AS-204 space-craft computer are given in reference 18. It reduces to the following formulas:

$$A_z = A_{z0} + \omega t$$

where: " $A_{z0}$  is the angle between the X-axis and the Greenwich Meridian at  $0^h$  on July 1, 1966,"  $t$  is the time since then and " $\omega$  is the angular rate of the earth."

$A_x$  and  $A_y$  are small angles about the X and Y axes due to precession and nutation.  $\underline{u}$ , a unit vector parallel to present position, measured in true earth coordinates, is given by

$$\underline{u} = \text{UNIT} \begin{bmatrix} \begin{bmatrix} 1 & 0 & A_y \\ 0 & 1 & -A_x \\ -A_y & A_x & 1 \end{bmatrix} \underline{r} \end{bmatrix}$$

where  $\underline{r}$  is the position vector measured in Besselian New Year mean coordinates.

Then

$$\text{Lat} = \tan^{-1} \frac{u_2}{\sqrt{u_0^2 + u_1^2} (b/a)^2}$$

$$\text{Long} = \tan^{-1} \left( \frac{u_1}{u_0} \right) - A_z$$

## Appendix A

$$\text{Alt} = r - r_e$$

$$r_e^2 = \frac{b^2}{1 - (1 - (\frac{b}{a})^2) \cos^2 \text{Lat}}$$

Or, conversely,

$$\underline{u} = \text{UNIT} \begin{bmatrix} \cos (\text{Long} + A_z) \\ \sin (\text{Long} + A_z) \\ (\frac{b}{a})^2 \tan \text{Lat} \end{bmatrix}$$

$$\underline{u}_r = \text{UNIT} \begin{bmatrix} \begin{bmatrix} 1 & 0 & -A_y \\ 0 & 1 & A_x \\ A_y & -A_x & 1 \end{bmatrix} \underline{u} \end{bmatrix}$$

$$\underline{r} = (r_e + \text{Alt}) \underline{u}_r$$

Latitude is geodetic latitude: the term " $(\frac{b}{a})^2 \tan \text{Lat}$ " equals the tangent of the geocentric latitude. Comparing the formulas concerning altitude with those given earlier in this appendix, it is seen that altitude is not treated correctly. The present formulas assume that altitude is measured along the radius vector and is the difference between the radius and the distance along the radius vector to the reference ellipsoid.

## Appendix A

Correctly, altitude is measured along a perpendicular to the reference ellipsoid from the sub-vehicle point to the vehicle. The error is zero at zero altitude, is less than 2,000 feet at 100 NM but may be as large as 3.6 million feet at lunar distances (being zero at  $0^\circ$  and  $90^\circ$  latitude and maximum at  $45^\circ$  latitude). Since the only use of the routine to convert latitude, longitude and altitude to XYZ coordinates is at the launch pad (at least to the writers' knowledge), the routine is satisfactory. Use for high altitudes should be considered carefully, and generally discouraged.

Note that the "precession nutation" matrix used in the software ignores the rotation about the pole. This is satisfactory if the angle  $A_z$  includes the effect. With such being the apparent case, then  $A_z$  must be the angle between the mean equinox at the Besselian New Year and true Greenwich at the present instant, and the rotational rate  $\omega$  must be the sidereal rate of the earth (including its annual motion).

The angle  $A_{zo}$  is computed by finding GTHA (thus including nutation) at  $0^h$ , July 1, 1966 and then adding the precession angle in right ascension between July 1 and the Besselian New Year. The 1966 Almanac gives this GTHA as  $18^h 34^m 24^s.195 = 278^\circ.6008125$ . The interval between  $0^h$ , July 1, 1966 (J.D. 2439307.5) and the Besselian New Year (J.D. 2439491.541) is 184.041 days. Taking a tropical year as  $365^d.24220284$  (1966), and the precession in right ascension as  $3^s.07357$  (1966) per tropical year, then the correction is  $1^s.548733667$  or  $0^\circ.0064530$ .  $A_{zo}$  is therefore  $278^\circ.6072655$ .

This technique succeeds because the nutational rotation about the pole changes only above  $1 \times 10^{-5}$  radians during the year, and is approximated in the formula by the value at July 1, 1966.

In computing  $\omega t$  over such a long time, care must be given to maintaining accuracy. The angular rate of the earth (1966) is 361.008317236 degrees/day and, with  $t$  in days, and neglecting multiples of  $360^\circ$  in the result,  $\omega t$  is best written as

$$\begin{aligned} \omega t &= 1.008317236 \text{ (integral number of days)} \\ &+ 361.008317236 \text{ (fractional number of days)} \end{aligned}$$

# BELLCOMM, INC.

## Appendix A

TABLE I-1

### Sample Matrices

Alignment Epoch: J.D. 2439474.5 + 40801<sup>s</sup>.92 after 0<sup>h</sup> u.t.  
(1966, December 15, 11<sup>h</sup>, 20<sup>m</sup>, 1<sup>s</sup>.92)

Besselian New Year: J.D. 2439491.541 (Jan. 1.041, 1967)

GMHA = 83°.20393, GTHA = 83°.20089, at alignment epoch

$\omega t = 170^\circ.47345$

### Nutation Matrix

	Mean Eqnx	Mean Y	Mean Pole	
True Eqnx	1.0	+5.299E-5	+2.298E-5	= N
True Y	-5.299E-5	1.0	-2.912E-5	
True Pole	-2.298E-5	+2.912E-5	1.0	

### Precession Matrix

Alignment	B.N.Y.			
	Mean Eqnx	Mean Y	Mean Pole	
Mean Eqnx	1.0	+1.014E-5	+0.441E-5	= P
Mean Y	-1.014E-5	1.0	0	
Mean Pole	-0.441E-5	0	1.0	

# BELLCOMM, INC.

## Appendix A

### Nutation-Precession Matrix

Alignment	B.N.Y.			
	Mean Eqnx	Mean Y	Mean Pole	
True Eqnx	1.0	+6.313E-5	+2.739E-5	= NP
True Y	-6.313E-5	1.0	-2.912E-5	
True Pole	-2.739E-5	+2.912E-5	1.0	

### Platform Alignment Matrix (REFSMAT)

Stable Member	B.N.Y.		
	Mean Eqnx	Mean Y	Mean Pole
SMX	-.714355536	+.575903475	+.397531595
SMY	-.502161466	-.026228430	-.864376038
SMZ	-.487370528	-.817096852	+.307932954

# BELLCOMM. INC.

TABLE I-2

## Sample Matrices

Alignment Epoch: J.D. 2439324.5 + 40801<sup>s</sup>.92 after 0<sup>h</sup> u.t.  
(1966, July 11<sup>h</sup>, 20<sup>m</sup>, 1<sup>2</sup>.92)

Besselian New Year: J.D. 2439491.541 (Jan 1.041, 1967)

GMHA = 295°.35681 , GTHA = 295°.35369 at alignment epoch

$\omega t = 170^\circ.47344$

### Nutation Matrix

	Mean Eqnx	Mean Y	Mean Pole
True Eqnx	1.0	+5.483E-5	+2.378E-5
True Y	-5.483E-5	1.0	-2.556E-5
True Pole	-2.378E-5	+2.556E-5	1.0

### Precession Matrix

	B.N.Y. Mean Eqnx	Mean Y	Mean Pole
Alignment			
Mean Eqnx	1.0	+10.193E-5	+4.433E-5
Mean Y	-10.193E-5	1.0	0
Mean Pole	- 4.433E-5	0	1.0



# BELLCOMM, INC.

## Nutation-Precession Matrix

Alignment	B.N.Y.		
	Mean Eqnx	Mean Y	Mean Pole
True Eqnx	1.0	+15.676E-5	+6.810E-5
True Y	-15.676E-5	1.0	-2.556E-5
True Pole	- 6.811E-5	+ 2.556E-5	1.0

## Platform Alignment Matrix (REFSMAT)

Stable Member	B.N.Y.		
	Mean Eqnx	Mean Y	Mean Pole
SMX	+.911247484	-.107313814	+.397632740
SMY	+.411252916	+.289453253	-.864342444
SMZ	-.022340206	+.951157495	+.307896663

# BELLCOMM. INC.

TABLE I-3

## Sample Matrices

Alignment Epoch: J.D. 2439654.5 + 40801<sup>s</sup>.92 after 0<sup>h</sup> u.t.  
(1967, June 13, 11<sup>h</sup>, 20<sup>m</sup>, 1<sup>s</sup>.92)

Besselian New Year: J.D. 2439491.541 (Jan. 1.041, 1967)

GMHA = 260°.62046, GTHA = 260°.6196 at alignment epoch

$\omega t = 170^\circ.47345$

## Nutation Matrix

	Mean Eqnx	Mean Y	Mean Pole
True Eqnx	1.0	+4.336E-5	+1.880E-5
True Y	-4.336E-5	1.0	-3.420E-5
True Pole	-1.880E-5	+3.420E-5	1.0

## Precession Matrix

	B.N.Y. Mean Eqnx	Mean Y	Mean Pole
Alignment			
Mean Eqnx	1.0	-10.000E-5	-4.349E-5
Mean Y	+10.000E-5	1.0	0
Mean Pole	+ 4.349E-5	0	1.0

# BELLCOMM, INC.

## Nutation-Precession Matrix

Alignment	B.N.Y.		
	Mean Eqnx	Mean Y	Mean Pole
True Eqnx	1.0	-5.665E-5	-2.469E-5
True Y	+5.665E-5	1.0	-3.420E-5
True Pole	+2.469E-5	+3.420E-5	1.0

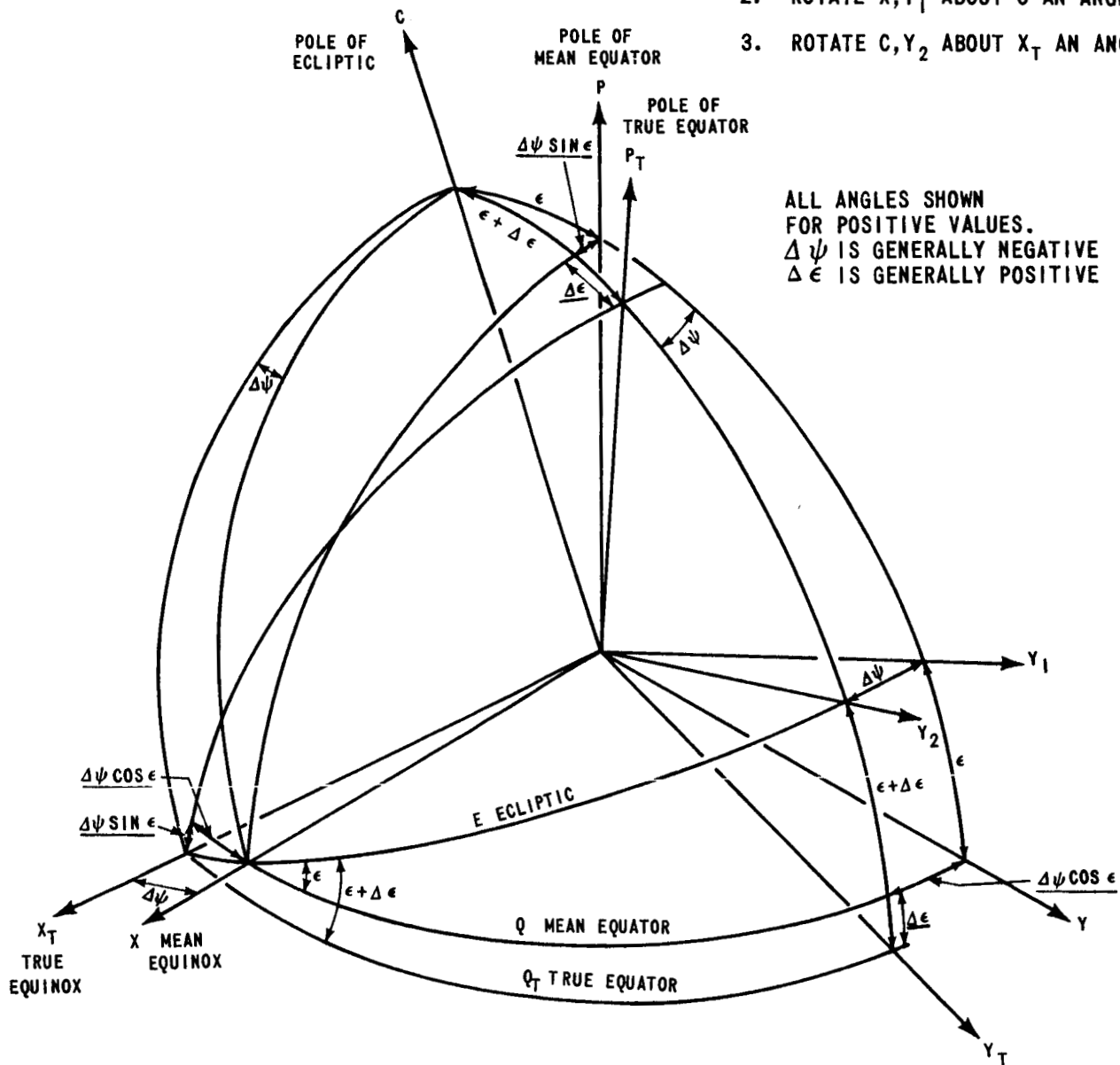
## Platform Alignment Matrix (REFSMAT)

Stable Member	B.N.Y.		
	Mean Eqnx	Mean Y	Mean Pole
SMX	+.687603213	-.607567728	+.397571724
SMY	+.502834886	+.003455737	-.864375584
SMZ	+.523792796	+.794260353	+.307882421

TO GO FROM  $P, X, Y$  TO  $P_T, X_T, Y_T$ :

1. ROTATE  $P, Y$  ABOUT  $X$  AN ANGLE  $\epsilon$ .
2. ROTATE  $X, Y_1$  ABOUT  $C$  AN ANGLE  $\Delta\psi$ .
3. ROTATE  $C, Y_2$  ABOUT  $X_T$  AN ANGLE  $(\epsilon + \Delta\epsilon)$ .

ALL ANGLES SHOWN  
FOR POSITIVE VALUES.  
 $\Delta\psi$  IS GENERALLY NEGATIVE  
 $\Delta\epsilon$  IS GENERALLY POSITIVE

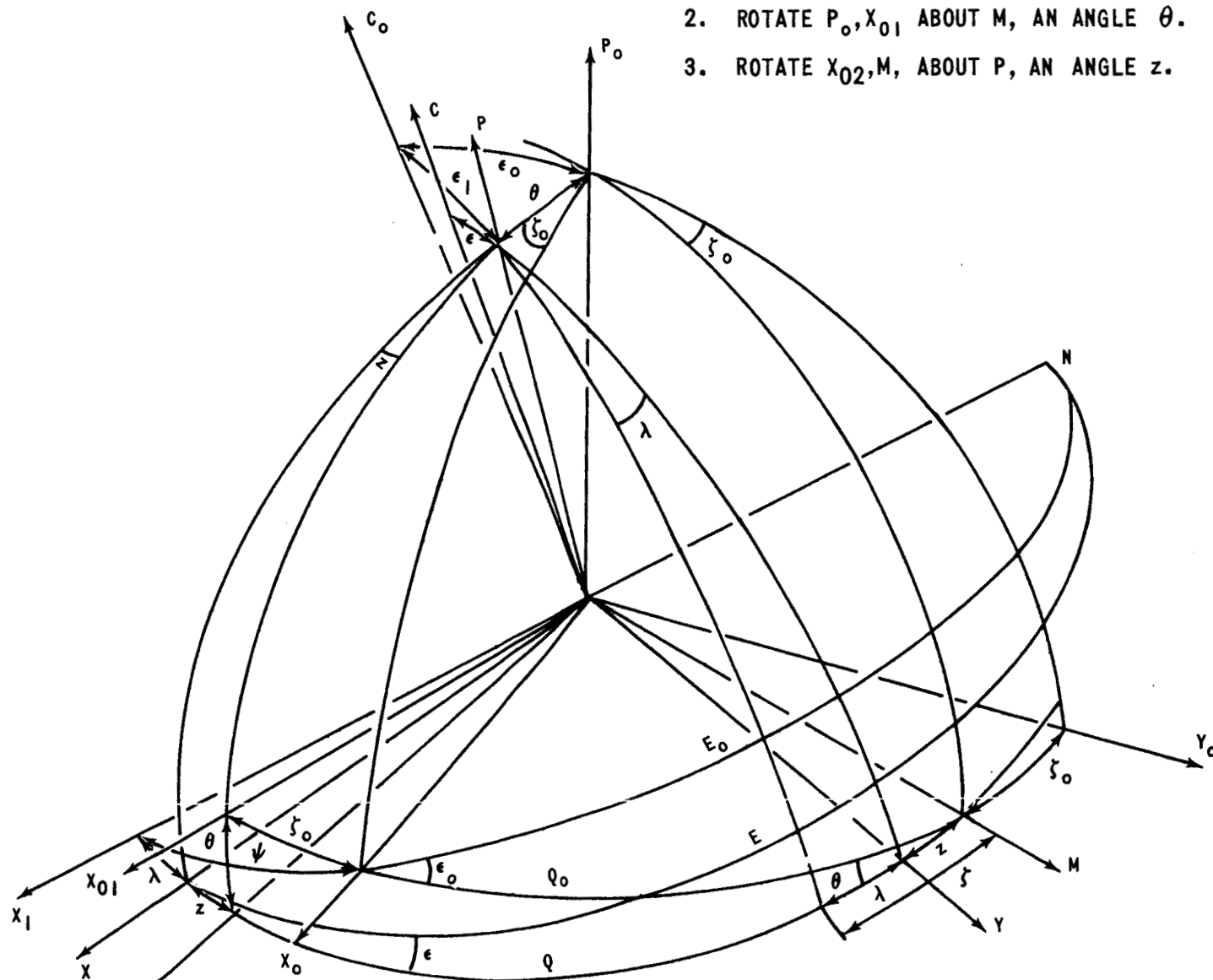


$P, X, Y$  POLE,  $X, Y$  AXES OF MEAN EQUATOR,  $Q$ .  
 $C$  POLE OF ECLIPTIC.  
 $P_T, X_T, Y_T$  POLE,  $X, Y$  AXES OF TRUE EQUATOR  $Q_T$ .  
 $\Delta\psi$  NUTATION IN LONGITUDE  
 $\epsilon$  MEAN OBLIQUITY  
 $\epsilon + \Delta\epsilon$  TRUE OBLIQUITY.  
 $\Delta\psi \cos \epsilon$  EQUATION OF THE EQUINOXES, (NUTATION IN RIGHT ASCENSION).  
 UNDERLINED QUANTITIES, BASED ON SMALL ANGLE APPROXIMATIONS,  
 ARE USED IN COORDINATE TRANSFORMATIONS.

FIGURE A-1 AXES DIFFERENCES DUE TO NUTATION

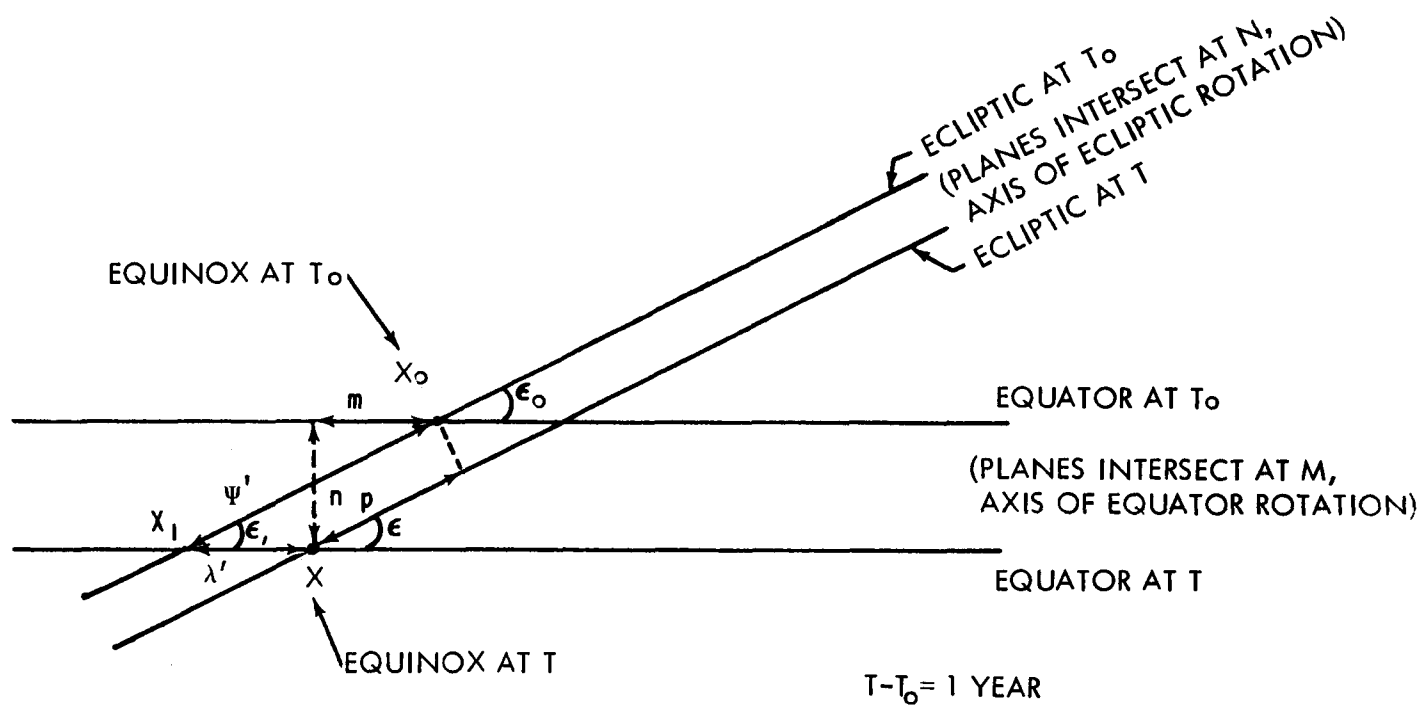
TO GO FROM  $P_o, X_o, Y_o$  TO  $P, X, Y$ :

1. ROTATE  $X_o, Y_o$  ABOUT  $P_o$ , AN ANGLE  $\zeta_o$ .
2. ROTATE  $P_o, X_{o1}$  ABOUT  $M$ , AN ANGLE  $\theta$ .
3. ROTATE  $X_{o2}, M$ , ABOUT  $P$ , AN ANGLE  $z$ .



- $C_o$  POLE OF ECLIPTIC  $E_o$  AT EPOCH  $t_o$ .  
 $C$  POLE OF ECLIPTIC  $E$  AT EPOCH  $t$ .  
 $P_o, X_o, Y_o$  POLE,  $X, Y$  AXES OF EQUATOR  $Q_o$  AT EPOCH  $t_o$ .  
 $P, X, Y$  POLE, AXES OF EQUATOR  $Q$  AT EPOCH  $t$ .  
 $\epsilon_o$  OBLIQUITY OF ECLIPTIC AT  $t_o$ .  
 $\epsilon$  OBLIQUITY OF ECLIPTIC AT  $t$ .  
 $\zeta_o, \theta, z$  ANGLES WHICH DEFINE PRECESSION.

FIGURE A-2 PRECESSION POLAR DIAGRAM AFTER SUPPLEMENT TO  
 AMERICAN EPHEMERIS AND NAUTICAL ALMANAC



$\epsilon$  = OBLIQUITY OF THE ECLIPTIC

$\Psi'$  = LUNI-SOLAR PRECESSION ON THE ECLIPTIC (BOTH  $\Psi, \Psi'$  USED IN [11])

$\lambda'$  = PLANETARY PRECESSION ON THE EQUATOR

$p$  = GENERAL PRECESSION IN LONGITUDE =  $\Psi' - \lambda' \cos \epsilon$ ,

$m$  = GENERAL PRECESSION IN RIGHT ASCENSION =  $\Psi' \cos \epsilon - \lambda'$

$n$  = GENERAL PRECESSION IN DECLINATION =  $\theta = \Psi' \sin \epsilon$ ,

$\zeta_0$  =  $90^\circ - X_0M$

$z$  =  $XM - 90^\circ$

FIGURE A-3 GENERAL PRECESSION - EQUATORIAL DIAGRAM

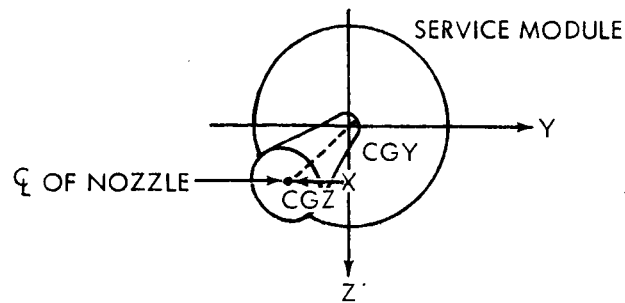


FIGURE A-4 REAR VIEW OF SERVICE MODULE SHOWING EFFECTS OF GIMBAL ANGLES CGY AND CGZ

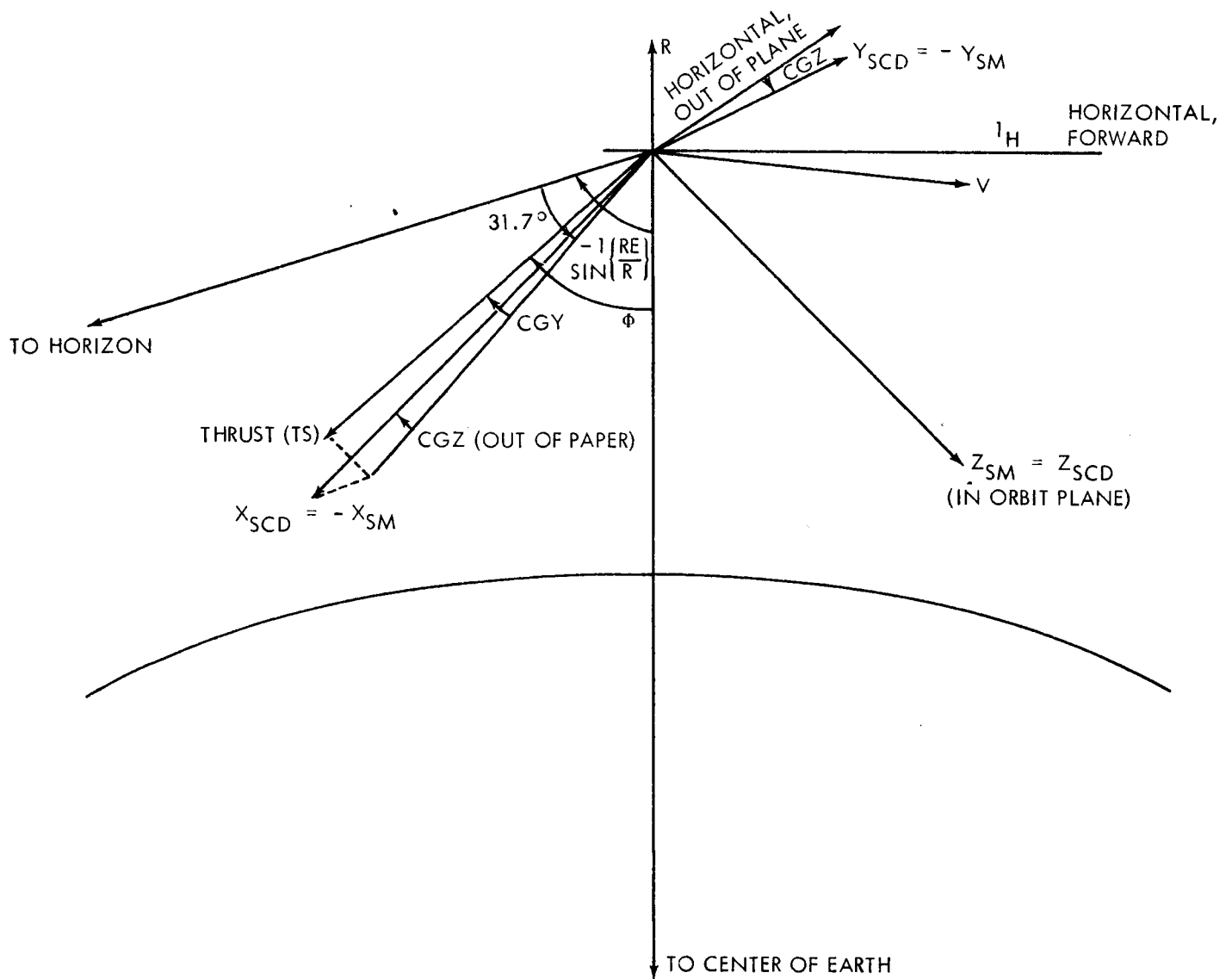


FIGURE A-5 VECTOR DIAGRAM AT RETROFIRE IGNITION (IN PLANE OF ORBIT)

APPENDIX B

Accelerometer Output Quantization Effects

This appendix contains an analysis of the effects of the quantization of the outputs of the accelerometers in the Inertial Measuring Unit. The accelerometers are called Pulse Integrating Pendulous Accelerometers; they output a pulse to the guidance computer each time the sensed velocity, along the accelerometer axis changes by 5.85 cm/sec (0.192 fps).

The analysis is taken from reference 19, but is adapted to the present case.

Accelerometer Model

At a set of discrete time instants,  $\{t_j\}$   
 $j = 0, 1, \dots, n$ , velocity measurements  $V_i(t_j)$ ,  $i = 1, 2, 3$  are made by three integrating accelerometers mounted orthogonally on an inertial platform

$$\bar{V}_a(t_j) = \int_0^{t_j} a_T(t) \bar{x}(t) dt + \bar{\delta}(t_j) \quad (1)$$

Here

$$(a) \quad \bar{V}_a(t_j) = \begin{bmatrix} V_1(t_j) \\ V_2(t_j) \\ V_3(t_j) \end{bmatrix} \quad (2)$$

represents the vector of accelerometer readings.

(b)  $a_T(t)$  represents the magnitude of the aerodynamic acceleration.



## Appendix B

- (c)  $\bar{\lambda}(t)$  is the direction cosine vector of the aerodynamic acceleration vector in platform coordinates.
- (d)  $\bar{\delta}(t)$  represents the vector of errors introduced by quantization.

For the purpose of this analysis it will be assumed that the aerodynamic acceleration is such as to cause the velocities in all three platform coordinates to be monotonically increasing functions of time. With this assumption the accelerometer readings will be lower than the true values. Each component of the quantization noise thus has the probability density function

$$p[\delta_i(t_j)] = \begin{cases} \frac{1}{b} & -b < \delta_i(t_j) < 0 \\ 0 & \text{elsewhere} \end{cases} \quad (3)$$

where  $b = .192$  ft/sec (.0585 meters/sec) is the value of the least significant bit in each accelerometer register.

Thus the mean of the quantization noise is

$$E\{\delta_i(t)\} = -\frac{b}{2} \text{ ft/sec} = -.096 \text{ ft/sec} \quad (4)$$

and the variance about the mean is

$$E\left\{\left(\delta_i(t) + \frac{b}{2}\right)^2\right\} = \frac{b^2}{12} \text{ ft}^2/\text{sec}^2 = .00307 \text{ ft}^2/\text{sec}^2 \quad (5)$$

The noise is also assumed to be uncorrelated, i.e.,

$$E\left\{\left(\delta_i(t_j) + \frac{b}{2}\right) \left(\delta_i(t_k) + \frac{b}{2}\right)\right\} = 0 \text{ for } j \neq k .$$

## Appendix B

Noise Response of the Navigation Equations ("Average G Equations")

The spacecraft navigation equations are

$$\bar{R}_n = \bar{R}_{n-1} + \bar{V}_{n-1} \Delta T + \frac{1}{2} \left[ \Delta \bar{V}_a(n) + \bar{G}_{n-1} \Delta T \right] \Delta T$$

$$\bar{G}_n = \bar{G}(\bar{R}_n) \quad (6a)$$

$$\bar{V}_n = \bar{V}_{n-1} + \Delta \bar{V}_a(n) + \frac{1}{2} \left[ \bar{G}_n + \bar{G}_{n-1} \right] \Delta T \quad (6b)$$

where

$\Delta \bar{V}_a$  is the change in velocity, due to lift and drag as measured by the accelerometers,

$\bar{R}_n$  is the estimate of the position vector at time  $t_n$ ,

$\bar{V}_n$  is the estimate of the velocity vector at time  $t_n$ ,

$\bar{G}_n$  is the gravitational acceleration vector.

To simplify the analysis of these equations the one dimensional problem will be considered and the model used for gravity will be

$$G_n = -\mu/R_n^2 \quad (6c)$$

Equations (6) represent a set of nonlinear, coupled, difference equations for the navigation position and velocity (the nonlinearity being due to the gravity term). In order to determine the statistics of the errors resulting from noisy

## Appendix B

measurements ( $\Delta V_a$ ), the gravity equation (6c) will be linearized about a nominal value. The position equation (6a) will then be uncoupled from (6b) in such a way as to yield a second order difference equation for the noise in position. This difference equation will then be solved to yield a weighting sequence (impulse response) which will be used to determine the statistics of the resulting noise. The weighting sequence is then used to determine the statistics of the navigation velocity errors caused by the coupling through the gravity terms. The error statistics will now be derived.

Taking the velocity equation out of recursive form and using the fact that  $V_a(0) = 0$  and  $\Delta V_a(n) = V_a(n) - V_a(n-1)$  yields

$$V_n = V_o + V_a(n) + \frac{1}{2} \Delta T [G_o - G_n] + \Delta T \sum_{i=1}^n G_i \quad (7)$$

Taking the position equation out of recursive form and inserting (7) for the navigation velocity yields

$$R_n = R_1 + (n-1) \Delta T [V_o - V_a(0)] + \frac{1}{2} (n-1) \Delta T^2 G_o + \frac{\Delta T}{2} [V_a(n) - V_a(1)] + \Delta T \sum_{i=1}^{n-1} V_a(i) + \Delta T^2 \sum_{i=1}^{n-1} \sum_{j=1}^i G_j$$

Using

$$\sum_{i=1}^{n-1} \sum_{j=1}^i G_j = \sum_{i=1}^{n-1} (n-i) G_i$$

and

$$V_a(0) = 0$$

## Appendix B

yields

$$R_n = R_1 + (n-1)\Delta T V_o + \frac{1}{2} (n-1)\Delta T^2 G_o + \frac{\Delta T}{2} [V_a(n) - V_a(1)]$$

$$+ \Delta T \sum_{i=1}^{n-1} V_a(i) + \Delta T^2 \sum_{i=1}^{n-1} (n-i)G_1$$

Now assuming that  $R_o$ ,  $V_o$ ,  $G_o$  are noise free the following equation for the deviation in position due to noise results:

$$\delta R_n = \frac{\Delta T}{2} [\delta V_a(n) - \delta V_a(1)] + \Delta T \sum_{i=1}^{n-1} \delta V_a(i)$$

$$+ \Delta T^2 \sum_{i=1}^{n-1} (n-i) \delta G_1 + \delta R_1 \quad (8)$$

In order to determine the deviation in gravitational acceleration due to a change in position the following is considered

$$\delta G = \frac{\partial G}{\partial R} \delta R = \frac{2\mu}{R^3} \delta R$$

Using  $\frac{\mu}{R^2} \approx 32$  and  $R \approx 2 \times 10^7$  ft yields

$$\delta G = 32 \times 10^{-7} \delta R = k \delta R$$

Forming  $\delta R_{n+1} - \delta R_n$  yields

$$\delta R_{n+1} - \delta R_n = \frac{\Delta T}{2} [\delta V_a(n+1) + \delta V_a(n)] + \Delta T^2 k \sum_{i=1}^n \delta R_n$$

## Appendix B

Taking the first difference of the above equation yields

$$\delta R_{n+2} - (2 + \Delta T^2 k) \delta R_{n+1} + \delta R_n = \frac{\Delta T}{2} [\delta V_a(n+2) - \delta V_a(n)] \quad (9)$$

Equation (9) is a linear, constant coefficient, second order difference equation for the position noise forced by the noise in the accelerometer readings.

The characteristic roots of this equation are (using  $\Delta T = 2$  and  $k = 32 \times 10^{-7}$ )

$$z_1 = 1.0036$$

$$z_2 = .9964$$

Taking the  $z$  transform of equation (9) yields the transfer function

$$H(z) = \frac{\frac{\Delta T}{2} (z^2 - 1)}{(z - z_1)(z - z_2)}$$

$$H(z) = \frac{\Delta T}{2} + \frac{\Delta T}{2} \left[ \frac{1}{(z - z_1)} + \frac{1}{(z - z_2)} \right] \quad (10)$$

The inverse transform of (10) yields the weighting sequence

$$h(k) = \begin{cases} \frac{\Delta T}{2} & k = 0 \\ \frac{\Delta T}{2} (z_1)^{k-1} + \frac{\Delta T}{2} (z_2)^{k-1} & k > 0 \end{cases} \quad (11)$$

## Appendix B

Equation (11) is the desired result, which gives the noise in position as a linear combination of the noise in the accelerometer measurements

$$\delta R_n = \sum_{i=1}^n h(n-i) \delta V_a(i) \quad (12)$$

To determine the mean of the error in position the expectation of (12) is taken

$$E\{\delta R_n\} = E\{\delta V_a\} \sum_{i=1}^n h(n-i)$$

This uses the fact that the mean of the accelerometer noise is time invariant. Using  $E\{\delta V_a\}$  as the mean of the quantization noise results in

$$E\{\delta R_n\} = -0.096 \sum_{j=0}^{n-1} h(j)$$

Since  $\sum h(j)$  is a power series the summation can be obtained in closed form to yield

$$E\{\delta R_n\} = -0.096 \frac{\Delta T}{2} \left[ 1 + \frac{z_1 - z_1^{n-1}}{1 - z_1} + \frac{z_2 - z_2^{n-1}}{1 - z_2} \right] \quad (13)$$

Now using  $\Delta T = 2$  seconds,  $n = 320$  (i.e.,  $n\Delta T \approx 640$  sec, the approximate time the spacecraft is in the atmosphere) the following result is obtained

$$E\{\delta R_{320}\} = -75.4 \text{ ft.}$$

## Appendix B

It should be noted that if the change in the gravitational acceleration, resulting from noise in position, is ignored the resulting mean of the position noise would be

$$E\{\delta R_n\} \Big|_{\delta G=0} = (n - \frac{1}{2})\Delta T E\{\delta V_a\}$$

$$E\{\delta R_{320}\} \Big|_{\delta G=0} = -47.1 \text{ ft.}$$

Thus 37.5% of the total position error is contributed by the gravitational terms. It is noted that the mean of the position noise can be reduced to zero, if desired, by initializing  $V_a(0) = -\frac{b}{2}$  rather than zero (in the processing).

Since the input is uncorrelated noise, with variance about the mean given by equation (5), the standard deviation of the noise in position, about its mean, is

$$\sigma_{\delta R_n} = \left[ \sum_{k=0}^{n-1} h^2(k) \right]^{1/2} \sigma_{in}$$

where  $\sigma_{in} = \frac{b}{\sqrt{12}} = 0.0554 \text{ ft/sec.}$

Using  $h(k)$  as given by (11) yields

$$\sum_{k=0}^{n-1} h^2(k) = \left( \frac{\Delta T}{2} \right)^2 \left[ 2n-1 + \frac{(1.0036)^{2(n-1)} - (.9964)^{2(n-1)}}{.0036} \right]$$

## Appendix B

For  $\Delta T = 2$ ,  $n = 320$  the result is

$$\sum_{k=0}^{319} h^2(k) = 3361 \text{ sec}^2 = 57.98^2 \text{ sec}^2$$

Thus

$$\sigma_{\delta R_{320}} = 57.98 \sigma_{in}$$

For quantization  $\sigma_{in} = 0.0554 \text{ ft/sec}$  and  $\sigma_{\delta R_{320}} = 3.21 \text{ ft.}$  about the mean.

The conclusion of this analysis of position errors is that the output of the position equation is biased by  $-75.4 \text{ ft}$  and has a standard deviation about this bias of  $3.21 \text{ ft}$ . The results of a simulation agree ( $67 \text{ ft}$  error in radial component of position) with the results of the above analysis. It should also be noted that the analysis reveals that very little fluctuation about the mean is to be expected and only one computer run need be made to determine the effect of quantization on position errors.

In passing, it is useful to note that the average  $g$  equations do an entirely adequate job during entry. With perfect accelerometers (no truncation effects) the estimated position and actual position differ by about  $100 \text{ ft}$  at the end of entry, while the velocity error is about  $0.27 \text{ fps}$ . With accelerometer output truncation, the error is about  $220 \text{ ft}$  and the velocity error is  $0.30 \text{ fps}$ .

The weighting sequence obtained for the position error will be very useful in determining the effect of quantization on velocity errors since position is coupled to the velocity navigation via the gravity term. It will now be shown that the errors in velocity estimates caused by quantization will have the following properties.



## Appendix B

- (a) Accumulated gravity errors represent 42% of the bias in the velocity estimate.
- (b) The variance about this bias is essentially due to the most recent accelerometer measurement.

The deviation of the velocity estimate obtained from (7) can be written (assuming  $R_o$ ,  $V_o$  and  $G_o$  noise free)

$$\delta V_n = \delta V_a(n) - \frac{1}{2} \Delta T \delta G_n + \Delta T \sum_{i=1}^n \delta G_i \quad (14)$$

Using  $\delta G_i = k \delta R_i$ ,  $E\{\delta V_a\} = -\frac{b}{2}$  and taking the expectation of the above equation yields

$$E\{\delta V_n\} = -\frac{b}{2} - \frac{1}{2} \Delta T k E\{\delta R_n\} + \Delta T k \sum_{i=1}^n E\{\delta R_i\}$$

Using equation (13) and performing the summation yields

$$E\{\delta V_n\} = -\frac{b}{2} [1 + 0.722] = -0.165 \text{ ft/sec}$$

The 1 in the square bracket is due to the mean of the noise in the most recent accelerometer measurement and the 0.722 term is due to the accumulated gravity error. Again this mean can be eliminated, if desired by using  $V_a(0) = -\frac{b}{2}$  in the processing.

By formal manipulation of (14) it can be shown that the variance of the velocity error about its mean is given by

$$\sigma_{\delta V_n}^2 = \frac{b^2}{12} \left[ 1 + \Delta T^2 k^2 \sum_{i=1}^{n-1} \sum_{j=1}^{n-1} \sum_{\ell=1}^{\min(i,j)} h(i-\ell)h(j-\ell) \right]$$

## Appendix B

Since

$$0 < h(j) < \frac{\Delta T}{2} [(1.0036)^{320} + 1] = 4.158$$

the triple summation can be bounded

$$\begin{aligned} \Delta T^2 k^2 \sum_{i=1}^{n-1} \sum_{j=1}^{n-1} \sum_{\ell=1}^{\min(i,j)} h(i-\ell) h(j-\ell) \\ < \Delta T^2 k^2 (4.158)^2 (n-1)^3 = 0.023 \end{aligned}$$

Thus

$$0.0554 \frac{\text{ft}}{\text{sec}} = \frac{b}{\sqrt{12}} < \sigma_{\delta V_{320}} < \frac{b}{\sqrt{12}} (1.023)^{1/2} = 0.0560 \text{ ft/sec}.$$

The error in velocity due to quantization was found to be 0.19 ft/sec from simulation. This figure agrees sufficiently well with the results of the analysis.

It has been shown that the position and velocity navigation equations are biased low because of quantization and that the variance about the velocity bias is essentially due to the most recent accelerometer measurement. It has also been shown that in evaluating the performance of the navigation equations the coupling of errors through the gravitational acceleration should not be ignored. Although the magnitude of the errors calculated here may not be significant compared to other error sources in the system, the model developed has provided useful information.

# BELLCOMM, INC.

## APPENDIX C

### AS-204 Requirements and Directives - Entry Phase

Insofar as entry is concerned, the following directives and requirements are pertinent.

"Apollo Flight Mission Assignments" (M-D MA 500-11, SE 010-000-1, September 10, 1965) states that mission AS-204 primary objectives include verification of: the operation of the CM heat shield (adequacy for entry from low earth orbit), and the G&N system.

"Apollo Program Specification" (SE 005-001-1, Revision A, March 1, 1966) states requirements as follows: (also see later)

3.5.1.22 Entry The CM shall be capable of controlled flight through the earth's atmosphere to any preselected impact point having a ground range between 1500 NM and 2500 NM from the entry point (defined as the point at which the vehicle first descends through the 400,000 feet altitude level). Additionally, the CM shall be capable of safe flight to all extended ranges between 2500 NM and 3500 NM. Both of these shall be possible without exceeding a 10 g deceleration for inertial velocities up to 36,500 fps and equatorial inclinations between  $+90^\circ$ . The design limit entry load for all CM systems shall be a 20 g deceleration.

3.5.1.23 Aerodynamic Characteristics The CM shall have an off-set center of gravity (cg) which will produce a lift-to-drag ratio of  $0.34 \pm 0.04$  at Mach 6. The direction of the lift vector shall be controllable through the use of the attitude control subsystem.\*

3.5.2.5.2 Accuracy .... The Primary Navigation Guidance and Control System shall be capable of guiding the CM during entry to the preselected point of parachute deployment within a 10 NM CEP.

"AS-204/205 Appendix to the Apollo Program Specification" (March 1966) states as follows:

1.0 Scope ... These requirements are presented in this Appendix as deviations to the requirements specified for equipment for the lunar landing mission... Unless otherwise noted, the paragraphs in this Appendix replace in their entirety the identically numbered paragraphs in the body of the specification.

---

\*Revised by MSC ASPO to be 0.28, + 0.04, - 0.00 for AS-204

## Appendix C

3.5.1.22 The CM shall be capable of controlled flight through the earth's atmosphere to a preselected water landing ares. This shall be possible without exceeding a 10 g deceleration for an Earth orbital entry. The design limit entry load for all CM systems shall be 20 g deceleration.

3.5.1.23 Aerodynamic Characteristics No Change.

3.5.2.5.2 Accuracy The navigation, guidance and control system shall be capable of guiding the CM during entry to the selected point of parachute deployment within a 10 NM CEP.

APPENDIX D

Simulation Computer Programs

The trajectories discussed in this report were computed using two computer programs called "Monte Carlo Entry" (MCE) and Bellcomm Apollo Simulation Program (BCMASP). Features of these programs are discussed in this section.

MCE is a program developed by W. G. Heffron and J. E. Holcomb of Bellcomm, and improved by Mrs. S. B. Watson. It is largely in FORTRAN. Integration is accomplished using the Adams-Bashforth four point predictor equation with "precision-and-a-half", with Runge-Kutta equations to start the process. MCE programming includes the effects of up to 106 changes in nominal data, e.g., position, velocity, and attitude readout uncertainties, deviations and/or perturbations from nominal values (correlated or uncorrelated), atmospheric density changes, vehicle mass change, Inertial Measuring Unit (IMU) errors, etc. It has three modes of operation called Monte Carlo, Sensitivity Matrix and Single Run. In a Monte Carlo run, error sources are assumed to be normally distributed, 1 sigma values are input, random values are computed based on the input, and a trajectory computed. This is repeated as often as requested; mean value and standard deviations (for some 78 quantities) are computed at selected trajectory events or times, as requested. In a Sensitivity Matrix run, a no-error trajectory is run first, followed by single error source trajectories for each non-zero error source input. The difference between the no-error trajectory and, say, the trajectory in which X gyro bias drift is non-zero is thus due to the non-zero X gyro bias drift and shows the sensitivity of the trajectory to that error source. An assumption of linearity in the sensitivity is implied (which turns out to be appropriate for the entry trajectory). From the sensitivity matrix and knowledge of the standard deviations of the error sources, the program develops covariance matrices at selected trajectory events or times by matrix methods.

In the Single Run mode of operation, the error sources are incorporated at the values input and a single trajectory computed.

The MCE program, in addition to normal listings of trajectory results, also creates a binary tape of data. A program called PLOTAP, developed by Mrs. S. B. Watson with the assistance of Mr. J. E. Holcomb, uses these data to create the plots shown in this report.

## Appendix D

In calculating a trajectory, MCE performs the following computations. It determines the CM attitude for aerodynamic trim with the roll angle controlled and computes the lift and drag forces and orientation (reentry standard atmosphere is used [9]; trim lift and drag coefficients and trim angle of attack come from tables). IMU drift rates and accelerometer readings are then computed. Gravity forces are computed for an oblate earth. Every two seconds the entry guidance computations are performed (including the average g navigation algorithm) resulting in a roll command (roll about the relative velocity vector). Required gimbal angles are computed and a "bang-bang" minimum time with limited rate and acceleration autopilot is simulated which produces a time history table of roll gimbal angles. The variables are then integrated and the program returns to the attitude computation routine. A Besselian New Year (1967) mean equinox and equator coordinate system is used, except that platform computations are made in platform axes. One entry trajectory, which requires some 840 seconds flight time, takes 2.0 minutes on the IBM 7044 computer using 1 second time steps for all computations except the guidance routine, or 1.2 minutes using 2 second time steps.

The BCMASP program was developed by Bell Telephone Laboratories for Bellcomm and modified for the present study by Mr. I. Bogner with the assistance of Mrs. S. B. Watson. BCMASP is largely in FORTRAN and uses four point Runge-Kutta equations for integration. It includes the JPL ephemeris for sun and moon, the effects of earth oblateness, and the 1962 standard atmosphere. (BCMASP has been furnished to MSC and MSFC at the present time).

For purposes of this study, BCMASP has two basic modes of operation - Single Run (as in MCE) and Perturb. Perturb mode is similar to the Sensitivity Matrix mode in MCE, one error source being inserted at a time and trajectory differences being listed. BCMASP includes the simulation of an Inertial Measuring Unit having the standard error sources.

In calculating a trajectory with BCMASP the roll attitude is computed using a simplified rate limiting autopilot, with pitch and yaw assumed to be in aerodynamic trim. Lift and drag are computed using tabulated lift and drag coefficients and resolved along aerodynamic trim axes. IMU drift rates and accelerometer readings are calculated. Gravity forces are computed for an oblate earth. (Sun and moon effects can be included.) The entry guidance computations are entered every two seconds (including the average g navigation algorithm) producing the new roll angle command. Variables are integrated and the program returns to lift and drag computations. Inertial axes of 1950.0

Appendix D

(first point of Aries) are the basic coordinate axes, but inertial axes of date of 1967 Besselian New Year, and platform axes are also used as appropriate. One entry trajectory requires some 1.5 minutes on the IBM 7044 using 2 second time steps.